Fall 2019

Ultra-Fast Sensors to Study the Fundamental Neurochemistry Underlying Disease

Alyssa West

ULTRA-FAST SENSORS TO STUDY THE FUNDAMENTAL NEUROCHEMISTRY UNDERLYING DISEASE

by

Alyssa West

Bachelor of Science
University of West Florida, 2015

Submitted in Partial Fulfillment of the Requirements

For the Degree of Doctor of Philosophy in

Chemistry

College of Arts and Sciences

University of South Carolina

2019

Accepted by:

Parastoo Hashemi, Major Professor

Stephen Morgan, Committee Member

Aaron Vannucci, Committee Member

Jane Roberts, Committee Member

Cheryl L. Addy, Vice Provost and Dean of the Graduate School

ACKNOWLEDGEMENTS

I would like to begin by acknowledging my mentor Dr. Hashemi for her guidance these past four years, she has been a role model for me in many ways and I will always appreciate her efforts to help me become the best scientist I can be. I would also like to acknowledge the members of my committee, including those who were not able to attend my defense and those that stepped in to fill their shoes, each member has been very helpful throughout my graduate degree. I would like the thank the members of the Hashemi lab who have all been very supportive in everything from editing papers and evaluating data to providing impromptu therapy sessions when things were overwhelming. My undergraduate students, Navid and Deanna, taught me to be a better mentor and made so many electrodes we started giving them away. Ou constantly set an amazing example as a post-doc and was always willing to help me with MatLab codes for data analysis. There were numerous collaborators without whom this thesis would not be possible. The mathematical modeling team, Dr. Reed, Dr. Nijhout, and Dr. Best, were all patient and helpful with developing the models we use for our data. Dr. Peña was always available to assist on statistics and develop new ways to evaluate our signals. Dr. Blakely provided the unique SERT-Ala56 mouse model I used in my genetic ASD experiments. Dr. Galli also provided the opportunity for me to assess a unique mouse model as well as facilitated my training in behavior. Finally, I would like to acknowledge my family for their continuous support and Anthony for moving so far from home with me and always believing in me.

ABSTRACT

Serotonin is a vital neurotransmitter whose exact roles are ill-defined. Dysfunctions in serotonin signaling are thought to underlie a myriad of neurological problems including depression and autism spectrum disorder (ASD). Prior to investigating serotonin's role in disease states, one must understand more about the functionality of serotonin in healthy *in vivo* models. To study serotonin *in vivo*, fast-scan cyclic voltammetry (FSCV) and fast-scan controlled adsorption voltammetry (FSCAV) are employed to measure evoked and basal serotonin concentration, respectively. These methods, combined with mathematical modeling, provide information regarding regulatory mechanisms of serotonin neurotransmission. FSCV and FSCAV are first applied to characterize serotonin chemistry in the medial prefrontal cortex (mPFC), a brain region with abundant serotonin projections and associations with various diseases. In this region, we discover two unique populations of serotonin axons terminating in discrete reuptake domains. The mPFC serotonin signals are unique when compared to previously established brain regions. Mathematical modeling of the regions provides a unique tool to determine local tissue architecture. Establishing a model of serotonin neurotransmission in the mPFC of healthy mice allows us to begin to explore alterations during disease states and determine etiology.

Peripheral serotonin dysfunction is a common phenotype of ASD despite the underlying pathophysiology of this disorder remaining poorly understood. ASD is thought to result from a combination of genetic and environmental risk factors. To better

understand serotonin's role in the brain during ASD, we investigate two genetic ASD models and find similar alterations in evoked serotonin reuptake. To evaluate the contribution of lead as a risk factor for ASD, we use a low dose perinatal exposure model. Though no convincing evidence of ASD typical behaviors is induced by this exposure paradigm, acute effects at such low doses provides cause for concern and implies that compensatory mechanisms are employed to maintain the homeostasis of serotonin during long-term exposures.

In this dissertation, I present evidence for unique serotonin transmission in the mPFC and establish further evidence of serotonin neurotransmission disruptions in mouse ASD models. I evaluate lead for its effects on the serotonin system and provided support for further research into its contribution to ASD.

TABLE OF CONTENTS

LIST OF TABLES

LIST OF FIGURES

LIST OF ABBREVIATIONS

5-HT.....5-Hydroxyhistamine/ Serotonin

ANOVA.....Analysis of Variance

ASD..... Autism Spectrum Disorder

BBB.....Blood Brain Barrier

BH.....Benjamini- Hochberg

Ca^{2+}.....Calcium (II)

CFM.....Carbon Fiber Microelectrode

CV.....Cyclic Voltammogram

DATs.....Dopamine Transporters

EPA.....Environmental Protection Agency

ESCIT ..... Escitalopram

FDR..... False Discovery Rate

FSCAV.....Fast Scan Controlled Adsorption Voltammetry

FSCV..... Fast Scan Cyclic Voltammetry

IACUC.....Institutional Animal Care Use Committee

i.p. .....Intraperitoneal

IT..... Current vs Time

MCL.....Maximum Contaminant Level

MCLG..... Maximum Contaminant Level Goal

MFB ..... Medial Forebrain Bundle

mPFC ..... Medial Prefrontal Cortex

NETs ..... Norepinephrine Transporters

OCTs ..... Organic Cation Transporters

Pb^{2+} ..... Lead (II)

PBS ..... Phosphate Buffer Solution

PFC ..... Prefrontal Cortex

SE ..... Stimulation Electrode

SEM ..... Standard Error of the Mean

SERT ..... Serotonin Transporter

SFARI ..... Simons Foundation Autism Research Initiative

SNr ..... Substantia Nigra pars Reticulata

SSRIs ..... Selective Serotonin Reuptake Inhibitors

USC ..... University of South Carolina

WE ..... Working Electrode

WHO ..... World Health Organization

CHAPTER 1:

INTRODUCTION

1.1 SEROTONIN

Serotonin (5-hydroxytryptamine, or 5-HT) is an essential biological molecule present primarily in the gut, blood, and brain. The function of serotonin differs depending on the area of the body. In the gut, this molecule primarily regulates intestinal movements and in the blood it facilitates hemostasis and blood clotting[1]. In the brain, serotonin acts as a neurotransmitter, playing roles in numerous functions, including sleep, mood, appetite, and anxiety to name just a few[2, 3]. The way in which serotonin regulates brain function is ill-understood. This shortcoming primarily because it is difficult to measure serotonin in the brain.

Serotonin has 7 distinct known receptor families (each with multiple sub-types)[4] and can be reuptaken by any of the monoamine transporters, as well as the organic cation transporter[5]. Understanding the role of each of these receptors and transporters has been the focus of decades of research. However, understanding how these proteins interact with serotonin and each other to regulate this molecule's transmission is difficult because it requires a technique capable of *in vivo* measurements while causing minimal damage to these circuits. The gap in understanding how serotonin contributes to the regulation of specific functions has also led to a gap in our understanding of how serotonin contributes to diseases in which it is implicated. One such disease is autism spectrum disorder (ASD). Abnormalities in serotonin concentration in the peripheral nervous system is well studied[6], but we know much less about this messenger in the central nervous system.

1.2 AUTISM SPECTRUM DISORDER

ASD is a collection neurodevelopmental disorders presenting with a wide range of symptoms, each with varying severity that can be observed in patients. Due to the large variety of symptoms, patients are diagnosed on three core behaviors: impaired social

interaction, communication and language deficits, and repetitive behaviors. In recent years, clinicians have begun to consider social and communication abnormalities under the same umbrella[7].

The prevalence of ASD has been growing since it was first recognized as a unifiable clinical disorder. As per the most recent data from the surveillance year of 2014, 1 in 59 children were diagnosed with ASD, an increase from 1 in 125 just 10 years prior[8]. This increasing rate of occurrence cannot solely be attributed to an improvement in early detection methods or a more established set of diagnosis attributes. Nonetheless, identification of the underlying cause of ASD has not yet been deduced. A plethora of research on the subject has led to the consensus that a combination of genetic and environmental risk factors likely contributes to the underlying pathology of the disorder[9].

Over 1,000 genes have been implicated through extensive peer reviewed studies. The Simons Foundation Autism Research Initiative (SFARI) curates this data and presents the genes on a ranked scale of 1-5. The scale indicates the strength of the evidence linking the gene to ASD, with 1 being the strongest. The ranking also indicates if the gene is linked to a co-morbid syndrome, since syndromic genes can be more confidently linked to ASD. Additionally, the genes discovered with a promising link have led to 1,638 mouse lines and 361 rat lines, among others, which are assessed on the same core behaviors that the disorder is diagnosed upon in humans[10]. Despite this extensive research though, genetics cannot wholly account for the pathology of ASD.

Roughly 85% of cases of ASD are idiopathic and cannot be explained by genetics alone[11]. It is thought, therefore, that environmental risk factors play a role in explaining the remaining cases. While several environmental factors are confirmed to have a role in ASD,

a list of potential risk factors with links to some ASD behavioral phenotypes warrant further investigation[12]. Studies into risk factors are often contradictory; positive correlations between risk factors and ASD are highly dependent on the biological pathway assessed and the time of exposure during development. Many of the proposed risk factors are common, such as lead and pesticides[12], and there is concern regarding the inconsistencies in methods used to determine if environmental toxins are risk factors for ASD[13].

To accurately assess the contribution of risk factors to ASD, a robust method for evaluating ASD models must be considered. Currently, behavioral tests govern the diagnosis of ASD in animal models. This is largely due to the wide variety of behavioral, physical, and molecular presentations. In looking for a commonality to study, arguably the most reproducible biomarker is hyperserotonemia, or high blood serotonin, which is present in about one-third of individuals with ASD[14]. While serotonin concentrations in the body are easy to measure, analysis of the central nervous system is notoriously difficult. This difficulty means that little is known about the interaction between serotonin in the peripheral and central nervous systems.

A variety of factors make serotonin an ideal target for studying ASD. The neurotransmitter is thought to play a role in regulating a range of behaviors which are commonly altered in ASD[6, 15]. Serotonin's role in brain development, specifically as a growth factor during embryogenesis and in brain structure development[16], suggest that alterations in the neurotransmitter could contribute to developmental disorders such as ASD. Recently, research has found serotonin plays a role in gene regulation in neurons[17], suggesting that any changes in the regulation of serotonin, such as from environmental

factors, could alter gene expression. Finally, and perhaps the most convincing argument that serotonin plays a role in ASD, is that selective serotonin reuptake inhibitors (SSRIs) (a class of antidepressants) are the most commonly prescribed psychoactive drug for treating ASD behaviors[18]. In endeavoring to find a commonality among ASD models, a compelling argument for serotonin as the missing link exists.

1.3 MEASURING SEROTONIN

Measuring serotonin in the brain is very difficult for a variety of reasons, including the fragile nature of the brain, the similarities between serotonin and other monoamine neurotransmitters, the low levels at which neurotransmitters are present, and the rapid time scale during which neurotransmission takes place. The most commonly used technique for measuring serotonin *in vivo* is microdialysis, however this method typically provides information on the basal concentrations of serotonin every 20 minutes, though some improvements have resulted in slightly faster time resolution[19]. To understand the functionality of the serotonin circuit and the evaluate the processes which regulate serotonin neurotransmission, fast-scan cyclic voltammetry (FSCV) is a landmark technique.

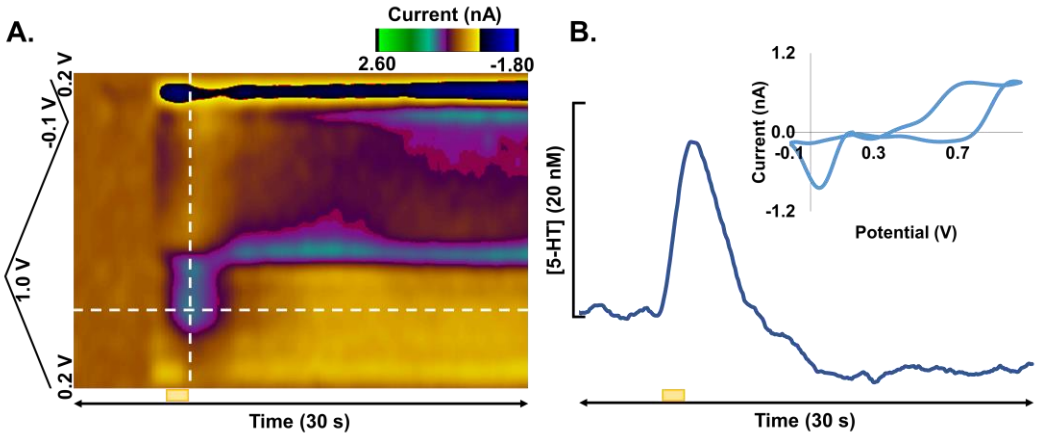

Figure 1.1: Fast-Scan Cyclic Voltammetry. Panel A of Figure 1.1 illustrates a representative color plot of serotonin, with the waveform shown on the left side.

The horizontal dotted line corresponds to the IT curve in Panel B which has been converted to concentration. The vertical dotted line corresponds to the inset CV in Panel B, which confirms the presence of serotonin with the oxidation peak at ~0.7 V.

FSCV for serotonin utilizes carbon fiber microelectrodes (CFMs) of 7 μm in diameter and 150 μm in length. The CFMs are electroplated with Nafion, a cation exchange polymer which serves to exclude species that poison CFMs. A serotonin specific waveform, shown in Figure 1.1, is applied to the electrode surface at a scan rate of 1000 V/s to selectively oxidize and reduce serotonin[20]. A stimulation electrode applies a brief electrical stimulation to evoke the release of serotonin *in vivo*. During this time, files are collected at 10 Hz, allowing observation of the release of serotonin into the extracellular space and subsequent reuptake back into the cells, as shown in Figure 1.1 current vs. time (IT) trace. Confirmation that the analyte is serotonin comes from the characteristic oxidation peak at 0.7 V found on the current vs voltage (CV) plot. The current from this oxidation can then be converted to concentration, allowing for the quantification of serotonin. Mathematical modeling can be utilized to glean information from the IT curve regarding the autoreceptors and transporters which regulate serotonin transmission[21]. While FSCV provides a wealth of useful information, the method is limited because it relies on background subtraction, meaning that ambient or basal levels cannot be known. To alleviate this restraint, the method was adapted to measure ambient concentrations of serotonin using fast-scan controlled adsorption voltammetry (FSCAV)[22].

FSCAV uses the same waveform as FSCV but applied at a higher frequency. FSCAV has three distinct steps, as shown in Figure 1.2. The first of these steps is application of the waveform at 100 Hz to minimize adsorption on the surface of the electrode, the second is a controlled adsorption step which holds a constant potential at the

electrode surface until maximum serotonin adsorption has been achieved. Finally, the waveform is reapplied and everything at the surface of the electrode is stripped, and all adsorbed serotonin is oxidized. The first CV with the characteristic serotonin oxidation peak is extracted, as shown in Figure 1.2 and the peak is integrated to yield the charge. Calibrations of each electrode inform upon the relationship between charge and concentration to allow *in vivo* values to be converted to concentration of serotonin. Combining this ambient serotonin concentration with the evoked release of serotonin provides a multi-faceted platform from which to evaluate serotonin neurotransmission. The combination of these techniques proves to be very advantageous for assessing the functionality of the serotonin system and detect any variations which may exist during disease states.

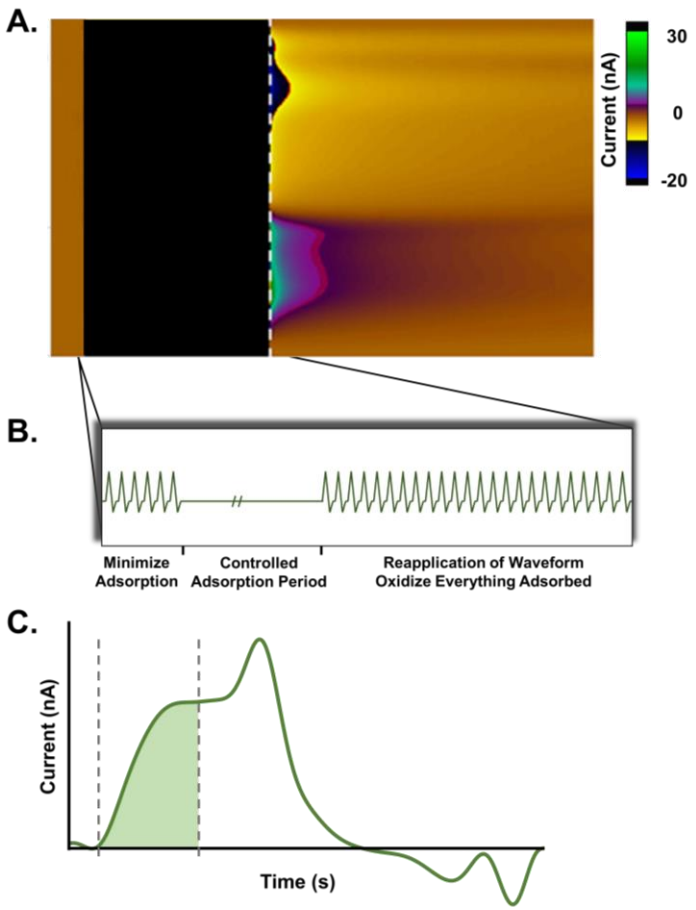

Figure 1.2: Fast-Scan Controlled Adsorption Voltammetry. Panel A of Figure 1.2 illustrates a representative color plot of serotonin, with a portion of this color plot zoomed in on for Panel B presenting the application of the waveform during the three stages of FSCAV. Panel C presents an unfolded CV with the area under the curve of the serotonin peak integrated to yield the charge needed to convert to ambient serotonin concentration.

FSCV and FSCAV were established in the brain regions, substantia nigra pars reticulata (SNr) and in the CA2 region of the hippocampus[22, 23]. However, to best evaluate serotonin in ASD a region with a more pronounced associated to the disorder should be studied. This brain area should ideally also have a high density of serotonin axons for measurement with FSCV and FSCAV. The prefrontal cortex (PFC) fits these criteria and is the most commonly documented region to have an overgrowth of neurons in ASD patients[24]. The PFC also mediates communication, cognitive development, and higher-order social and emotional behavior[25], all of which are heavily implicated in the core behavioral symptoms of ASD and make the PFC an ideal target for evaluating serotonin with FSCV.

1.4 SCOPE OF DISSERTATION

This dissertation will focus on establishing and modeling serotonin neurochemistry in the prefrontal cortex with FSCV and FSCAV. The unique serotonin signals found in this region will be compared to those in previously established regions, including the SNr and the CA2. These methods will be applied in well accepted genetic models of ASD. Finally, a perinatal lead exposure will be used to assess lead as a risk factor for ASD with behavioral and neurochemical serotonin analysis.

CHAPTER 2:

VOLTAMMETRIC EVIDENCE FOR DISCRETE SEROTONIN CIRCUITS, LINKED TO SPECIFIC REUPTAKE DOMAINS, IN THE MOUSE MEDIAL PREFRONTAL CORTEX[1]

[1] West, A., Best, J., Abdalla, A., Nijhout, F., Reed, M., Hashemi, P.; *Neurochemistry International*. **2019**. *123:50-58*.

Reprinted here with permission of publisher.

2.1 INTRODUCTION

The medial prefrontal cortex (mPFC) has garnered substantial interest in recent times amongst a diverse group of experts [26-28]. Cutting-edge research has centered on the role of the mPFC in differentiating memories [27] and suppressing reward-seeking behavior [28] *via* projections to other brain regions. Recent work has identified a key factor in the mPFC which may be imperative to treating addiction without the potential for abuse [26]. These studies, among others, highlight the many functions of the mPFC and the importance they play in a variety of contexts.

The role of the mPFC in modulating behavior is widely encompassing, with only a few functions mentioned above. As such, changes during development, including stress, drugs or social interactions, can affect the organization and function of the mPFC possibly leading to behavioral impairment [25]. To this end, our laboratory is interested in investigating the mPFC in the context of developmental disorders. Our specific interest is to understand how the chemistry in this area underlies the behavioral phenotypes of pathologies such as autism spectrum disorder (ASD). Since serotonin plays significant roles in early brain development [29] and the mPFC is densely innervated with this messenger's neurons [30], we find it meritorious to focus our chemical studies on serotonin. Serotonin chemistry in the periphery is impaired during ASD [31] however, there is currently no consensus on how or if the brain's serotonin chemistry, specifically in the mPFC, is altered during ASD. For example, human positron emission studies and animal autoradiographic studies are contradictory in their reports of serotonin transporter (SERT) density and binding capacity, with some reporting decreased SERT binding compared to controls, yet others showing no change in SERT density [32, 33] in ASD cases and models. These studies are then necessarily at odds with other animal-only ASD models that show

region-dependent abnormalities in the density of serotonin neurons [34], reduced SERT binding [35] and reduced excitatory transmission [36].

Given the uncertainties outlined above, here we seek to better define serotonin chemistry in the mPFC by applying cutting edge analytical methods, fast-scan cyclic voltammetry (FSCV) and fast-scan controlled adsorption voltammetry (FSCAV), for real-time *in vivo* serotonin analysis in the mPFC. The small size (~7 µm) of the carbon fiber microelectrode (CFM) and excellent selectivity and sensitivity of these techniques allows for sub-second measurements of stimulated serotonin release and reuptake as well as rapid (<1 minute) ambient level measurements.

Our previous work with FSCV revealed a single phase evoked serotonin response in the substantia nigra, pars reticulata (SNr) upon medial forebrain bundle (MFB) stimulation [21]. We noted a curious phenomenon in the reuptake profile of serotonin in this region. In some cases, the response would be cleared "fast" (<10 seconds) with a single reuptake curve. In other instances, the response decayed with a "slow" (>20 seconds) profile but in most cases, a combination of 'fast' and 'slow' clearance profiles resulted in a 'hybrid' reuptake. The 'fast' and 'slow' responses were identified as two distinct clearance mechanisms: Uptake 1, mediated by the serotonin transporters (SERTs), and Uptake 2, mediated by other monoamine transporters (dopamine transporters (DATs), norepinephrine transporters (NETs), and organic cation transporters (OCTs)). These mechanisms had previously been identified and while Uptake 2 was defined as high capacity, low affinity uptake, DATs and NETs can be included since each has multiple types of transporters that band together to simultaneously remove serotonin [5, 37]. We mathematically modeled our experimental curves and reported two sets of Michaelis-

Menten parameters corresponding to Uptake 1 (high affinity, low efficiency) and Uptake 2 (low affinity, high efficiency).

Here in the mPFC, we found similar single phase evoked responses with a hybrid clearance profile. Additionally, for the first time, we observed two evoked responses to a single MFB stimulation; of particular significance, the two phases had different reuptake profiles. We found a strong correlation between the occurrence of single or dual responses and the position of the CFM within the mPFC layers. Additionally, the magnitude of the second phase in the dual phase response was dependent on the position of the stimulating electrode. These findings allowed us to hypothesize that there are distinct subsets of serotonin axons traversing the MFB, that terminate in discrete domains with specific reuptake profiles. We utilized pharmacology, histology and an elaboration of our prior model in the SNr to test this hypothesis. We subsequently showed that a comprehensive and highly organized cellular network underlies the control of serotonin chemistry in the mPFC. Our findings will, in the future, serve as a base chemical model to study serotonin dysfunction in models of ASD.

2.2 METHODS

2.2.1 ANIMALS AND SURGICAL PROCEDURES

All procedures described herein are in agreement with The Guide for the Care and Use of Laboratory Animals and approved by the Institutional Animal Care and Use Committee (IACUC) of the University of South Carolina (USC). Male C57BL/6 mice (Jackson Laboratory, Bar Harbor, ME) between 20-30 grams were used for all stereotaxic surgical experiments. Mice were housed in the USC animal care facility under a 12-hour light/dark cycle with access to food and water *ad libitum*. Experiments were performed

during the light phase. Mice were injected with a 25% urethane solution (dissolved in 0.9% saline, Hospira, Lake Forest, IL, USA) *intraperitoneally* (*i.p.*) and maintained on a heating pad (Braintree Scientific, Braintree, MA, USA) at 37°C. Fully anesthetized mice were placed in a stereotaxic frame (David Kopf Instruments, Tujunga, CA, USA) for intracranial surgery. Stereotaxic coordinates were each taken in reference to Bregma [38]. A Nafion coated carbon fiber microelectrode was lowered into the medial prefrontal cortex (AP: +1.70, ML: -0.20, DV: -2.20 to -2.90) and a stainless-steel stimulating electrode (SE) placed in the medial forebrain bundle (MFB) (AP: -1.58, ML: -1.00, DV: -4.80). A Ag/AgCl reference electrode was placed in the contralateral hemisphere (AP: -3.15, ML: +1.70). Placement of the working electrode (WE) was adjusted in the dorsal/ventral plane until the desired serotonin signal was observed.

2.2.2 VOLTAMMETRY

2.2.2.1 CARBON-FIBER MICROELECTRODES (CFMS)

CFMs were fabricated in house using ~7 µm diameter carbon fibers (Goodfellow Corporation, PA, USA). The carbon fibers were aspirated into glass capillaries (ED 0.6 mm, ID 0.4 mm; A-M systems, Inc., Sequim, WA, USA) and pulled *via* a vertical micropipette puller (Narishige Group, Tokyo, Japan). Under an optical microscope, carbon fibers were cut to 150 µm. An electrical connection was forged between the carbon fiber and connection wire using silver paint. CFMs were then electroplated with nafion [23].

2.2.2.2 FAST-SCAN CYCLIC VOLTAMMETRY

The serotonin waveform was generated using a PCIe-6341 DAC/ADC (National Instruments, TX, USA) card. The working electrode was scanned at 1000 V s^{-1} from 0.2 V to 1.0 V, down to -0.1 V then back to 0.2 V and cycled at 10 Hz [20]. Bi-polar electrical

stimulations induced serotonin release (60 Hz, 120 pulses, 350 µA, 4 ms pulse width), delivered through a linear constant current stimulus isolator. A CHEM-CLAMP potentiostat (Dagan Corporation, MN, USA) measured current. Potentials were measured against a Ag/AgCl reference electrode. A predetermined calibration factor of 49.5 ± 10.2 nA μM^{-1} was used to convert current to concentration [23].

2.2.2.3 FAST-SCAN CONTROLLED ADSORPTION VOLTAMMETRY

FSCAV was performed using a CMOS precision analog switch, ADG419 (Analog Devices) to control the application of the computer-generated waveform to the electrode. The logic was controlled programmatically with a series of ramps. The waveform (0.2–1.0 V to −0.1–0.2 V, scan rate = 1000 V s^{-1}) was applied at a frequency of 100 Hz for 2 seconds, followed by holding at a constant potential (0.2 V) for 10 seconds, and finally followed by the recommencement of the waveform for a total file collection time of 30 seconds. [22].

2.2.2.4 STIMULATION LOCATION EXPERIMENTS

Experiments were carried out to explore the contribution of stimulations along the MFB to the double peak signal amplitude. For these experiments, control files were collected, and the stimulation electrode was then removed from the brain and placed either anterior or posterior to the original placement before being lowered into the brain again. Control files were collected at the secondary SE placement and the procedure was repeated a third time with the SE moved opposite its initial placement (either anterior or posterior). Following collection of control files with the three SE placements, the experiment was terminated.

2.2.2.5 ANALYSIS AND STATISTICS

Custom software (WCCV 3.0, Knowmad Technologies LLC, Tucson, AZ, USA) was used for data collection, processing, and analysis. Data was background subtracted and filtered at zero-phase using a fourth order Butterworth 5 kHz low pass filter. FSCV yields cyclic voltammograms (CVs) which can be used both qualitatively and quantitatively. CVs are stacked in time to produce a 2-D color plot which allows for extrapolation of current vs. time (IT) plots as well as CVs. IT plots were written as text files and imported to Excel where they were averaged across each time point and converted to concentration using a predetermined calibration factor (*vide supra*). An average concentration vs. time trace is generated from this process and the standard error of the mean, taken across each time point, is added to the plot.

FSCAV data was processed and electrodes calibrated as previously described [22].

2.2.2.6 PHARMACOLOGY

Mice were administered a bolus intraperitoneal (*i.p.*) injection of 10 mg kg^{-1} escitalopram (ESCIT) (Sigma-Aldrich, St. Louis, MO) during the experiment. Files were collected for up to two hours following injection.

2.2.2.7 EXCLUSION CRITERIA

If the cyclic voltammograms (CVs) collected with FSCV and FSCAV did not match the characteristics of serotonin CVs collected *in vitro*, the mice were excluded from this study. Mice that died before the end of the collection time were excluded. Mice were also excluded if the electrode was found not be located in the MFB after histology. All other mice were included in this study.

2.2.3 HISTOLOGY

Following data collection, a large potential (13 V for 90 seconds) was passed through the working electrode to lesion the brain. Mouse brains were harvested, following euthanasia, and stored in 4% paraformaldehyde until ready for slice analysis. Brains were transferred to 20% sucrose solution 48 hours prior to sectioning. Each brain was sectioned (30 µm) using a cryotome and sections were analyzed for working and stimulating electrode placement. Electrode placements were verified, and mPFC subsection location of the CFM determined based on the Allen Mouse Brain Atlas (Allen, 2004).

2.2.4 MODELING

Our model for this work is an elaboration of a prior model [21], with addition of two domains, which are two distinct types of termini clusters. Domain 1, Dmn_1, is subject to both Uptake 1 and 2 and receives input from Population 1. Domain 2, Dmn_2, subject only to Uptake 1 and receives input from Population 2. Let x be a variable that goes from Dmn_2 (x =0) to Dmn_1, where we expect that L (maximum distance between Dmn_1 to Dmn_2, as estimated from the maximum distance across characteristically similar layers) (Allen Mouse Brain Atlas, 2004) will be of the order of magnitude of 500 µm.

As depicted in Figure 2.1, Dmn_2 is the region $0 < x < a$ and Dmn_1 is the region $b < x < L$ where x is a distance variable indicating the position of interest. Let u(t,x) be the extracellular concentration of serotonin at x at time, t. Then u(t,x) satisfies the partial differential equation (1):

$$\frac{\partial u(t,x)}{\partial t} = Input\ (t,x) - \ Uptake\ (t,x) + \mathrm{k} \cdot \frac{\partial^2 u(t,x)}{\partial^2 x} \quad (1)$$

$$u(0,x) = 60\ nM \quad (2)$$

$$\frac{\partial u(t,0)}{\partial x} = 0 = \frac{\partial u(t,L)}{\partial x} \quad (3)$$

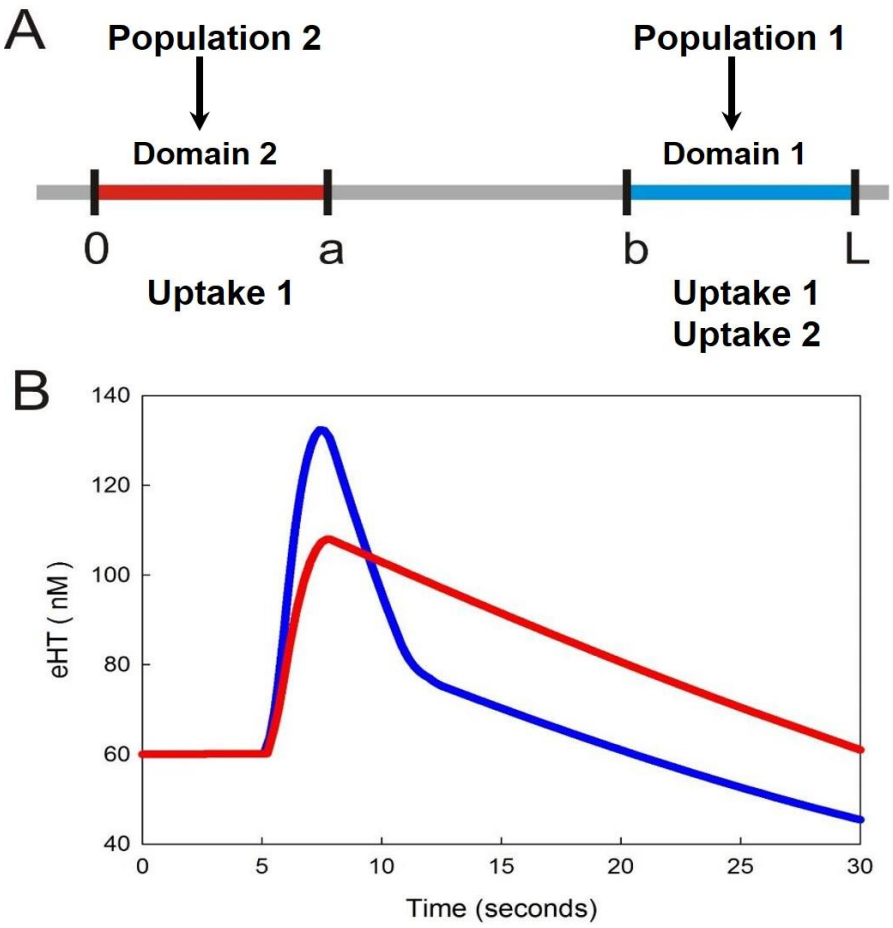

Figure 2.1: Representation of the Mathematical Model. Panel A of Figure 2.1 shows a geometric sketch of a physiological hypothesis. Population 1 provides input to Dmn_1, located between x = b and x = L. Dmn_1 has both Uptake 1 and Uptake 2. Population 2 provides input to Dmn_2, located between x = 0 and x = a. Dmn_2 has Uptake 1. In the middle region (between x = a and x = b), there is no input and no reuptake but extracellular serotonin is free to diffuse. The response (blue) in Panel B shows the time course of extracellular serotonin if only population 1 were stimulated. The response (red) in Panel B shows the time course of extracellular serotonin if only population 2 were stimulated. Experimentally, sole stimulation of population 2 has not been observed.

Where k is the diffusion coefficient of serotonin in the extracellular space. The initial condition (2) states that at time = 0 the system is at steady state and the extracellular concentration of serotonin is equal to 60 nM at all x (estimated from prior models and

experimental data Appendix Figure A.4) [22]. The boundary condition (3) guarantees that serotonin cannot diffuse out of the interval [0,L].

Input(t,x) is constant at the steady state level until t = 5 seconds, which is the start of MFB stimulation. For a few seconds after t = 5, impulses arriving from populations 1 and 2 increase the serotonin concentrations in Dmn_1 and Dmn_2 creating FSCV peaks. After that the peak amplitudes dip below basal level until 30 seconds because of prolonged autoreceptor effects discussed previously [21]. The strength of the inputs to Dmn_1 and Dmn_2 depend on the position and strength of the MFB stimulation and are varied in our simulation experiments. There is no input between x = a and x = b.

In Dmn_1, Uptake(t,x) is both by Uptake 1 and Uptake 2. Uptake 1 has a Michaelis-Menten profile with $V_{max1} = 19.25$ nM s^{-1} and $K_{M1} = 5$ nM. Uptake 2 also follows Michaelis-Menten kinetics with parameters $V_{max2} = 780$ nM s^{-1} and $K_{M2} = 170$ nM. These parameters are almost identical to those we previously established in the SNr [21]. The constraints of this model include that Dmn_2 is subject to Uptake 1, that Uptake 2 operates only at concentrations above 75 nM, and that there is no uptake between x = a and x = b.

The question that we investigate in the simulations in this paper is what will happen in the extracellular space if serotonin can diffuse from type 2 domains (Dmn_2), to the electrode surface, which is enveloped by type 1 domains (Dmn_1). In all of our simulations we assume Dmn_1 are ubiquitous around the electrode. The parameter r, s_1, and s_2, are proportional to serotonin release in Dmn_1 and Dmn_2, respectively. Model simulations were performed using MatLab R2017b (MathWorks, Natick, MA, USA) using ODE solver ode23s implemented on an iMAC with operating system OS X version 10.12.6.

2.3 RESULTS AND DISCUSSION

2.3.1 TWO SEROTONIN RELEASE EVENTS IN RESPONSE TO A SINGLE STIMULATION

The MFB was stimulated and serotonin was detected in the mPFC at an implanted CFM. Examples of serotonin release are shown in the color plots in Figure 2.2 (*vide supra* for color plot interpretation). This kind of stimulation - measurement method is well established in dopamine voltammetry; for example, dopamine release is induced in the nucleus accumbens upon MFB stimulation [39]. It is generally well accepted in the voltammetry community that MFB stimulated dopamine release, which is abolished *via* lidocaine-induced cell body inactivation, is antidromic [40]. We believe that this principle applies to MFB stimulated serotonin release in the mPFC.

Figure 2.2A shows the average serotonin response in the mPFC with error bars signifying standard error of the mean for responses averaged between animals. This average response is tallied as a function of two distinct response types. Specifically, in some experiments, we recorded a single evoked serotonin peak with primarily Uptake 2 clearance. However, an equal amount of times we observed a double peak, or dual event, in response to the stimulation. The second peak appeared to be delayed and the amplitude varied with respect to the first. The appearance of these dual responses varied substantially, and representative examples of the five most common types we observed are shown in Figure 2.2B. The CVs of both peaks, shown in the inset, clearly identified each release event as serotonin with an oxidation peak around 0.7 V. Capacitive currents were observed on the color plots and CVs at the switching potentials in Figure 2.2B, though they did not interfere with serotonin quantification [41].

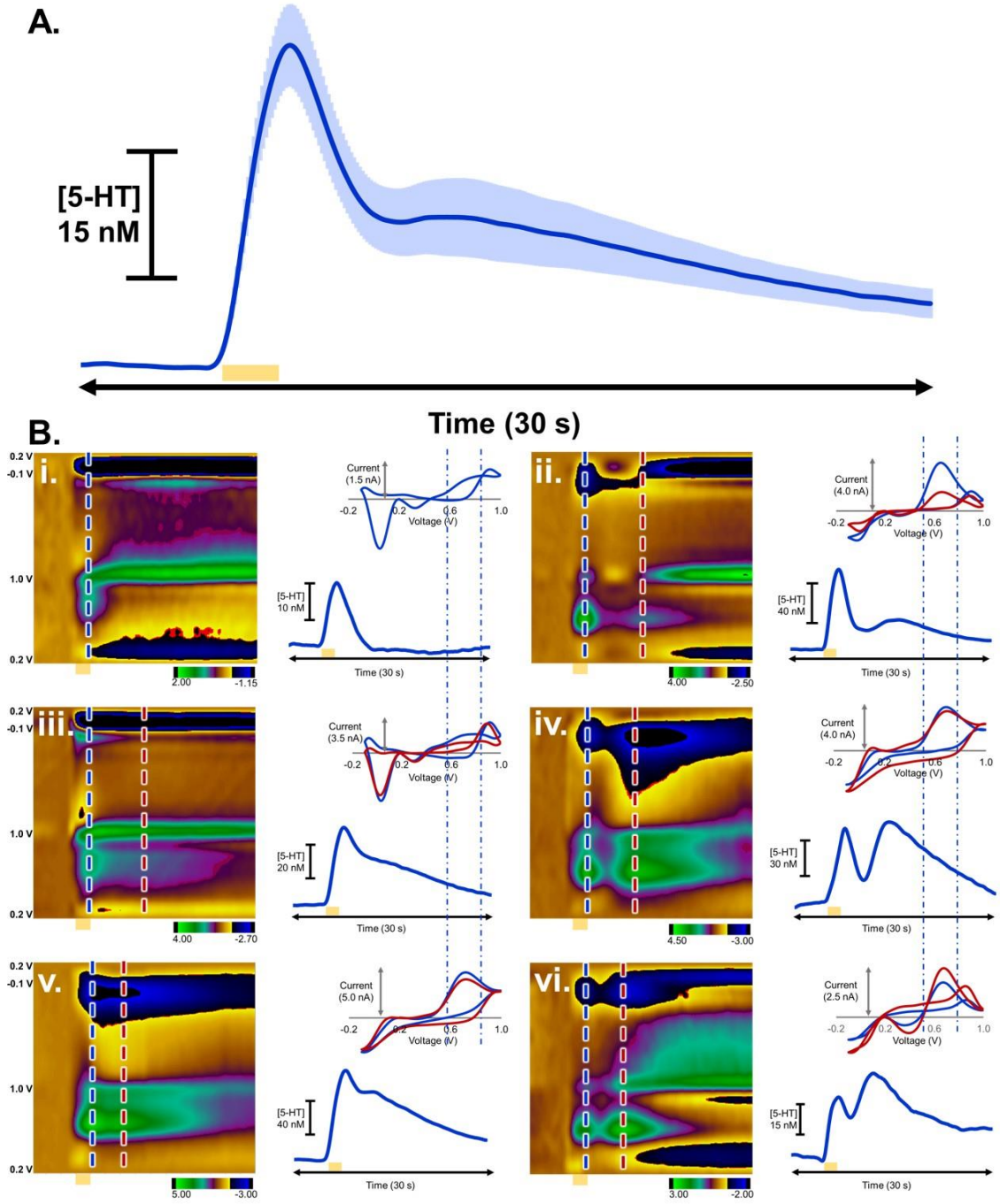

Figure 2.2: Serotonin Responses in the mPFC. The average response of all signals recorded in the mPFC can be seen in (A) with error bars showing SEM. The variety of these signals can be seen in (B) with color plots, concentration vs. time traces, and inset CVs corresponding to the peaks identified from the color plot. The traditional single peak is shown in (i.) along with the variety of double peaks seen in (ii.-vi.). Inset CVs confirm that each peak is serotonin by the oxidation peak at ~0.7 V. The correlation between the individual signals and their experiment number (seen in Table 2.1) is as follows: i.-17, ii.-3, iii.-2, iv.-7, v.-9, vi.-5.

To the best of our knowledge, this is the first time that biphasic responses have been observed with serotonin. Dopamine has been previously observed, with FSCV, to exhibit a variety of profiles depending on measurement location, though the reasoning for these responses cannot wholly be applied to this instance for serotonin [42].

While several hypotheses were considered for this biphasic phenomenon, including mobilization of different vesicular pools and second messenger effects, we believe that the data are best explained *via* a combination of two theories. First, parallel projection systems have previously been postulated to underpin dopamine circuitry from the ventral tegmental area [43]. Likewise, parallel serotonin pathways from the dorsal and median raphe nuclei project to the mPFC [44, 45]. Second, biochemically distinct compartments form the basis of the striosome-matrix hypothesis [46-48]. Thus, here we hypothesize two different, parallel populations of serotonin axons in the MFB that terminate in different biochemical compartments (not to be confused with mPFC layers), which here we term domains, Dmn_1 and Dmn_2. Dmn_1 receives input from population 1 and clearance occurs *via* both Uptake 1 and Uptake 2. Dmn_2 receives input from population 2 and the serotonin released here is cleared *via* Uptake 1. An illustration of this hypothesis, with two scenarios illustrating the CFM location either in layers 1-3 or in layers 5-6, can be found in Figure 2.3. The prospect of Uptake 2 clearing serotonin is substantiated as DATs, NETs, and OCTs have been found in the mPFC. While rodent studies have shown a higher expression of SERTs compared to DATs and NETs in the mPFC [49], their high efficiency allows them to suitably clear serotonin. OCTs have been found with some abundance in the mPFC [50] but information regarding their expression relative to DATs and NETs is less available.

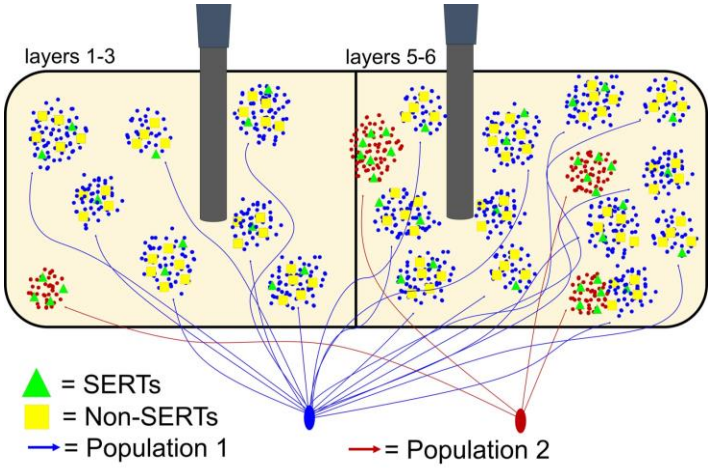

Figure 2.3: Theory Schematic. Population 1 (blue) has input to all layers and terminates in Dmn1 with Uptake 1 (SERTs, green triangles) and Uptake 2 (non-SERTs, yellow squares) transporters. Population 2 (red) has input primarily to layers 5 and 6 and terminates in Dmn2 where Uptake 1 dominates. The time delay of the second peak is due to diffusion, since Dmn2 is more sparse, thus farther from the CFM. This phenomenon also explains why the second peak is only observed in layers 1-3 after administering ESCIT (see Figure 2.5); where amplitude of serotonin released in Dmn2 is now high enough to be measured.

Our experimental data (*vida infra*) suggests that Dmn_2 occurs sparsely across layers and that Dmn_1 is ubiquitous. The sparse innervation of Dmn_2 is such that we believe that our electrode is never close enough to detect peaks from Dmn_2 first, but the ubiquitous nature of Dmn_1 makes our electrode constantly consistently surrounded by this domain. Our hypothesis is that the second peak is caused by the diffusion of serotonin from Dmn_2, *via* activation of population 2, to the electrode surface. We now explore this notion in more detail.

Figure 2.4 shows data from a representative experiment where a dual response is observed pre (blue trace) and post (red trace) 10 mg kg^{-1} ESCIT administration. Pre-drug, the extracellular serotonin rises rapidly after the stimulation followed by a rapid, Uptake 2

mediated, decline. At about t = 11 seconds the curve begins to rise again because of diffusion of serotonin from Dmn_2 to the CFM. In this example the initial reuptake profile of the second peak is primarily mediated by Uptake 2 as serotonin from Dmn_2 has diffused to the electrode surface which is surrounded by Dmn_1 and the high concentrations of serotonin have activated Dmn_1 Uptake 2 transporters. Once the concentration falls below a certain threshold, Uptake 2 ceases and Uptake 1 dominates. Post ESCIT, the first peak is not largely affected because ESCIT does not significantly target Uptake 2 transporters [51]. The second peak, conversely, increases in amplitude and the decay is significantly slowed, because clearance here is mostly mediated by Uptake 1 (SERTs). This response to ESCIT was a consistent trend seen across the dual response signals obtained. An additional representative experiment with these conditions can be found in the Appendix (Figure A.1).

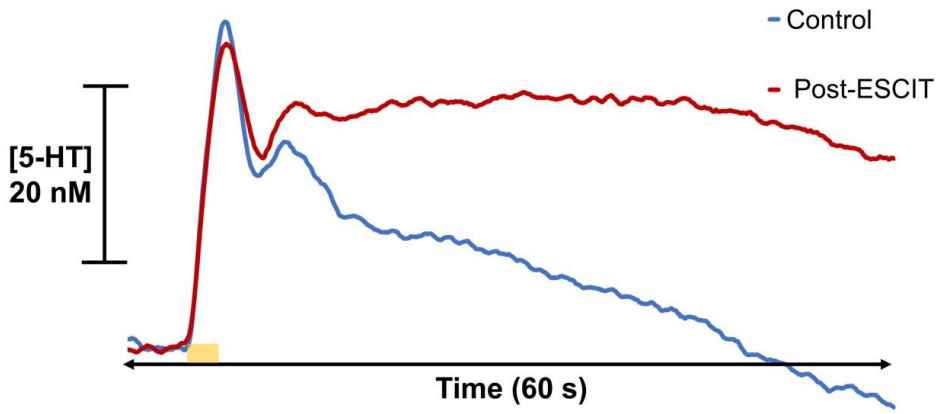

Figure 2.4: A Double Peak pharmacological experiment. A representative response (experiment 18) is shown before (blue) and after (red) *i.p.* administration of 10 mg kg^{-1} ESCIT. Both curves show a biphasic response. Our hypothesis of diffusion from Dmn_2 to Dmn_1 explains the differences between the curves.

These results confirm that the two individual peaks are selectively associated with different uptake mechanisms. This uptake specificity exists regardless of whether a second

peak is observed or not. Above we hypothesized that the two peaks result from activation of separate populations and explore this in more detail in the following sections.

2.3.2 SINGLE OR DUAL EVOKED RESPONSE ARE DEPENDENT ON SUB-REGION LAYERS

In defining the origin of the two evoked serotonin peaks, we first explored the correlation of the position of the CFM in the mPFC tapestry to the prevalence of single vs. double peaks. Following data collection, a large potential was applied to the working electrode, which we previously found successfully created an identifying lesion in the brain tissue (otherwise undetectable due to the miniature dimensions of the CFM). The lesions were categorized on the sub region (prelimbic, infralimbic, and anterior cingulate cortex) and layer (1-6) of the mPFC. We found no trend between sub regions, but single vs. double peaks were distinctly dependent on layer. Table 2.1 correlates the signal type (single vs. double) with the sub-region and layer in which the CFM made measurements. Visual representation of the histology can be found in the Appendix (Figure A.2).

Double peaks were consistently observed in layers 5-6, while single peaks were seen only in layers 1-3. This trend was consistent across all subregions of the mPFC. While layers are traditionally defined by the synaptic density [52], the data shown here supports the theory that the layers may also define the topographical limits of functionally different serotonin neurons. In support of this, morphological differences between cortex varicosities have been identified [53]. These different varicosities can be directly associated with specific projections from the dorsal and medial raphe which have been shown to terminate in a layer dependent manner [44, 45, 53]. In addition, there is genetic [54] and

electrophysiological [55] evidence for functionally different serotonin neurons in the frontal cortex.

Table 2.1: Correlating Peak Response to Measurement Location.

Experiment Number	Number of Peaks	WE Sub-region	WE Layer
1	Two	Anterior Cingulate	5
2	Two	Prelimbic	5
3	Two	Anterior Cingulate	5
4	Two	Anterior Cingulate	5
5	Two	Anterior Cingulate	6a
6	One	Anterior Cingulate	2/3
7	Two	Prelimbic	5
8	One	Infralimbic	2/3
9	Two	Anterior Cingulate	5
10	One	Anterior Cingulate	2/3
11	One	Infralimbic	1
12	One	Infralimbic	1
13	One	Infralimbic	1
14	Two	Anterior Cingulate	5
15	One	Prelimbic	2/3
16	One	Anterior Cingulate	1
17	One	Infralimbic	1
18	Two	Infralimbic	5
19	One	Anterior Cingulate	2/3
20	Two	Prelimbic	5

An interesting phenomenon was observed following administration of ESCIT in experiments where only single peaks were observed; a second peak could emerge after ESCIT. Figure 2.5 shows a representative experiment where single evoked events were measured before (control, blue) and 40-60 minutes after (red) ESCIT. Histology confirmed that the CFM was located in layer 1-3, as above for single peaks. An additional representative experiment with the same conditions can be found in the Appendix (Figure A.3).

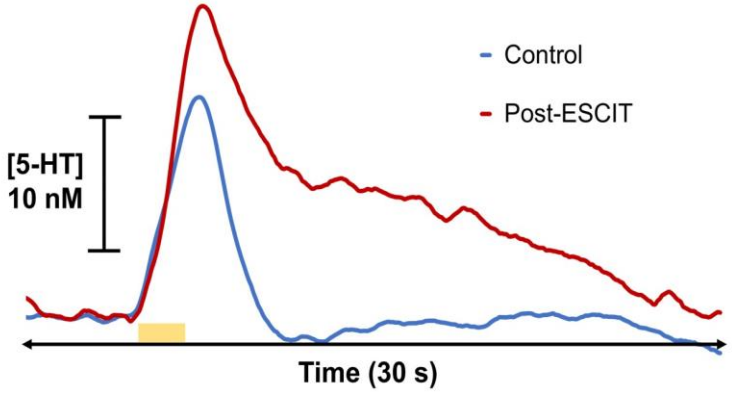

Figure 2.5: A Single Peak Pharmacological Experiment. The [5-HT] vs time traces are shown for a representative (experiment 15) single peak serotonin response before (blue) and 60 minutes after (red) 10 mg kg^{-1} ESCIT administration. Histology confirmed that the CFM was in layers 1-3.

The experiments listed in Table 2.1 revealed that the occurrence of single or dual evoked events are dependent on the layer in which the CFM is located. Figure 2.5 experiments indicated layer 1-3 have the potential for the second peak, but that prior to ESCIT the amplitude is too low to be detected. The capacity for a second peak provides support for the presence of Dmn_2 in layers 1-3, though much more sparse than in layers 5-6, resulting in an amplitude too low to be detected without pharmacological intervention.

We observed another phenomenon related to the dual response. In different animals there was a large variance in the ratio of the amplitude of the second to first serotonin peak even when the CFM was in the same layer and sub region, pointing towards an important role for the stimulation location. We next investigated this notion.

2.3.3 SECOND PEAK AMPLITUDE IS HEAVILY DEPENDENT ON MFB STIMULATION

To further define the origin of the two evoked serotonin peaks, we test the hypothesis that the two evoked serotonin events occur *via* stimulation of separate axonal populations, traversing the MFB. We found that stimulating different locations along the MFB, in the AP axes, changed evoked serotonin amplitude, with the most significant effect on the second peak. We postulate that these stimulation electrode placements have less effect on the first peak because axonal population 1 must be more consistently located along the MFB tract that we probed.

Figure 2.6A depicts three double peak signals obtained in one animal. Each signal was collected by stimulating a different location along the MFB moving anterior (i) to posterior (iii). The second peak amplitude increases with the anterior placement of the SE and decreases posterior. In the third signal (iii), and most posterior SE placement, the second peak is almost completely eliminated. In Figure 2.6B the experiment was repeated when a single peak was observed, and movement of the SE did not cause a double peak to appear. This allows us to conclude that while the stimulation along the MFB controls the amplitude of the second peak, the presence of a single or double peak remains wholly dependent on the CFM placement within the mPFC layers.

We next study the discrete reuptake mechanisms tied to each domain.

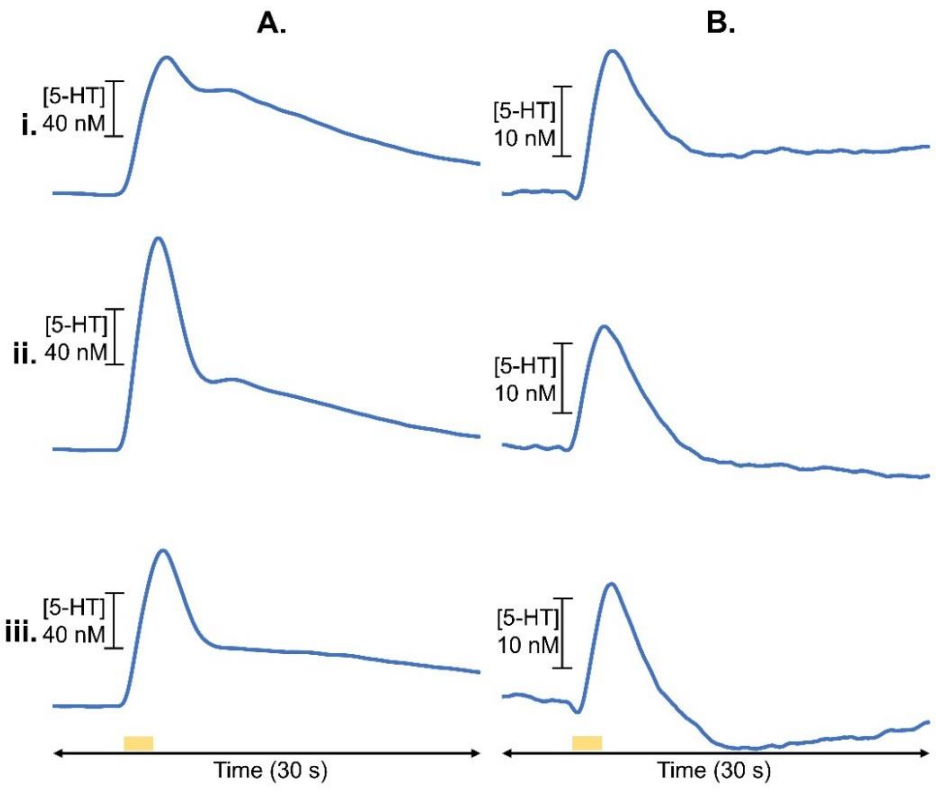

Figure 2.6: Investigating the Effects of Stimulation Location. The left panel (A) shows a serotonin double peak response in a single animal (experiment 9). The right side (B) shows a serotonin single peak response in a single animal (experiment 11). In each experiment, control files were collected with three different SE placements (i.-iii.) while the WE remained in the same place. The SE was removed from the brain and reinserted twice, anterior (i.) and posterior (iii.) to the original (ii.) placement.

2.3.4 MODELING TWO DISCRETE AXONAL POPULATIONS THAT TERMINATE ONTO SPECIFIC TRANSPORTER DOMAINS

Figure 2.2B shows five different experimental response curves measured in layers 5-6, and one response measured in layers 1-3 of the mPFC. Our fundamental hypothesis is that there are two types of domains in layers 5 and 6: Dmn_1 is innervated by population 1 of axons from the MFB and once released into this domain, serotonin is reuptaken by

Uptake 1 and 2 transporters. Dmn_2 is innervated by population 2 axons and once serotonin is released into this domain, it is uptaken by Uptake 1 transporters. We experimentally demonstrated that Dmn_1 is ubiquitous and Dmn_2 occurs more sparsely. Therefore, we assumed that the CFM always measures serotonin released from Dmn_1. The potential for the CFM to measure serotonin released from Dmn_2 depends on several factors including: input to population 2, the diffusion length L, and coefficient k. As the serotonin released from Dmn_2 diffuses through the extracellular tissue it is reuptaken by the transporters of surrounding domains, thus its reuptake profile is heavily dependent on the extracellular serotonin concentrations. In the Materials and Methods Section 2.2.4, we formulated a mathematical model based on these hypotheses. Our mathematical model fails if serotonin from Dmn_2 was either cleared exclusively cleared by Uptake 2 or initially cleared by Uptake 2 and the subsequently cleared by Uptake 1.

Our model represents a highly complex physiological system and the intent is not to exactly match the experimental curves in Figure 2.2B. Rather, the purpose is to show, using the model, that by varying s_1 and s_2, the strengths of the stimulation from populations 1 and 2, respectively, the diffusion length L and coefficient k, and the basal extracellular serotonin, that we can obtain the variety of behaviors seen in the experimental curves in Figure 2.2. We next discuss the response and model curves (i)-(vi) individually. Of note: although the aspect ratios of the curves are the same, the scale of the y-axis varies in both the experimental curves (Figure 2.2B) and the model curves (Figure 2.7).

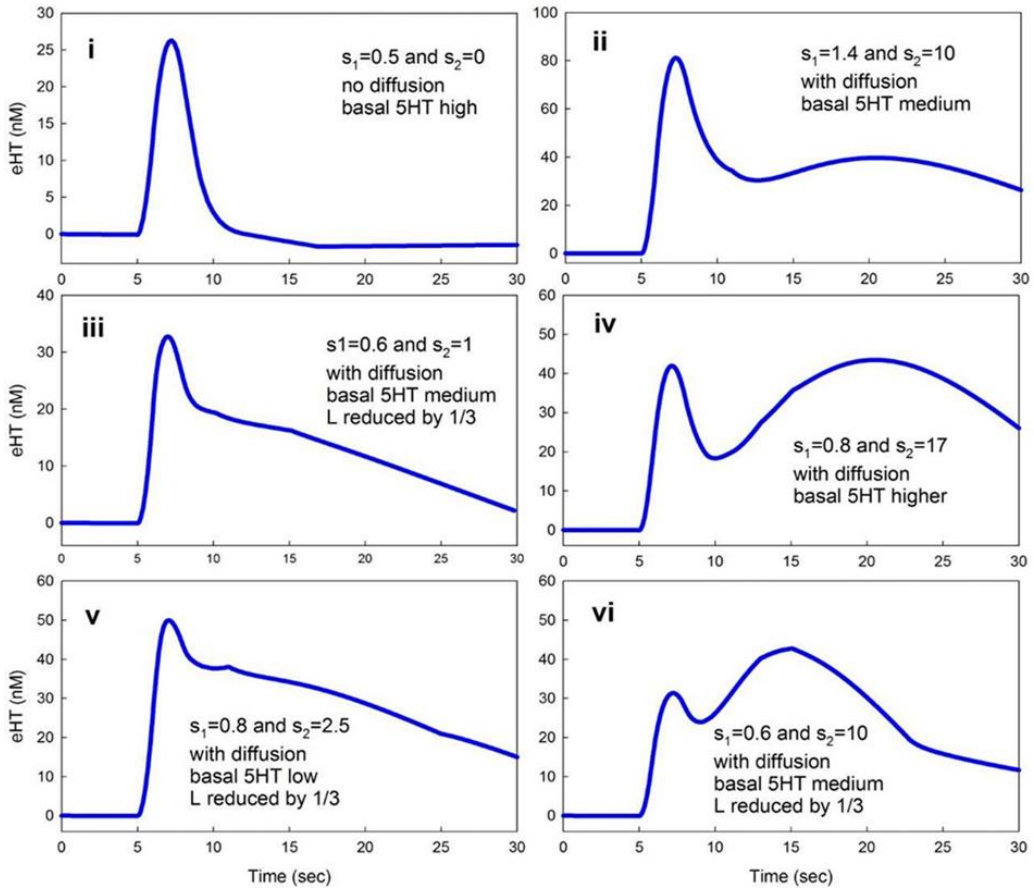

Figure 2.7: Model Simulations. Panels i.-vi. show the extracellular serotonin response with different choices of parameters. s_1 and s_2 represent the strength of the neural inputs to Domains 1 and 2, respectively. In Panel (i) there is no diffusion, so the response only represents serotonin released from Dmn_1. In Panels (ii), (iii), (iv), (v), and (vi) the diffusion coefficient is the same, k=0.3 $(nM)^2\ s^{-1}$. In each panel the approximate basal level of extracellular serotonin is indicated. We have shown, using FSCAV, that basal serotonin levels in the mPFC vary over a range of 50-75 nM (see Appendix Figure A.4). In Panels (iii), (v), and (vi) the diffusion length (L) from Dmn_2 to Dmn_1 is reduced by 33%. These simulations can be compared with experimental curves in Figure 2.2B.

Response (i). The single peak simulated here arose from stimulation of population 1 (s_1=0.5), uptaken rapidly, indicating mainly Uptake 2 mediated transport [21]. To fit this peak the following parameters were implemented: diffusion coefficient k = 0, indicating no diffusion took place from Dmn_2 to Dmn_1 where the CFM is located.

The basal level of serotonin in the extracellular space was assumed to be in the higher range, making Uptake 2 operational. Thus Uptake 2 quickly brought the released serotonin back down to baseline. The curve then descended below baseline as a result of the autoreceptor effect previously discussed [21].

Response (ii). For this simulation, population 2 was stimulated in addition to population 1 resulting in diffusion of serotonin from Dmn_2 to the electrode surface, resulting in two peaks. The first peak descended quickly because the extracellular serotonin is within the range which Uptake 2 operated. The second peak was reuptaken more slowly by the Uptake 1 transporters as the extracellular serotonin descended below the range of Uptake 2, in addition to the fact that serotonin continued diffusing from Dmn_2.

Response (iii). This resembled a typical hybrid response previously observed [21], with the exception that a second peak shortly followed the first. To simulate this response, the stimulation of population 1 was $s_1 = 0.6$, and that of population 2 was $s_2 = 1$. The basal level of serotonin was in the middle range. The model then produced a hybrid response with a slight second peak that occurred close to the first peak as the diffusion length between the two domains was reduced by 33%.

Response (iv). The simulation shown here had input to population 1, $s_1 = 0.8$, and input to population 2, $s_2 = 17$. This resulted in a lower amplitude of the first peak and higher amplitude of the second peak. The reuptake of the second peak was faster in this simulation as a result of the extracellular serotonin remaining in the range necessary for Uptake 2 to function up to t = 30 sec.

Response (v). This response was simulated in the model by setting the input of population 1, $s_1 = 0.8$, and population 2, $s_2 = 2$, and reducing the diffusion length between Dmn_1 and Dmn_2. The basal level of serotonin was in the lower range so serotonin was reuptaken by Uptake 1 transporters, because Uptake 2 transporters were inactive.

Response (vi). In the experimental curve in Figure 2.2B.vi, which this simulation resembles, the first peak was lower in amplitude than the second, while the second peak occurred earlier in time than in the other curves shown. This effect was produced in the model simulation with input of the population 1, $s_1 = 0.6$, and shortening the diffusion length from Dmn_2 to Dmn_1. The resulting curve showed a pulse of extracellular serotonin from Dmn_2 arriving earlier to the electrode, in Dmn_1.

These simulations, generated with our new model, described the features of the experimental serotonin responses observed in the mPFC. Additional simulations (not shown) with varying parameters can give a multitude of other single and double-peak shapes of response curves**.** Thus, this mathematical model accurately supports the hypothesis that we constructed based upon our experimental data.

2.4. CONCLUSION

The medial prefrontal cortex plays a critical role in a variety of functions and behaviors. In working towards characterizing the functionality of the mPFC, we directed our efforts towards delineating serotonin transmission in this area. The application of FSCV and FSCAV allowed us the capacity to, for the first time, produce real-time *in vivo* serotonin measurements in the mPFC. We had previously modeled evoked serotonin

release in the substantia nigra, pars reticulata, and identified two clearance mechanisms: Uptake 1 and Uptake 2, each mediated by different transporters [21]. Our current work in the mPFC, presented here, revealed two distinct evoked serotonin events, resulting from a single stimulation of the MFB, which were each bound to a discrete reuptake profile. We hypothesized that distinct populations of serotonin axons traverse the MFB and terminate in discrete reuptake domains. This hypothesis was explored and substantiated *via* pharmacology, histology, and mathematical modeling. In this work, we presented evidence for the complex organization and regulation of serotonin transmission in the mPFC. The model developed from this work lays the groundwork for our future studies of the function of the mPFC and its relation to behavioral outcomes.

CHAPTER 3:

FAST SEROTONIN VOLTAMMETRY AS A VERSATILE TOOL FOR MAPPING DYNAMIC TISSUE ARCHITECTURE: I. RESPONSES AT CARBON FIBERS DESCRIBE LOCAL TISSUE PHYSIOLOGY[2]

[2] West, A.[+], Abdalla, A.[+], Jin Y., Saylor, R., Qiang, B., Peña, E., Linden, D.J., Nijhout, H. F., Reed, M. C., Best, J., Hashemi, P.; Accepted by *J. Neurochem*. 08/13/19. **(**[+]= these authors contributed equally)

Reprinted here with permission of publisher.

3.1 INTRODUCTION

Neuromodulators, such as serotonin, are thought to regulate the brain's major excitatory and inhibitory processes. As such, subtle alterations in the function of these modulators are thought to underlie the phenotypes of many disorders of the brain [6, 56-59]. To better understand the functional importance of messengers like serotonin in the brain, analytical measurements of neurotransmitters is a thriving and rapidly evolving field [60-62]. To this end, we have thus far focused on pioneering *in vivo* measurements of evoked and ambient serotonin using fast-scan cyclic voltammetry (FSCV) and fast-scan controlled adsorption voltammetry (FSCAV) at carbon fiber microelectrodes (CFMs) [22, 23].

Quantitative chemical measurements of brain serotonin *in vivo* are highly challenging because of very low extracellular concentrations [63]. An additional difficulty for electroanalytical measurements is that serotonin and serotonin metabolites are detrimental to electrode stability due to polymer filming [20]. In our initial efforts to develop an FSCV tool for serotonin measurements, we chose to make measurements in the substantia nigra, pars reticulata (SNr) because this region contains the most dense innervation by serotonin axons in the brain [64]. When it comes to interest in serotonin's actions in the brain however, there is much focus on psychiatric, cognitive and developmental disorders [6, 56-59] which implicate brain regions other than the SNr. These brain regions include the hippocampus [65], amygdala [66], hypothalamus [67] and prefrontal cortex (PFC) [68]. Our own research interests incline us towards the hippocampus and medial prefrontal cortex (mPFC). Biophysical alterations are seen in these regions during disease. For example, volume changes in the hippocampus and the prefrontal cortex have been associated with depression [69-72]

It is very important to address the chemical functionality associated with such biophysical changes. We have performed pilot studies in these and other brain areas [22, 73, 74], here we present a formal characterization of the voltammetry stimulation and measurement circuits for serotonin in the CA2 region of the hippocampus and the mPFC, compared with the SNr.

Serotonin is shown to be evoked in the CA2 region of the hippocampus, the mPFC and the SNr *via* a common electrical stimulation of the medial forebrain bundle (MFB). Comparison of the evoked and ambient serotonin chemistry in these three regions reveals significant differences which we postulate to arise from differences in tissue physiology local to the CFM, specifically in the characteristics of serotonin reuptake *via* different monoamine transporters. The chemical signals are modeled mathematically according to our previously established models of serotonin transmission which accounts for Uptake 1 (Serotonin transporter (SERT) mediated) and Uptake 2 (Dopamine transporter (DAT), norepinephrine transporter (NET), and organic cation transporter (OCT) mediated) [21] and single vs. dual evoked events [73]. Our modeling also, independently, hypothesizes differences in how serotonin is reuptaken *via* Uptake 1 and 2, while bringing forth additional hypotheses about the strength of input to the three locales and autoreceptor contribution. Our models' predictions are subsequently verified with confocal imaging of axons and stimulation parameter experiments.

We thereby show that FSCV and FSCAV are multi-faceted tools that provide information on the proteins directly around the CFM and tell us about the strength of the input circuit. This combination of techniques presents an innovative approach for chemical brain mapping which has future implications for chemically defining the functionality of

local circuitry during health and disease. A better understanding of the circuits within specific brain regions will ultimately allow for improved drug targeting for disease treatment.

3.2 MATERIALS AND METHODS

3.2.1 STUDY DESIGN AND EXCLUSION CRITERIA

Previously collected sample data (see Appendix B) informed upon values necessary to determine statistical difference between two serotonin signals. This data was input into a power analysis according to literature standards [75]. The following formula to calculate sample size between two groups with a quantitative endpoint was used:

$$n = 2 \times SD^2 \times (Z^{\alpha} + Z^{\beta})/d^2$$

The pooled standard deviation from the sample data was found to be 1.06, and the effect size 1.96, resulting in a calculated Cohen's d of 1.85 [76]. The Z^{α} term used was 1.96 according to a 95% confidence interval and the Z^{β} term was 0.842 according to the 80% power assumed. This power analysis resulted in a n=5.25, which was rounded to 5. Finally, the sample size was corrected to account for loss of animals due to death or exclusion criteria[75]. We began with 141 animals to accommodate this adjustment and still achieve sufficient power. The percent of animals expected to die due to urethane anesthesia, based on empirical observations from our own lab, was about 38% (54of 141 animals). This number appears high, though research has shown that many studies severely under-report unexpected death from anesthesia[77]. Urethane is a terminal anesthetic and the dose is difficult to adjust. However, the fact that our experiments require long periods of stable anesthesia, combined with the non-survival nature of our experiments makes urethane an ideal choice for our purposes. Of the remaining 87 animals, 34 were excluded for because

of exclusion criteria fully detailed below, leaving 53 animals that were included in the data analysis (16 in the SNr, 16 in the CA2 and 21 in the mPFC). No randomization was used to determine which mice would be used for measurement in each region.

For all FSCV experiments, the CV of the evoked signal was compared to well-established serotonin cyclic voltammograms (CVs) *in vivo* and *in vitro* and mice in which the CVs did not contain the characteristic serotonin redox peaks or included interference by dopamine were excluded. For FSCAV experiments, a stimulated serotonin response was collected prior to the start of FSCAV and the same aforementioned test was performed. Data which contained a stimulation artifact resulting from the stimulation electrode touching the skull that masked, delayed, or minimized the serotonin response (stimulation glitch) were excluded. Electrodes that displayed drift or instability during file collection, as a result of damage during insertion, were excluded. While stereotaxic technique was utilized for this study, individual variation between mice often times limits the control we have over the exact position of the working electrode. We confirmed placement of the electrode in our target region in two ways, first during surgery, if the cyclic voltammogram is characteristic for serotonin and second, post-surgery histology confirmed if the electrode was in the target region. Signals not collected in the target regions were excluded from the study.

3.2.2 CARBON-FIBER MICROELECTRODES

CFM's were constructed through the aspiration of a single T-650 carbon fiber (7 μm, Goodfellow, Coraopolis, PA) through a cylindrical glass capillary (internal diameter: 0.4 mm, external diameter: 0.6 mm, Product # 624500, A-M Systems, Carlsborg, WA). This capillary was then placed in a vertical pipette puller (Narishige Group, Setagaya-Ku,

Tokyo, Japan) to make a carbon – glass seal by gravity. The protruding carbon fiber was then cut to 150 µm in length. Subsequently, a solution of Nafion (LQ-1105-US-25, 5% by weight Nafion, Ion Power, DE) was electrodeposited, as previously described, onto the exposed carbon fiber [23]. The CFM was then dried for 10 minutes at 70°C.

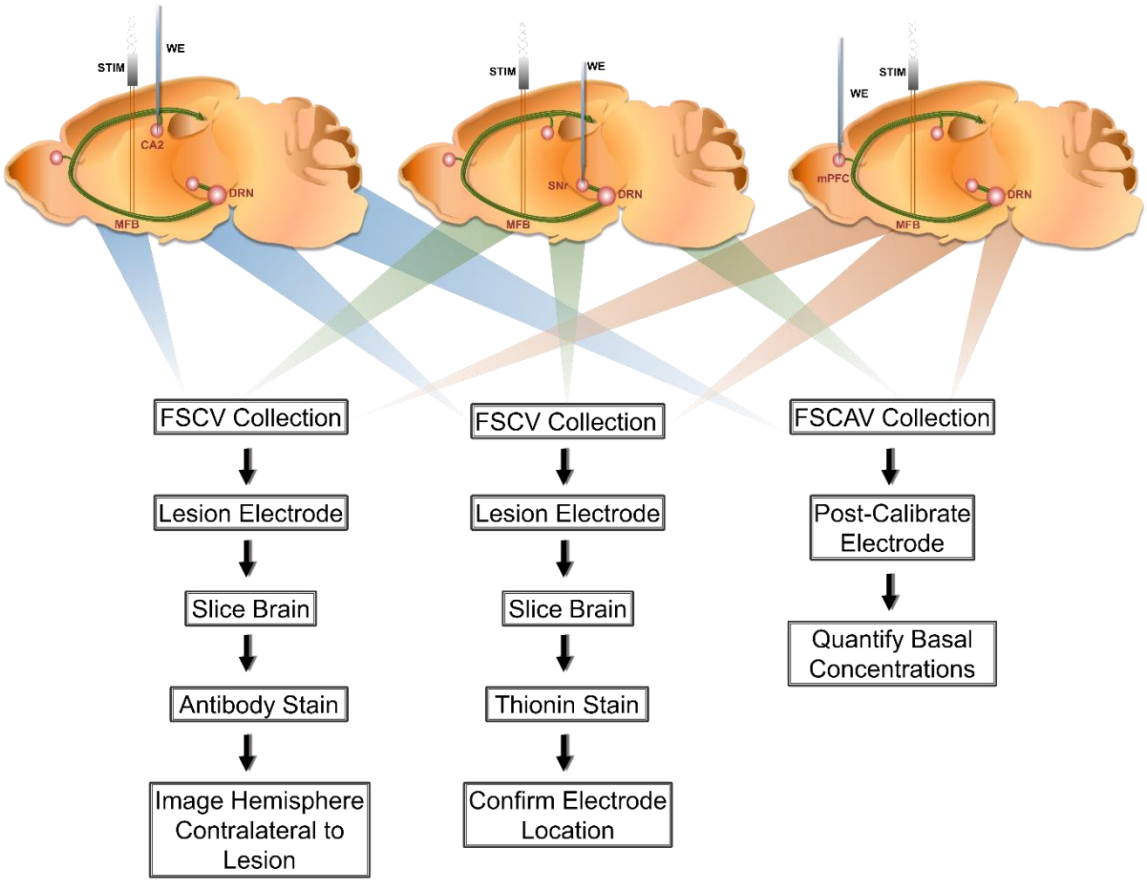

Figure 3.1. Methods Diagram. In each of the three brain regions (CA2, SNr, mPFC) serotonin measurements were taken using either FSCV or FSCAV. The three main methods, outlined here, led to the collection of evoked control (SNr: n=5, CA2: n=5, mPFC: n=10), evoked stimulation parameter experiments (SNr: n=5, CA2: n=5, mPFC: n=5), and basal (SNr: n=5, CA2: n=5, mPFC: n=5) serotonin measurements, and staining of serotonin axons (SNr: n=1, CA2: n=1, mPFC: n=1) in each of the three regions of interest. (n= number of animals)

3.2.3 ANIMAL SURGERY

C57BL/6J (RRID: IMSR_JAX:000664) male mice, 6 to 12 weeks old and between 20-30 g, were procured from Jackson Laboratories (Bar Harbor, ME). The study was

originally started with 156 mice. Mice were offered food and water *ad libitum* and housed in 12 hours light/dark cycles. The Guide for the Care and Use of Laboratory Animals, as accepted by the Institutional Animal Care and Use Committees of the University of South Carolina (Institution Approval # A3049-01), was followed in all animal care and procedures. A urethane solution was produced (25% (w/v)) by dissolving urethane (Product # U2500, Sigma Aldrich Co., St. Louis, MO, USA) in sterile saline (0.9% NaCl solution, NDC 0409-4888-20, Hospira, Lake Forest, IL). The anesthetic urethane, was administered *intraperitoneally* (*i.p.*) at a volume of 7 μL per 1 g mouse weight, followed by stereotaxic surgeries (Model 962, David Kopf Instruments, Tujunga, CA) during the light cycle. To maintain the ideal mouse body temperature of 37° C, a heating pad from Braintree Scientific was utilized. For stereotaxic coordinates of MFB [AP: -1.58, ML: +1.0, DV: -4.8 to -5.0], SNr [AP: -3.28, ML: +1.40, DV: -4.21 to -5.0] CA2 [AP: -2.9, ML: +3.35, DV: -2.5 to -3.0], and mPFC [AP: +1.7, ML: +0.2, DV: -2.0 to -3.0], bregma was used as a reference from Franklin and Paxinos (2008). In order to access the MFB, CA2, SNr, and mPFC holes were drilled in line with the above stereotaxic coordinates. No randomization method was used to assign mice for measurements in a specific region. For stimulation, a stainless-steel electrode (diameter 0.2 mm, MS303/2-A/SPC; Plastics One, Roanoke, VA) was inserted into the MFB. For measurements, the Nafion-coated CFM was then inserted into either the CA2, SNr, or the mPFC. The reference electrode is made of a silver wire (diameter: 0.010 in, 787000; A-M Systems, Sequim, WA), which was electroplated with chloride through immersion of in hydrochloric acid for 30 seconds (0.1 M, 4 V vs. tungsten). This is then placed into the contralateral hemisphere of the CFM placement.

3.2.4 DATA COLLECTION

FSCV and FSCAV were both performed through instrumentation and software (WCCV 3.05) developed by Knowmad Technologies LLC (Tucson, AZ) (available upon request). FSCV was performed by applying the "Jackson" waveform [20]. Measurements were collected every 10 minutes with a 30-60 second file. Five seconds into the file, a stimulation was applied (60 Hz biphasic 360 μA, 120 pulse stimulation, 2 ms per phase) through employing a linear constant current stimulus isolator (NL800A Neurolog; Digitimer Ltd.) to elicit the serotonin response. This stimulation was varied slightly, one parameter at a time, for the stimulation parameter experiments. FSCAV was applied through a CMOS precision analog switch, ADG419 (Analog Devices), which is used to control the application of the computer-generated "Jackson" waveform to the CFM. The logic was software - controlled to either apply a series of ramps (0.2 V to 1.0 V to -0.1 V to 0.2 V, scan rate = 1000 V/s) every 10 ms (100 Hz) or apply a constant potential of 0.2 V to the CFM for a specified controlled adsorption period (10 s) [22].

3.2.5 DATA ANALYSIS

Signals collected from FSCV and FSCAV were processed using custom software (*vide supra*) using LabVIEW 2009 (available upon request). The processing used includes signal deconvolution, filtering, and smoothing. For FSCAV, the cyclic voltammogram (CV) at the 3rd scan (following the controlled adsorption period) was extracted to integrate the serotonin oxidation peak approximately between 0.4 V and 0.85 V. The charge value found, in pC, was plotted versus [serotonin] to generate calibration curves that were then used to calculate *in vivo* values which were specific to each electrode [22]. No blinding was necessary for the purpose of the experiments presented herein.

3.2.6 STATISTICAL ANALYSIS

Post-Hoc Validation of Sample Size: A sample size of 5 mice for each of the three groups was utilized. This choice of sample size was initially estimated by previous studies (see Study Design) as the data necessary for proper sample size calculation was not yet collected. Following collection of experimental data, this sample size was reevaluated based on power considerations. We assumed that two-sample t-tests applied at 5% level of significance and an 80% power with a Cohen's d of 2.0 (associated with an effect size of 2), when the common standard deviation is 1.0. Note that based on the obtained sample data, the pooled standard deviation was found to be 1.06, which is close to 1.0. Based on the sample size formula, the appropriate sample size to use is thus n = 3.92, rounded to a sample size of 4 for each group. Taking into consideration that the assumed common standard deviation of 1.0 may have been too liberal (in light of the sample standard deviation of 1.06), a sample size of 5 per group appears acceptable for determining statistical differences.

Basal Level Analysis: In vitro calibrations related charge with the concentration, as explained previously [22]. We compared the basal responses for the three regions (CA2, SNr, mPFC; five animals for each region), where the basal value was measured every minute for 60 minutes. Hence, a repeated measures two-factor model was fitted, with the factors being the region and time. To accommodate the repeated-measures feature, random effects were included in the model, as well as the possible interaction effects between region and time. The model developed is presented here:

$$Y(I,j,t) = M + A(i) + B(t) + C(i,t) + V(I,j) + E(I,j,t)$$

Where i = 1, 2, 3 represents the region; j = 1, 2, …, 5, represents the animal number (within the group), and t = 0, 1, 2, …, 60, represents the time. M is a common mean; the A(i)'s are the effects of the region levels; the B(t)'s are the effects of the time levels; the C(I,t)'s are the interaction effects; V(i,j) is a random term (which is normally distributed) to account for the repeated measurements over time; and E(I,j,t)'s are the error terms (which are also normally distributed and independent of the V(I,j)'s).

A test of the null hypotheses that the B(t)'s and C(I,t)'s are all zeros based on the repeated-measures analysis of deviance, implemented through the R Statistical Package, resulted in not being able to reject these null hypotheses, hence both the interaction effect and the time effect were not significant. The p-value for testing for no interaction effects was 0.8539, while the p-value for testing that there is no time effect is 0.8249.

Because the time and region*time effects were not significant, we therefore combined the concentration over the 60 minutes for each of the animals in each group by obtaining their sample means. These sample mean values were then used to compare whether there were differences between the three regions; this analysis was performed using a one-way analysis of variance (ANOVA). By analyzing the sample means of the observations over time, we were able to eliminate dependencies over time among the observations. This analysis of variance showed that at least two of the regions are indeed different statistically with a p-value of 0.00000756 (ANOVA).

To determine which regions are different, we performed pairwise t-tests with the Welch-Sattertwaite's degrees-of-freedom approximation to allow for unequal variances, and we implemented a multiple testing correction, using the Holm procedure. We concluded that CA2 and mPFC regions are not statistically different (adjusted p = 0.23),

while the SNr and CA2 are different (adjusted p = 0.000012), and the SNr and mPFC are also different (adjusted p = 0.000043). A summary of the statistics from these group means are provided in Table 3.1 below, which includes 95% confidence interval for the group means.

Table 3.1 Statistical Analysis of Group Means for Each Brain Region.

Region	Sample Size	Mean (mean of the sample means)	SD (standard deviation)	ME (margin of error)	95% CI for the group mean response
SNr	5	39.706	4.391	5.452	34.254 - 45.158
CA2	5	72.822	7.170	8.903	63.919 - 81.725
mPFC	5	67.565	7.636	9.481	58.084 - 77.046

Depletion Analysis: Repeated stimulations were employed to determine if serotonin release could be depleted in each of the three regions over time. Maximum serotonin release for each animal in each group was measured in response to stimulations every minute for 20 minutes. The main goal was to compare the maximum amplitude during the first stimulation (t=1) with those at later times to see whether serotonin release was depleted in response to repeated stimulations. Because this is a repeated measures experiment, for any fixed time t (taking values from 2, 3, …, 20), we took the differences in the level at time t and at time 1 for each of the animals within each group. Using these differences, we then performed a one-sample t-test to test the null hypothesis that the population mean difference is zero versus less than zero (indicating a decrease from time 1 to time t). We performed this procedure for each of the time values t, yielding a t-test statistic value and a p-value. Since we performed multiple tests (19), we applied the

Benjamini-Hochberg (BH) false discovery rate (FDR) mulitplicity correction. The results are as follows, based on the BH-adjusted p-values:

For the CA2 data set, we concluded that the maximum amplitude at t=20 is significantly lower than at t=1, with BH-adjusted p-value of 0.0325. This is the only time point for which we concluded significance based on the BH-adjusted p-values. It should be noted that some of the unadjusted p-values arising from these t-tests were less than .05, however the necessity of the multiplicity adjustments increased these values. It is possible that with more animals, statistical significance could be achieved. Another way to globally test if the serotonin level was decreasing over time is *via* an analysis of covariance with the covariate being the serotonin level at t=1. This analysis of covariance yielded an estimate of the regression coefficient associated with time of -0.4542 (p-value = 0.00048) and with estimate of the coefficient of determination of R^2 = 59.66%. The sign of the estimated regression coefficient (negative), indicates that the serotonin level decreases over time from t=1.

For the SNr data set, we did not find any significant differences between t=1 and any of the other time points, even before the BH adjustment for multiplicity. An analysis of covariance also did not show a significant decrease.

For the mPFc data set, prior to the BH multiplicity adjustments, there were p-values that were less than 0.05. After employing the BH-adjustments the analysis concluded no significant differences between the t=1 and later time values. An analysis of covariance did not show a significant difference in the serotonin level over time.

3.2.7 MODELING

We use the mathematical model that we previously presented [21]:

$$\frac{d[S(t)]}{dt} = R(t)(1 - A(t)) - \alpha \frac{V_{max1}[S(t)]}{K_{m1} + [S(t)]} - \beta \frac{V_{max2}[S(t)]}{K_{m2} + [S(t)]}$$

S(t) is the concentration of serotonin in the extracellular space, R(t) is the firing rate of the serotonin neuron that rises briefly after stimulation, and A(t) represents the strength of the autoreceptor effect. The first negative term represents reuptake by SERTs with V_{max1} = 19.25 nM/hr and K_{m1} = 5 nM. The second term represents Uptake 2 (DATs, NETs, and OCTs) with V_{max2} = 780 nM/hr and K_{m2} = 170 nM. Uptake 2 operates only above the steady state concentration of serotonin. α and β give the balance between Uptake 1 and Uptake 2. For details and discussion, see Wood *et al.* 2014. To model the double hump in the mPFC we use the extended model presented in West *et al.* 2018 that allows diffusion of serotonin from regions with only Uptake 1 to regions that have both Uptake 1 and Uptake 2.

3.2.8 HISTOLOGY

In order to confirm the spatial placement of the CFM *in vivo*, a small lesion was created at the end of the FSCV experiment, by applying a constant potential at the CFM (~10 V for 1 min). Subsequently, the mice were euthanized *via* cervical dislocation followed by decapitation, and the brain was removed from the skull and stored in 4% paraformaldehyde in PBS solution. At least 2 days prior to sectioning, the brain was transferred into a 30% sucrose solution, until it was saturated with the medium. The brain was then flash-frozen, sectioned into 30 μm slices mounted onto frosted glass slides, and stained with 0.2% thionin. The slices were then photographed with an optical microscope.

3.2.9 IMMUNOHISTOCHEMISTRY

Slc6a4-EGFP male mice (RRID: MMRRC_030692-UCD), 6-12 weeks old, were anesthetized with urethane (25% dissolved in 0.9% NaCl solution, Hospira, Lake Forest, IL) administered *intraperitoneally* (*i.p.*) at a volume of 7 μL per 1 g mouse weight. Mice

were then perfused intracardially with phosphate-buffered saline (PBS) followed by 4% paraformaldehyde in PBS at 4 °C. The entire brain was removed and fixed in 4% paraformaldehyde for 3 hours at room temperature and then cryoprotected in 15% sucrose in PBS overnight at 4 °C, followed by a switch to 30% sucrose on the next day and continuing overnight. Sections of the mouse brain (40 µm thick) were prepared using a microtome and were washed with PBS and then blocked with 5% normal goat serum and 0.3 % Triton X-100 in PBS for 2 hours at room temperature. The sections were incubated in primary antibody diluted in blocking buffer, overnight at 4 °C. The primary antibodies used were chicken anti-GFP (1:5000, Aves Labs #GFP-1010, RRID: AB_2307313), guinea pig anti-SERT (1: 1,000, Frontier Institute #HTT-GP-Af1400), rabbit anti-TH (1: 1,000, Millipore #AB152), and mouse anti-NeuN (1:500, Millipore #MAB377, RRID: AB_2298772). The sections were then washed with PBS and incubated in the secondary antibody in a blocking buffer for 2 hours at room temperature. The secondary antibodies used were Alexa Fluor 488-labeled goat anti-chicken (1:1000, Life Technologies #A11039), Cy3-labeled goat anti-guinea pig (1:800, Jackson ImmunoResearch Laboratories #106-165-003), Cy3-labeled goat anti-rabbit (1:800, Jackson ImmunoResearch Laboratories #111-165-003), and Cy5-labeled goat anti-mouse (1:200, Jackson ImmunoResearch Laboratories #115-175-146). Then, the sections were mounted on slides, and images were acquired using a single-photon confocal microscope (Zeiss). Maximum projection images of 10 z-planes 1 micron apart were analyzed using NIH ImageJ (https://imagej.nih.gov/ij/), and % pixel intensity of EGFP signal above threshold was measured as an index of SERT innervation.

3.3 RESULTS

3.3.1 SEROTONIN IS EVOKED *VIA* A COMMON MFB STIMULATION IN THREE DISTINCT BRAIN REGIONS

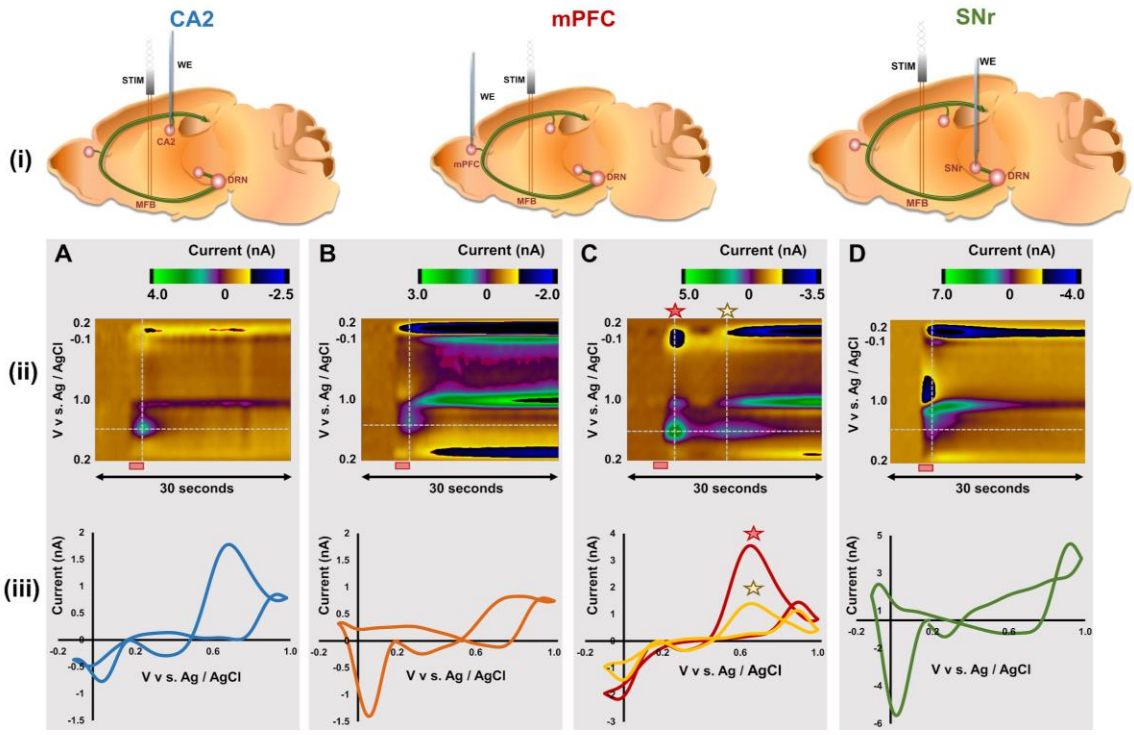

Figure 3.2. Representative Serotonin Signals of the Three Regions. (i) Representation of a sagittal section of a mouse brain. WE shows the position of the working electrode and STIM shows the stimulating electrode. Green track represents the serotonergic axons that originate in the raphe nucleus and traverse the MFB to innervate different brain regions. (ii) Representative FSCV color plots of the CA2 (A) (n=5), the mPFC (B) (n=5) and (C) (n=5), and the SNr (D) (n=5). The red bar below the color plots denote the stimulation period (2 s) iii) Cyclic voltammograms extracted from the vertical dashed lines in A(ii), B(ii), C(ii), and D(ii) with current on the y-axis and voltage vs. Ag / AgCl on the x-axis. Red and yellow stars on C(ii) denote the two successive oxidation events seen in the mPFC. Cyclic voltammograms extracted at both these positions are seen in C(iii), marked with their respective stars. (n=number of animals)

Stimulation of the MFB at one location evokes serotonin in the CA2 region of the hippocampus, the mPFC and the SNr. Figure 3.2 displays representative examples of color plots and CVs collected in each of these 3 brain areas upon stimulation. In Panel i are illustrations of the positions of the stimulating and working electrode in sagittal sections of

the mouse brain. Panel ii shows representative 30 second color plots enveloping the 5 seconds before and 25 seconds after the stimulation. Interpretation of color plots is explained in detail elsewhere [78], briefly voltage is on the y-axis, time on the x-axis, and current illustrated in false color. Panel iii shows CVs extracted from the vertical dashed lines on the color plots with the oxidation peak of serotonin at approximately 0.7 V.

In contrast to the CA2 and SNr where a single serotonin release and uptake event is evoked upon stimulation, in the mPFC we often also observe a dual peak, the origins of which we've recently described [73]. Two representative examples of mPFC signals are illustrated in Figure 3.2C.

To study whether there is physiological relevant information in these traces, we carry out a comparison of how serotonin concentration changes over the file collection time. Serotonin concentration [serotonin] vs. time traces are extracted at the position of the peak oxidation current and averaged between 5 animals per region. Figure 3.3 shows the averaged serotonin time courses per region (n=5, ± standard error of the mean ((SEM)). The responses are confirmed to be in the target region *via* lesioning the tissue adjacent to the CFM after the experiment. A representative stained slice from each region, along with the location of the CFM, for each experiment performed can be found in Panel B of Figure 3.3. The decay of these traces indicates the transporters responsible for removing serotonin from the extracellular space. A fast decay is a result of Uptake 2 (DATs, NETs, and OCTs), a slow decay results from Uptake 1 (SERTs), and a trace which has both fast and slow decay is a hybrid response and results from a combination of the two uptakes. Serotonin release in the CA2 appears primarily mediated by Uptake 2. The mPFC serotonin responses, as we previously characterized [73], involve clearance by both Uptake 1 and 2

transporters, which are linked inextricably to the two release domains.

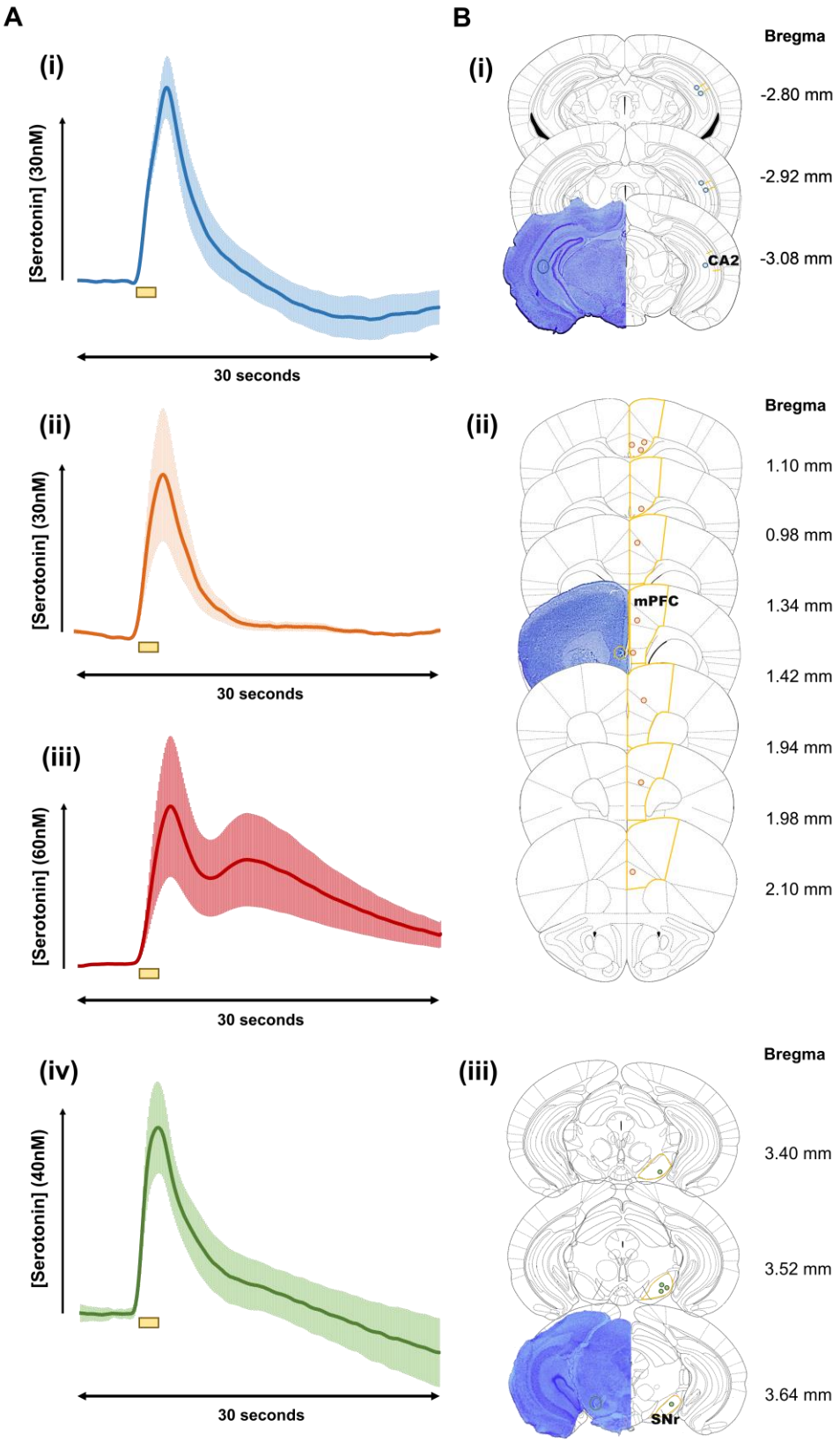

Figure 3.3. Average Serotonin Concentration vs. Time Profiles and Histology. (A) Averaged [Serotonin] – time profiles (n=5 ± SEM) i) CA2, ii) mPFC single peak response, and iii) mPFC double peak response, and iv) SNr. Yellow bars beneath the plot denote the stimulation period (2 s). (B) Thionin stained representative brains displayed on the left with a colored circle denoting the actual placement of the CFM. On the right, yellow lines represent the outlines of the i) CA2 ii) mPFC, and iii) SNr regions. Blue, orange, and green circles denote the placement of the CFM in each individual mouse, for the CA2 (n=5), the SNr (n=5), and the mPFC (n=10), respectively. Coordinates with respect to Bregma are shown to the right of each coronal slice. Region specific coordinates are explained in the methods section. (n=number of animals)

Serotonin released in the first domain, observed as a single peak, is reuptaken by Uptake 2 mechanisms, while serotonin in the second domain is solely reuptaken by Uptake 1 processes. This was verified pharmacologically using escitalopram. Domain 2 is only readily observed when measurements occur in layers 5-6 of the mPFC and is more sparsely innervated, resulting in a second peak due to the longer diffusion time to reach the electrode surface. In the SNr, serotonin seems to be reuptaken *via* a hybrid of Uptake 1 and 2.

This data lead us to formulate a hypothesis that the chemical decay profile after stimulation offered by the CFM is indicative of the ratio of SERT (Uptake 1) : non-SERT (Uptake 2), specifically that serotonin in the SNr is cleared by a higher Uptake 1 : Uptake 2 ratio when compared to the other two regions. To strengthen this hypothesis, we perform ambient serotonin measurements with FSCAV in the three brain areas, shown in Figure 3.4.

3.3.2 SEROTONIN BASAL LEVELS DIFFER BASED ON BRAIN REGION

To measure ambient serotonin levels in each of three brain localities, a new method, FSCAV is applied [22]. First MFB stimulation is employed in mice to verify the presence of serotonin with FSCV. FSCAV is then performed on the same CFM for 60 mins to obtain

a baseline reading of ambient serotonin concentrations. The dark blue, green, and orange circles on the central trace of Figure 3.4 represent the weighted average response (n=5 ± SEM) in the three regions. Individual mice traces are displayed by faint markers, of similar color, on the same plot. Representative *in vivo* color plots, along with CVs extracted from the 3rd scan (vertical dashed line), post controlled adsorption period, can be seen on Figure 3.4. All CVs demonstrate the characteristic redox serotonin peaks, thus confirming the identity of the signal measured. To convert this signal to serotonin concentration in the 3 zones, we use a chemometric approach, to take into account the variability between the CFMs used, along with the *in vivo* variability. This approach was explained in detail previously [22].

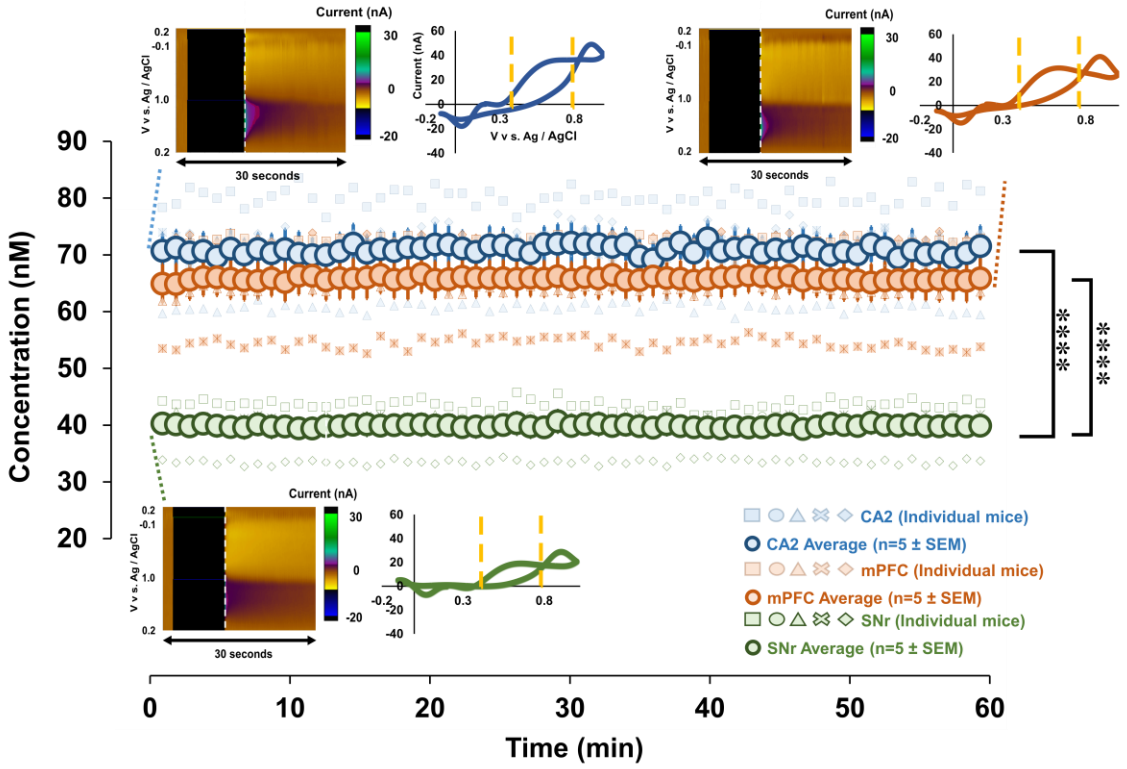

Figure 3.4. Ambient Serotonin Concentrations. Blue, orange and green circles represent the weighted averaged response (n=5 mice each region ± SEM), and faint blue, orange, and green markers represent individual mice responses. Files were collected for 60 mins to obtain a baseline reading. Representative FSCAV color plots and CVs (extracted from

vertical dashed lines) are inset, on top left for the CA2, top right for the mPFC, and at the bottom for SNr. Yellow lines on the CV denote the limits of integration. ****p<0.0001.

Using 5 mice for each region, the average ambient serotonin level in the CA2 is 72.82 ± 3.21 nM (n = 5 mice, weighted average ± standard error), the mPFC is 67.57 ± 3.42 nM (n = 5 mice, weighted average ± standard error), whilst the level in the SNr is 39.71 ± 1.96 nM (n = 5 mice, weighted average ± standard error). A pairwise t-test confirms statistically significant differences in the basal levels between the CA2 and SNr (p= 0.000012), and the mPFC and SNr (p= 0.000043). While the CA2 and mPFC are not statistically different from one another (p= 0.23). See the analysis reported earlier.

3.3.3 MATHEMATICAL MODELING OF EVOKED RELEASE

The ambient measurements support the idea that serotonin release in the SNr is reuptaken with a higher Uptake 1: Uptake 2 ratio than in the CA2 or mPFC. Here we analyze the experimental curves with previously established models and allow the model to generate an independent hypothesis to explain the experimental data. The model utilizes the Uptake 1, Uptake 2, autoreceptor, and two domain theories to determine the best parameters for fitting the experimental data presented here [21, 73]. Figure 3.5 shows the mean experimental curves for the CA2, mPFC and the SNr (solid are experimental and dotted are models).

This analysis gives us an opportunity to compare the three areas by comparing the models' parameters that were optimized to fit each curve. We allow ourselves to vary the strength of the input (R(t)), the strength of the autoreceptor effect (A(t)), and the strengths of Uptake 1 and Uptake 2 (α and β). And, to obtain the double hump in the mPFC, we allow diffusion from a region with only Uptake 1 to a region with both Uptake 1 and 2 (see

West *et. al.* 2018). The table in Figure 3.5 shows the qualitative differences in the parameters for different regions.

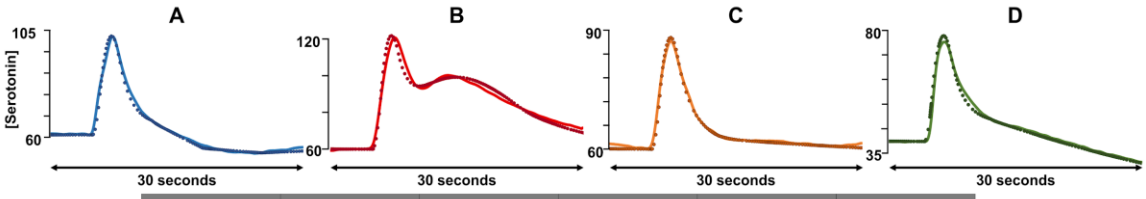

Region	Input	Uptake 1	Uptake 2	Autoreceptors	Diffusion
CA2	Moderate	Moderate	High	High	No
mPFC Layers 5-6	High	Moderate	Low	Low	Yes
mPFC Layers 1-3	Low	Moderate	Low	Low	No
SNr	Moderate	High	High	High	No

Figure 3.5. Comparison of Experimental Data with Model Predictions. The [Serotonin] vs. time plots display the experimental data (solid) and model curves (dotted) for each region: CA2 (A), mPFC layers 5-6 (B), mPFC layers 1-3 (C), and the SNr (D). The table below outlines the parameters used to generate the model curves for each region.

The results from the modeling are as follows:

(a) Diffusion is needed to explain the double humps seen in the PFC.

(b) There is higher contribution of Uptake 1 in the SNr than in the other regions.

(c) The autoreceptor effect is strong in the SNr and CA2 but weak in the mPFC.

(d) The input strength to regions of the mPFC is more variable than to the SNr and CA2.

The model's results bring forth 2 additional hypotheses, (b) and (d) that we are able to test below.

3.3.4 IMAGING AXONAL DENSITY IN THREE BRAIN REGIONS

To test the hypothesis brought forth by the model's 2nd result (higher contribution of Uptake 1 in SNr) we employ a single photon imaging approach, whereby axons are imaged in brain slices of adult serotonin transporter-EGFP BAC transgenic mice [79]. The imaging locations are chosen to correspond to the regions of our voltammetric measurements as ascertained with the histological analysis in Figure 3.3. Figure 3.6 shows

exemplar confocal images taken from the mPFC, CA2, and SNr from serotonin transporter-EGFP BAC transgenic mice.

To compare the degree of innervation between the regions, the percent pixels were calculated across the same number of focal planes for each region. The results, seen in Table 3.2, illustrate a higher degree of serotonin axon innervation in the SNr compared to the two regions (innervation depends on layer and sub-region of CA2 and mPFC).

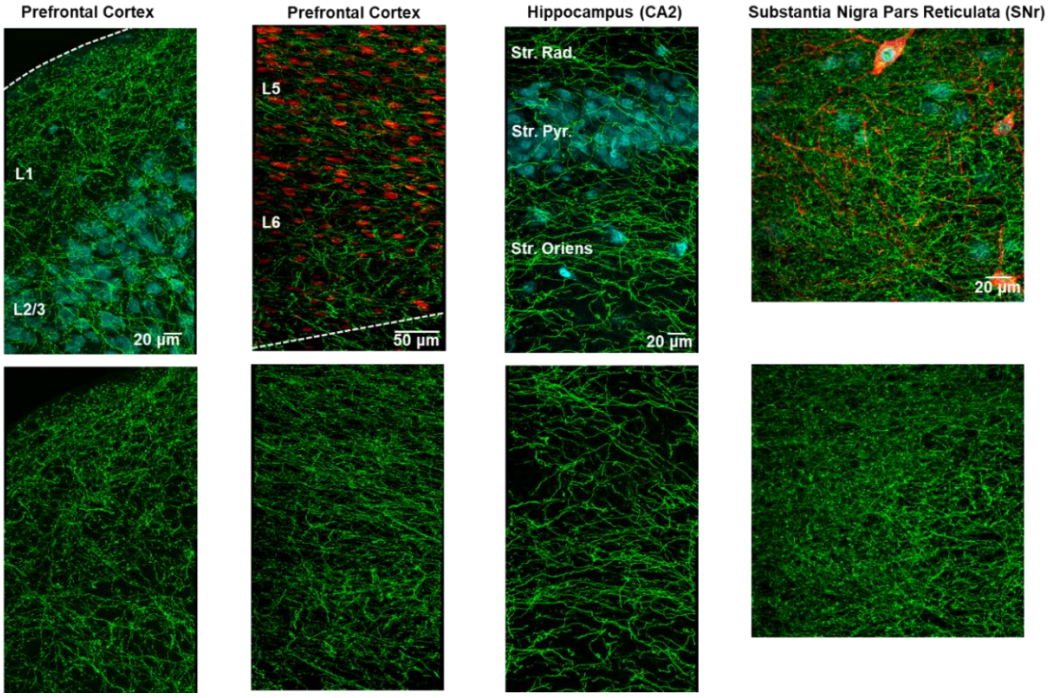

Figure 3.6. Immunohistochemical Staining. Immunohistochemistry for GFP in serotonin transporter-EGFP BAC transgenic mice reveals serotonin axon density across brain regions (n=1 mouse per region). Top panels: The SERT signal is shown in green with NeuN in cyan in all regions except the prefrontal cortex layer 5 and 6 where NeuN is shown in red. Layers 1-6 are all clearly defined in the prefrontal cortex and the stratum radiatum (Str. Rad.), stratum pyrimidale (Str. Pyr.), and the stratum oriens are labeled in the hippocampus. In the SNr, the red immunofluorescence is signal from an antibody directed against tyrosine hydroxylase, a marker of dopamine neurons. The top panels show single photon confocal micrographs of axonal innervation in the three brain areas. The bottom panels show the green channel alone to allow for the clear comparison of serotonin axon density.

Table 3.2. Serotonin Axon Innervation

Region	Sub-Region/ Layer	% Pixels
CA2	Oriens	16.3
	Pyramidale	10.6
	Radiatum	15.9
SN	Pars Reticulata	27.4
mPFC	L 1	19.7
	L 2/3	14.6
	L 5	17.4
	L 6	14.9

3.3.5 AXONAL REACTION TO ELECTRICAL STIMULATION

To test the hypothesis brought forth by the model's 4th result (input strength to mPFC is more variable than other two regions) we perform a stimulation parameter study. Figure 3.7 (top panel) shows the maximum evoked concentration of serotonin after systematic variation of stimulation conditions frequency, amplitude and pulse width. This data shows that the axons react in a similar manner to stimulation since increased terminal serotonin accompanies increased stimulation intensity, frequency and pulse width. It is only the mPFC response that does not substantially plateau during any of the stimulation paradigms, whereas the CA2 and SNr responses plateau during one or more of the experiments (CA2 and SNr during amplitude and SNr during frequency). The plateau of the curves are confirmed utilizing the first derivative of each point with respect to the previous one. In one or more of the parameter studies, the first derivative of the CA2 and SNr data fall below zero, indicating that the slope is plateauing. A depletion study where serotonin release is stimulated once a minute over a one-hour period is shown in Figure 3.7 (bottom panel). Here, when accounting for multiplicity, serotonin release in the CA2, but

in the SNr or mPFC, shows significant depleted over 20 stimulations (see Statistical Analysis section)

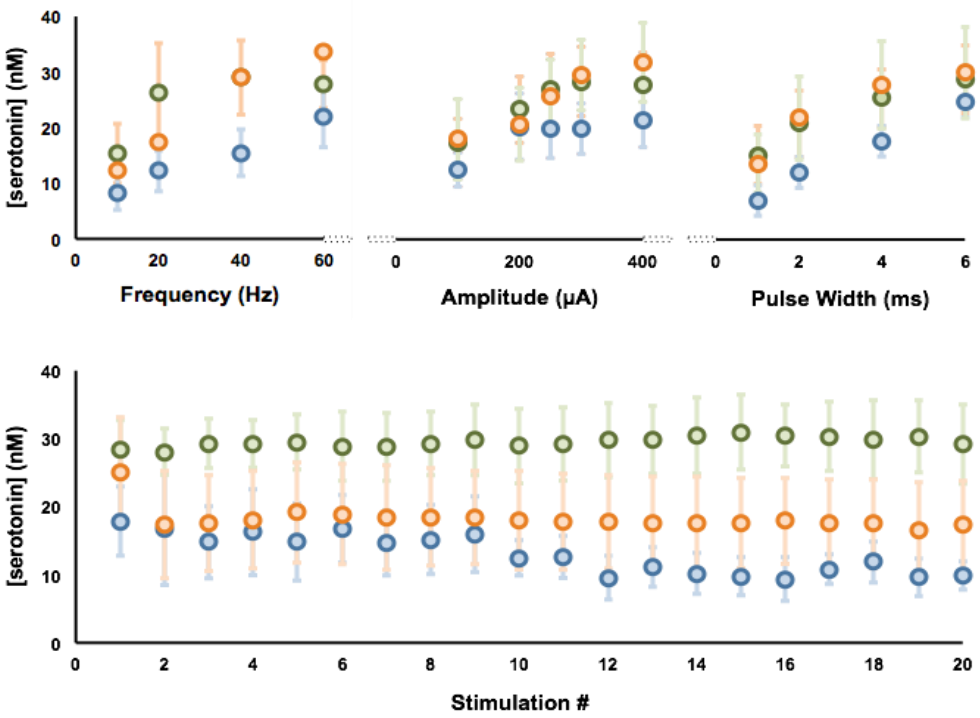

Figure 3.7. Serotonin Axon Innervation. Top Panel– Averaged serotonin responses (n=5, ± SEM), CA2 (blue), mPFC (orange) and in the SNr (green) with variation in the stimulation frequency (top left), stimulation amplitude (middle), and stimulation pulse width (top right). Bottom Panel – Average serotonin response (n=5, ±SEM) to a stimulation train for 20 mins at 60 Hz, 4 ms pulse width, and 360µA in the SNr (green), CA2 (blue), and mPFC (orange). (n=number of animals)

3.4 DISCUSSION

3.4.1 EXPANDING SEROTONIN VOLTAMMETRY BEYOND THE SNR

In vivo FSCV measurements are largely limited to dopamine. Serotonin is significantly more problematic to electroanalyze *in vivo* for two reasons. First, during the oxidative scan, serotonin and similarly structured metabolites form unstable intermediary species that rapidly restabilize by forming polymers [20]. Unfortunately, as this happens on

the electrode surface, serotonin films are created which poison the electrode. Second, extracellular serotonin levels are low, being subject to a thorough level of regulation, likely because of serotonin's well-established neurotoxic effects [80]. The former issue was largely resolved *ex vivo via* a combination of kinetic and physical modifications to the electrode and detection scheme [20, 23]. The latter challenge was addressed by targeting an *in vivo* brain region with the highest density of serotonergic innervation, the SNr [64], under the rationale that the extracellular serotonin levels in that region should be high. Paradoxically, for reasons described below, we now know that extracellular serotonin levels in the SNr are not as high as in the other regions we studied.

Recent interest in serotonin dynamics is largely for its roles in affective, cognitive and developmental disorders [6, 56-59]. To investigate these diseases, brain regions other than the SNr are thought to play important roles. For example, the hippocampus is heavily implicated in emotion and memory, and as such is often the focus of depression studies [65]. Similarly, the amygdala, nucleus accumbens, and hypothalamus are investigated for their roles in depression and anxiety [67, 81]. The prefrontal cortex plays a role in controlling cognition, motor function, affective and social behaviors [25]. The region also has a prolonged development period which means particular susceptibility to influence from exposure to environmental risk factors [82]. As such, the PFC is often associated with and considered in the study of developmental disorders. General and our own interest in these regions shifted our efforts towards serotonin FSCV measurements in the CA2 region of the hippocampus and the mPFC.

It is not trivial to simply apply our current FSCV approach to serotonin measurements in new brain regions. This is primarily because of interference from other

transmitters, metabolites and ions, and the heterogeneity of serotonin release sites within each region. Nonetheless, we optimized stereotaxic coordinates that yield serotonin FSCV signals in the CA2 region of the hippocampus, the mPFC and the SNr, in separate animals, through electrical stimulation of a common MFB site. Figure 3.2 shows 3 representative color plots and corresponding CVs for signals obtained in these regions. It is important to mention that the examples we choose in this figure are highly representative of the signals we obtain in each region. The color plots and CVs are different in these regions, with unique additional features, speak to the different interferences and microenvironment around the CFM. One such unique feature is the 'switching' peaks of each region that occur when analytes adsorb to the electrode surface and change the capacitative current that occurs as a function of the electrical bilayer on the electrode surface. This capacitative or charging current is normally subtracted out, however when analytes adsorb and change the current, a signal is manifested at the positive and negative switching potentials. It is not easily possible to identify which analytes are responsible for the switching peaks, but the switching peaks are different in region depending on the microenvironment. The characteristic serotonin oxidation peak is at around 0.7 V and we use this to quantify serotonin. Upon initial inspection of the CV, this peak can occasionally be difficult to observe due to the large switching peaks. However, upon closer inspection, including subtracting out the large switching peaks, the characteristic serotonin oxidation peak is observed.

The mPFC is an intrinsically unique brain region in the context of evoked serotonin responses where two types of signals are routinely observed. In contrast to the CA2 and SNr where a single serotonin release and uptake event is evoked upon stimulation, in the

mPFC we often also observe a dual peak. We recently characterized mPFC responses and showed that the dual response was due to stimulation of two distinct axonal bundles that traverse the MFB with diffusion to the electrode surface resulting in the two distinct peaks. Each domain was also found to have a specific reuptake mechanisms (Uptake 1 or Uptake 2) which was verified pharmacologically using escitalopram [73].

These data thus confirm serotonin release in three regions *via* stimulation of the same MFB coordinate. This common stimulation site is significant because it will enable future, simultaneous measurements of serotonin in multiple brain localities in one animal.

We perceive that the most striking feature of these responses is the difference in reuptake profiles. To better provide a visual comparison, in Figure 3.8, these responses are normalized such that the maximum amplitude in each case is at the level of the horizontal blue dotted line. In Wood *et al*. 2012, we modeled the uptake of serotonin in the SNr *via* two mechanisms, Uptake 1 and 2, first coined by Sol Snyder in the 1970s [37]. Uptake 1 is reuptake by the serotonin transporters (SERTs) at high affinity and low efficiency. We observe the Uptake 1 mechanism as a single, slow decay curve (approx. 12-15 seconds). Uptake 2 transpires due to the activity of non-serotonin (non-SERT) transporters, that uptake serotonin with high efficiency, but with low capacity. Uptake 2 generates a decay curve with a single slope that reaches baseline quickly (around 5 seconds). When there is a combination of SERTs and non-SERTs, the result is a hybrid signal, with a curve that decays quickly for a few seconds, followed by a slow decay until it reaches baseline, resulting in decay with two different slopes [21].

While the latter portions of the reuptake curves appear to be the most different between the curves, important information is garnered by comparing the entirety of the

reuptake profiles. Serotonin release in the CA2 appears primarily mediated by Uptake 2. The mPFC serotonin responses, as we previously characterized [73], involve clearance by both Uptake 1 and 2 transporters, which are linked inextricably to the two release domains. Serotonin released in the first domain, observed as a single peak, is reuptaken by Uptake 2 mechanisms, while serotonin in the second domain is solely reuptaken by Uptake 1 processes. Domain 2 is only readily observed when measurements occur in layers 5-6 of the mPFC. In the SNr, serotonin seems to be reuptaken *via* a hybrid of Uptake 1 and

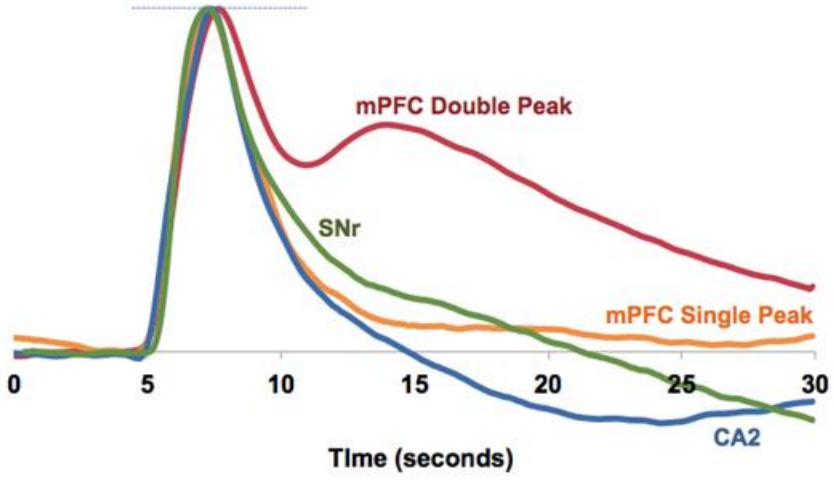

Figure 3.8. Comparison of Reuptake Curves. The averages from each region have been normalized such that the maximum amplitude of each curve is at the horizontal blue dotted line. This allows for simple visual comparison of the reuptake curves.

This data lead us to formulate a hypothesis that the chemical decay profile after stimulation offered by the CFM is indicative of the ratio of SERT (Uptake 1) : non-SERT (Uptake 2) mediated serotonin reuptake. It follows that serotonin in the SNr and mPFC is more subject to Uptake 1 than serotonin in the CA2. It is important to note that in the mPFC, we measure as many single evoked events mediated by Uptake 2 (exclusively in

layers 1-3) as we do double events (layers 5-6) incorporating both Uptake 1 and 2 [73]. For this reason, we narrow down our postulate to serotonin in the SNr being cleared by a higher Uptake 1 : Uptake 2 ratio when compared to the other two regions.

To strengthen this hypothesis, we perform ambient serotonin measurements with FSCAV in the three brain areas, shown in Figure 3.4. In this study we find that extracellular serotonin levels in the SNr are significantly lower than in the other two regions. This finding is in contrast to our early rationale, that because the SNr is highly innervated by serotonin fibers and this region contains a high tissue content of serotonin, that the SNr should contain a higher extracellular serotonin concentration.

We believe this low SNr basal level can also be explained by a higher ratio of SERT mediated reuptake in the SNr. At rest, ambient serotonin levels are primarily controlled by SERTs that are located, at high density, in the synaptic area [83]. However, because serotonin communication is characterized by volume transmission, this modulator can escape the synapse where it is more likely cleared by Uptake 2 mechanisms. Our electrical MFB stimulation is intense, with a high frequency and as such causes an atypically heavy efflux of serotonin, large enough to significantly escape the synapse. Thus, we observe Uptake 2 once the extracellular serotonin concentration is high enough to overcome a specific threshold. The stimulation allows us to test the local physiology of serotonin reuptake, yet the ambient level is more indicative of local SERT density (higher SERT density = lower extracellular serotonin).

This finding further supports our hypothesis that the SNr serotonin is reuptaken by a higher Uptake 1 : Uptake 2 ratio. To corroborate the rationale, we next turned to computational models to analyze the experimental data.

3.4.2 MATHEMATICAL MODELING SUGGESTS PHYSIOLOGICAL DIFFERENCES AROUND CFM

We bring forth the idea that serotonin release in the SNr is reuptaken with a higher Uptake 1: Uptake 2 ratio than in the CA2 or mPFC (*vide supra*). Here we use previously established models to model experiment data and generate independent hypotheses (Figure 3.5). As a reminder, the conclusions from the modeling are:

(a) Diffusion is needed to explain the double humps seen in the PFC.

(b) There is a higher contribution of Uptake 1 in the SNr than in the other regions.

(c) The autoreceptor effect is strong in the SNr and CA2 but weak in the mPFC.

(d) The input strength to regions of the PFC is more variable than to the SNr and CA2.

Result (a) has already been validated and discussed in detail in prior work [73]. Conclusion (b) is in line with hypotheses brought forth from experimental data. The model has additionally suggested two more ideas in conclusions (c) and (d). We next further verify the Uptake 1 : Uptake ratio 2 hypothesis and address these two novel concepts.

3.4.3 VERIFICATION OF MODEL HYPOTHESES

The data and modeling thus far are highly interesting in that they imply that the voltammetric signal can provide information about local tissue physiology and the voltammetric circuitry. According to our model, the SNr evoked serotonin is subject to a higher ratio of Uptake 1 vs. Uptake 2. It is not possible to say for certain, because the model reports a ratio, but this finding implies a higher density of SERTs in the SNr compared to the other regions. To address SERT density in each region, we first turned to the literature but were unable to find a single study that utilized a common technique to compare SERTs in the specific areas of all three regions we are interested in. Thus we employ a single

photon imaging approach, whereby axons are imaged in brain slices of adult serotonin transporter-EGFP BAC transgenic mice [79]. It is well established that axonal innervation corresponds to SERT density [68]. Images of axons and subsequent quantification of density (Figure 3.6 and Table 3.1) illustrate a higher degree of serotonin axon innervation in the SNr compared to the two regions (innervation depends on layer and sub-region of CA2 and mPFC). This is consistent with our model's hypothesis of higher ratio of Uptake 1 to 2 serotonin reuptake in the SNr. Thus these images provide support for the experimental and model Uptake 1 : Uptake 2 hypothesis.

We next explore an additional postulation offered by the model, that the excitation input to the mPFC is more variable than to the other two regions. While serotonin is elicited in all three regions *via* the common MFB stimulation, this does not mean that the stimulation location is optimal for evoking maximal serotonin in all regions. If the stimulation location is optimal for eliciting maximal serotonin in all areas, systematically increasing the stimulation intensity, frequency and width should provide three serotonin profiles that plateau with the same characteristic. Thus, we perform experiments in 5 separate mice in each region whereby electrical stimulation frequency, amplitude and pulse width are systematically altered. The standard stimulation utilized in our FSCV experiments is 120 pulses at 60Hz and 360 μA, so the parameters are varied around this range Figure 3.7 (top panel). The results from the stimulation paradigm study show that while the axons react in a similar manner to stimulation, the mPFC response does not plateau during any of the stimulation trains, whereas the CA2 and SNr responses clearly plateau during one or more of the experiments. This experiment shows that the stimulation location is less optimal for evoking maximal serotonin release in the mPFC, in accord with

the model's postulate that the excitation input to the mPFC is more variable than to the other two regions.

An interesting side note is that a key difference between regions is observed during a depletion study where serotonin release is stimulated once a minute over a one-hour period in Figure 3.7 (bottom panel). Here, only CA2 serotonin release are significantly depleted over 20 stimulations while the SNr shows no depletion. A simplistic explanation for this difference is the tissue content differences between these regions, of which SNr contains much higher serotonin levels than the other regions (21.0 ± 1.6 ng/mg in the SNr vs. 0.98 ± 0.13 ng/mg in the hippocampus and 0.81 ± 0.065 ng/mg in the frontal cortex) [37, 84]. While it is worth noting that none of these experiments demonstrate the profound depletion that occurs in similar depletion studies with dopamine, this was previously attributed to the high cytosolic serotonin compared to the low amount released during each stimulation [39].

Thus, independently, two of the model's hypotheses are verified, again providing context that the chemical signals at the CFMs provide important information about localities and circuits. Another aspect of the model is to hypothesize that serotonin in the CA2 is more strongly autoregulated in comparison to the other two locals. It would be extremely challenging to independently verify this notion due to the large scope of serotonin autoreceptors and autoreceptor sub-types, and these autoreceptors' ability to synergize. However, the chemical signal and modeling that allude to autoreceptor control provide direction for future interest in autoreceptor mediated serotonin regulation.

In sum, serotonin neurochemistry is important to study in the context of many brain disorders. FSCV and FSCAV are important tools to probe *in vivo* serotonin chemistry. In

this paper, we compared two new voltammetric serotonin stimulation - measurement circuitries, in the CA2 region of the hippocampus and the mPFC, to well established SNr measurements. A common MFB stimulation evoked serotonin in all three brain localities where evoked and ambient serotonin were measured at the same electrode. We found differences in the serotonin chemistry between these three regions that we postulated to arise from differences in tissue physiology local to the CFM. By taking mathematical and imaging approaches, we validated this hypothesis. We therefore highlight the strength of fast voltammetric tools for providing physiological information that has implications for circuit mapping. A map of the circuits within specific brain regions ultimately allows for improved drug targeting for disease treatment.

CHAPTER 4:

FAST VOLTAMMETRY OF SEROTONIN REVEALS SIMILARITIES ACROSS GENETIC MODELS OF AUTISM SPECTRUM DISORDER

4.1 INTRODUCTION

Autism spectrum disorder (ASD) is a developmental disorder affecting 1 in 68 children in the United States[8]. This behavioral disorder can present with a large variety of symptoms, though 3 core common behaviors define it: communication deficits, repetitive behaviors and social abnormalities. The severity in which these symptoms present also varies widely, resulting in the spectrum upon which children are diagnosed. Some of these symptoms can be managed with behavioral therapy and medication, while others are often quite debilitating, all leading to a high cost of care for patients and their families[85]. The growing prevalence and high cost of care has resulted in a vast amount of research into the cause and treatment of the disorder, identifying genetic and environmental risk factors as having a significant role[9, 86].

Genetic studies, particularly sibling and twin studies[87], have revealed that ASD may rest on a genetic foundation since over 1000 genes have been linked to the disorder[10]. To better understand the pathophysiology of ASD, we must focus on the known causes which can be used to generate animal models of the disorder. ASD animal models are traditionally assessed on behavioral phenotypes which are characteristic of the disorder in humans. Difficulty in replicating human behaviors in mice can result in inconsistencies in behavioral scoring and interpretation between labs, potentially discounting the validity of some genetic models. This issues with model assessment would be alleviated if a common biomarker could be identified.

In humans, high blood serotonin is arguably the most reproduceable biomarker, with 1 in 3 patients presenting with this phenotype[14]. Despite not all patients having hyperserotonemia, this high prevalence still warrants further examination; specifically,

investigation of serotonin in the brain. Serotonin plays many important roles as a neurotransmitter and is thought to be implicated in the behavioral phenotypes of ASD[6, 88]. Since serotonin cannot cross the blood brain barrier, the levels between the peripheral and central nervous system are not easily correlated and studying brain serotonin is further complicated by the fragile nature of the brain.

Serotonin has been studied in the brain using a variety of techniques; however, to understand the functionality of the circuit and the processes that play a role in serotonin regulation, we need to utilize a technique capable of detecting serotonin in in-tact tissue in real-time. Fast-scan cyclic voltammetry (FSCV) is an ideal technique for this task as it is capable of recording the stimulated release and reuptake of serotonin *in vivo*. Recently, FSCV was used to characterize serotonin chemistry in the prefrontal cortex[73], a region commonly associated with morphological changes in ASD patients and therefore an ideal place to begin investigations[24].

We begin our studies by looking at a model with a confirmed serotonin alteration, the SERT-Ala56 mouse. This model has been designed to present the high blood serotonin seen in 1/3rd of ASD patients[89]. It provides the unique opportunity to correlate serotonin brain chemistry with that of the peripheral nervous system. The genetic variation resulting in the SERT-Ala56 model has been observed in ASD patients and when this genetic alteration is present in mice[14], it results in all three of the characteristic autism like behaviors[89].

A secondary model with no direct link to serotonin is used to determine if altered serotonin neurochemistry persists across multiple, diverse ASD models. This second model contains an alteration to the Shank3 gene and displays two of the three ASD typical

behaviors[90]. The Shank3 gene is scored with a high association through Simons Foundation Autism Research Initiative (SFARI), meaning the evidence linking this gene to ASD is strong. It is also a syndromic model offering the opportunity to study a genetic model linked to a disorder which can occur comorbidly with ASD. The Shank3 gene encodes the protein which creates the scaffolding between glutamatergic neurons[91, 92]. While this does not directly affect serotonin neurons, the excitatory nature of glutamate could lead to downstream effects on other neurotransmitters.

Evaluating the serotonin chemistry in the brains of two distinct genetic models of ASD will allow us to determine if there are any underlying commonalities in the pathophysiology.

4.2 METHODS

4.2.1 BREEDING AND GENOTYPING

The Guide for the Care and Use of Laboratory Animals, as accepted by the Institutional Animal Care and Use Committees of the University of South Carolina (Institution Approval # A3049-01), was followed in all animal care and procedures. C57BL/6J (RRID: IMSR_JAX:000664) mice, and B6(Cg)-Shank3$^{tm1.2Bux/J}$ (RRID: IMSR_JAX:017890) were procured from Jackson Laboratories (Bar Harbor, ME). SERT-Ala56 mice were transferred from Dr. Randy Blakely at Florida Atlantic University. Mice were offered food and water ad libitum and housed in 12 hours light/dark cycles. Male and female mice were paired for breeding at 8 weeks old. Heterozygous- heterozygous pairings were used for SERT- Ala56 breeding and heterozygous-wildtype pairings were used for Shank3 breeding. Pups were weened at 21 days and a tail-snip obtained. The SERT-Ala56 mice were genotyped utilizing Transnetyx services. The Shank3 mice were genotyped

using PCR with REDTaq ReadyMix (Sigma Aldrich), and following previously established genotyping protocol by the Jackson Laboratory.

When the mice reached 7-12 weeks old, they underwent stereotaxic surgery and FSCV was used to evaluate their serotonin neurochemistry.

4.2.2 CARBON-FIBER MICROELECTRODES

Carbon fiber microelectrodes (CFMs) were generated in-house by aspiration of a single T-650 carbon fiber (7 μm, Goodfellow, Coraopolis, PA) through a cylindrical glass capillary (internal diameter: 0.4 mm, external diameter: 0.6 mm, Product # 624500, A-M Systems, Carlsborg, WA). A carbon – glass seal was made using a vertical pipette puller (Narishige Group, Setagaya-Ku, Tokyo, Japan). The protruding carbon fiber was cut to 150 μm in length. A cation exchange polymer, Nafion (LQ-1105-US-25, 5% by weight Nafion, Ion Power, DE), was then electrodeposited onto the carbon fiber as previously described[23].

4.2.3 SURGERY AND FSCV

A urethane solution (25% (w/v)) was made by dissolving urethane (Product # U2500, Sigma Aldrich Co., St. Louis, MO, USA) in sterile saline (0.9% NaCl solution, NDC 0409-4888-20, Hospira, Lake Forest, IL). When the mice were 7 to 12 weeks old they received an *intraperitoneally* (*i.p.*) injection of urethane solution at a volume of 7 μL per 1 g mouse weight. Once fully under the effects of the anesthesia, they underwent stereotaxic surgeries (Model 962, David Kopf Instruments, Tujunga, CA) during the light cycle. A heating pad from Braintree Scientific was used for maintaining the ideal mouse body temperature of 37° C. The stereotaxic coordinates for the MFB [AP: -1.58, ML: +1.0, DV: -4.8 to -5.0] and mPFC [AP: +1.7, ML: +0.2, DV: -2.0 to -3.0] were marked according to Franklin and Paxinos (2008), using bregma was used as a reference. Holes were drilled

at the marked stereotaxic coordinates, with an additional hole drilled in the contralateral hemisphere for the reference electrode. A pseudo Ag/AgCl reference electrode was used, made of a silver wire (diameter: 0.010 in, 787000; A-M Systems, Sequim, WA) electroplated with chloride through immersion in hydrochloric acid for 30 seconds (0.1 M, 4 V vs. tungsten). A stainless-steel stimulation electrode (diameter 0.2 mm, MS303/2-A/SPC; Plastics One, Roanoke, VA) was lowered into the MFB, and the Nafion-coated CFM was lowered into the mPFC.

FSCV was performed through instrumentation and software (WCCV 3.06) developed by Knowmad Technologies LLC (Tucson, AZ). A serotonin selective waveform, known as the "Jackson" waveform [20], was applied to the CFM. A 30 second file was collected every 10 minutes; five seconds into the file, a stimulation was applied (60 Hz biphasic 360 μA, 120 pulse stimulation, 2 ms per phase) using a linear constant current stimulus isolator (NL800A Neurolog; Digitimer Ltd.). Signals were processed using signal deconvolution, filtering, and smoothing in custom software using LabVIEW 2009.

4.2.4 DATA ANALYSIS

Signals were analyzed to compare the maximum amplitude and $t_{1/2}$. The maximum amplitude was taken as the highest concentration of serotonin elicited following the stimulation. These values were compared using a one-way t-test. The $t_{1/2}$ was calculated using the curve fitting tool with a custom equation for plotting exponential decay in MatLab R2018B, the natural log of 2 was divided by the mean lifetime yielded to calculate $t_{1/2}$. One-way t-test were used to test for statistical significance. Statistical significance was defined as a $p<0.05$.

4.2.5 EXCLUSION CRITERIA

For all FSCV experiments, the CV of the evoked signal was compared to well-established serotonin cyclic voltammograms (CVs) *in vivo* and *in vitro* and signals which lacked the characteristic serotonin redox peaks were excluded. Signals which contained a peak resulting from the stimulation electrode touching the skull that masked, delayed, or minimized the serotonin response (stimulation glitch) were excluded. Electrodes that displayed instability during file collection were also excluded.

4.2.6 HISTOLOGY

To confirm the placement of the CFM in the targeted region *in vivo*, a small lesion was created at the end of the FSCV experiment by applying a constant potential at the CFM (~10 V for 1 min). The mice were then euthanized *via* cervical dislocation followed by decapitation, and the brain was removed from the skull and stored in 4% paraformaldehyde in PBS solution. The brain was transferred into a 30% sucrose solution prior to sectioning. Once the brain was saturated with the medium, it was then flash-frozen, sectioned into 30 μm slices, mounted onto frosted glass slides, and the slices were then photographed with an optical microscope. Lesions were confirmed to be in the targeted regions.

4.3 RESULTS AND DISCUSSION

The SERT-Ala56 mice appear to display differences in serotonin transmission in comparison to control animals. In SERT-Ala56 mice, evoked serotonin release has a lower maximum amplitude and is taken up at a faster rate than in control animals. This effect can be observed in Figure 4.1 where the average evoked serotonin release of the SERT-Ala56 mice has been plotted along with an average control response. The peak concentration of serotonin released following stimulation (Max_A) and the time it takes to decay to half of

this amplitude ($t_{½}$) was calculated for each animal's serotonin response, as described above. These results are tallied in Table 4.1 along with the p-value outcomes of the t-test preformed to compare each measure.

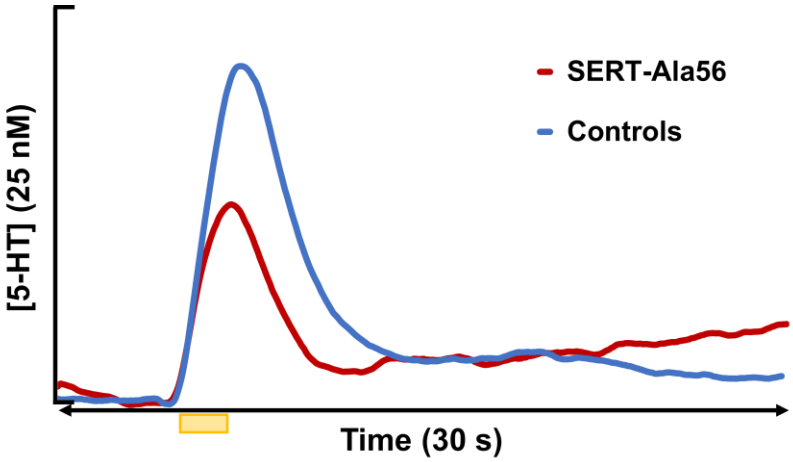

Figure 4.1. Evoked Release of SERT-Ala56 vs Control Mice. The evoked serotonin release (stimulation is noted by the yellow box) from SERT-Ala56 mice and Control mice have each been averaged and are compared here.

Table 4.1. $T_{1/2}$ and Maximum Release of SERT-Ala56 vs Mice.

Identification	**$T_{1/2}$ (s)**	**Max_A (nM)**
Knock-In 1	1.206	17.45
Knock-In 2	1.895	9.37
Knock-In 3	0.866	9.86
Knock-In 4	1.036	14.36
Control 1	1.560	17.49
Control 2	1.853	17.16
Control 3	2.067	26.52
Control 4	2.178	25.99
T-Test	**p=0.0870**	**p=0.0155**

The faster reuptake and decreased amplitude found in these animals are both supported by previous data presented by Blakely and colleagues[89]. The significantly decreased amplitude observed in the SERT-Ala56 mice can be explained *via* two possible hypotheses. Blakely and colleagues demonstrated that these mice have overactive SERTs

which caused the animals to exhibit a faster rate of serotonin clearance[89]. These overactive transporters may potentially explain the decreased amplitude observed since the SERTs will restrict the amount of serotonin detected following stimulated release. This phenomenon has been observed previously in tissue slice preparations and Wightman et al. postulated it was a result of the uptake of serotonin occurring between the time of the stimulation pulses, restricting the summation of extracellular serotonin[93]. The second explanation for the decreased amplitude is hypersensitive autoreceptors. Autoreceptors are inhibitory receptors that when bound to serotonin provide negative feedback to inhibit the release of serotonin. Veenstra-VanderWeele *et al.* demonstrated that the SERT-Ala56 genetic model displays increased autoreceptor activity, specifically naming the 5-HT_{1A} and 5-HT_{2A} receptors[14, 89]. The two explanations posited here may be at work, a theory further supported by the fact that 5-HT_{1B} autoreceptors have been shown to modulate SERT[94].

The change in $t_{1/2}$ observed was not statistically significant though an increased rate of serotonin clearance was also previously shown by Veenstra VanderWeele et al. using chronoamperometry[89]. Interestingly, previous models of FSCV serotonin dynamics indicate that the reuptake of a single peak in the prefrontal cortex is primarily mediated by other monoamine transporters such as dopamine transporters (DATs), norepinephrine transporters (NETs), and the organic cation transporters (OCTs)[73]. These transporters do not have a high affinity for serotonin but very efficiently reuptake serotonin. However, if the SERTs are significantly overactive they may still contribute to the increased clearance observed here.

The serotonin neurotransmission of Shank3 mice was compared to control animals and demonstrated unique features. Figure 4.2 displays the plot of the average evoked

serotonin release of the Shank3 mice over time along with an average control response. To evaluate the differences between the two cohorts, the peak concentration of serotonin released following stimulation (Max_A) and the time it takes to decay to half of this amplitude ($t_{½}$) was calculated for each animal's serotonin response, as described above. These results are tallied in Table 4.2 along with the p-values associated with the t-test preformed to compare each measure. Though no differences are found in the maximum evoked concentration of serotonin, the Shank3 mice do display a significantly faster reuptake.

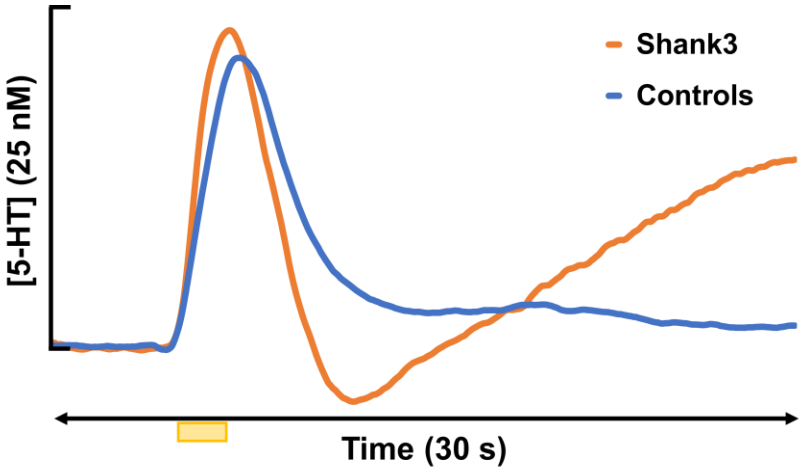

Figure 4.2. Evoked Release of Shank3 vs Control Mice. The evoked serotonin release (stimulation is noted by the yellow box) from Shank3 mice and Control mice have each been averaged and are compared here.

Table 4.2. $T_{1/2}$ and Maximum Release of Shank3 vs Control Mice.

Identification	**$T_{1/2}$ (s)**	**Max_A (nM)**
Heterozygous 1	1.373	29.55
Heterozygous 2	1.892	21.14
Heterozygous 3	0.8328	17.44
Heterozygous 4	1.406	31.50
Control 1	1.560	17.49
Control 2	1.853	17.16
Control 3	2.067	26.52
Control 4	2.178	25.99
T-Test	**p=0.0399**	**p=0.245**

The statistically faster reuptake displayed by the Shank3 mice indicates that the one or more of the DATs, NETs, OCTs, and SERTs are more active than in the control animals. There is no direct association between the genetic modification of Shank3 and these transporters and thus indirect explanations must be considered. There is limited information on the neurochemical changes present in this genetic modification to rationalize changes to other neurotransmitter transporters. The original study of this model found that these mice display lower amplitude but higher frequency post-synaptic excitatory currents and have fewer AMPA receptors. Though the amplitude is lower, the higher frequency excitatory currents may result in more frequent glutamate firing[90]. As the primary excitatory neurotransmitter, glutamate would potentiate the release of other neurotransmitters including serotonin, norepinephrine, and dopamine. In turn, the higher frequency release could cause upregulation in DATs, NETs, OCTs, and SERTs to maintain the homeostasis of these neurotransmitters. While quantification of AMPA receptors has been previously determined, it was not determined that NMDA and mGluR receptors are not upregulated as a compensatory mechanism. If more of these receptors were present, they could also lead to an increase in release of dopamine, norepinephrine, and serotonin. While these theories cannot yet be confirmed, it is reasonable to state that the excitatory and inhibitory balance of neurotransmission is disrupted in the Shank3 mice due to alterations in glutamate transmission. This disruption has indirectly resulted in an increased reuptake rate of serotonin.

A faster rate of serotonin reuptake is observed in both of these ASD models (Shank3 mice and SERT-Ala56) compared to control mice. This reuptake is primarily indicative of the non-SERTs including DATs, NETs, and OCTs[73]. In both genetic models,

it seems that these transporters more efficiently reuptake serotonin. Theories for this increased efficiency have been offered for both models, though they cannot be confirmed at this time. However, the faster reuptake of serotonin observed in the models provides an explanation for why selective serotonin reuptake inhibitors (SSRIs) are often prescribed as treatments for ASD and can be successful[95]. SSRIs work by blocking the reuptake of serotonin, and while these drugs are designed to have the highest affinity for SERT, many also display affinities for other monoamine transporters.

To investigate the functionality of SERTs in these models, we must next analyze the bi-phasic peaks often found in the prefrontal cortex and detailed in previous work[73]. This analysis will be the focus of future work and requires mathematical modeling for interpretation to distinguish between reuptake and diffusion components of the second peak.

CHAPTER 5:

BEHAVIORAL AND VOLTAMMETRIC ANALYSIS OF PERINATAL LEAD EXPOSURE AS A MODEL OF AUTISM SPECTRUM DISORDER

5.1 INTRODUCTION

Knowledge of the detrimental health effects of lead (Pb^{2+}) can be traced back to the 2nd century B.C. and as our scientific tools have improved, the list of symptoms resulting from lead poisoning has grown[96]. While Pb^{2+} is harmful to the peripheral nervous system, the central nervous system is especially sensitive to Pb^{2+} since this small cation readily crosses the blood brain barrier (BBB) and is similar in structure and size to other small metal ions that are essential to brain function[96, 97]. The damage caused by Pb^{2+} in the brain is extensive and includes oxidative stress, mitochondrial dysfunction, neuroinflammation, protein turnover dysregulation, decreased cellular energy metabolism, lipid peroxidation, abnormal neurotrophic factor expression, and altered gene transcription[97-99]. Many of these issues are a direct result of Pb^{2+}'s ability to mimic and compete with calcium (II) (Ca^{2+})[100]. This phenomenon also means that Pb^{2+} directly affects neuronal signaling with some studies reporting enhanced transient neurotransmission and inhibited stimulated release[101].

Over the last century it has been acknowledged that children are far more susceptible to lead poisoning than adults and that these effects persist across the lifespan. A number of factors contribute to this susceptibility including that children's digestive systems more readily absorb Pb^{2+} and the developing brain is far more vulnerable[102]. Likewise, there is extreme concern of the exposure of pregnant and lactating women to Pb^{2+} as it can cross to the fetus and child through the placenta and milk ducts[103, 104]. In children exposed to Pb^{2+} during development, a myriad of symptoms have been reported to last long after exposure including cognitive, attention, and behavioral impairments[105]. These have been replicated in animal studies of lead exposure *in utero* which found that mice exposed to millimolar concentrations of Pb^{2+} from pregnancy up to weaning resulted

in learning and memory impairments[106]. Thus, early life and gestational Pb^{2+} exposure is highly implicated as a risk factor for developmental disorders.

The large body of literature characterizing the many harmful effects of Pb^{2+} exposure, as well as the progressive reduction in the exposure levels being tested has caused the World Health Organization (WHO) to acknowledge that there is no safe level of lead exposure. Humans are exposed to Pb^{2+} from a variety of sources, including paint, leaded gasoline, cosmetics, fruit juices, and drinking water. The inclusion of Pb^{2+} in paint and gasoline has been banned in most countries, reducing the likelihood of exposure *via* those sources. As for cosmetics, fruit juices, and drinking water, regulatory agencies in the US have placed limits of 10 ppm, 50 ppb, and 15 ppb, respectively. Unfortunately, these standards are not always upheld, exposing populations to dangerous levels of Pb^{2+}, often times without their knowledge. These were exactly the circumstances in the highly publicized cases of D.C and Flint, Michigan when local populations were exposed to extremely high levels of Pb^{2+} for months and in some cases years before the problem was addressed[107, 108]. While these events highlight the dangers of chronic exposure to high levels of Pb^{2+}, they also beg the question, is the standard itself safe. The EPA acknowledges that the maximum contaminant level goal (MCLG) for Pb^{2+} is zero, yet based mostly on cost, the maximum contaminant level (MCL) is actually 15 ppb[109].

Pb^{2+} has been shown to induce inflammation in the peripheral and central nervous system. Acute exposure studies have found that Pb^{2+} accumulates in microglial cells and can cause astrocyte activation, while this ion can promote chronic glial cell activation with coexisting inflammatory and neurodegenerative features. Perinatal $^{Pb2+}$ exposure studies in mice have revealed DNA methylation and gene expression alterations. Some of these genes

include those that play a role in immune system function and brain development. This could explain why studies have previously found impaired synapse formation and altered synaptic plasticity. In conjunction with these gene effects, vesicular release was also inhibited. It is thought that $Pb2^{+}$ exposure disrupts excitatory and inhibitory (E/I) balance of neurotransmission due to action on GABA and glutamate, the primary inhibitory and excitatory neuromodulators, respectively.

It remains to be seen what the exact effects of these many changes have on a molecule such as serotonin. As a neurotransmitter, serotonin will likely be disrupted by the inhibition of vesicular release. However, serotonin will also be affected by the changes in brain development as it also plays a role in this process[16]. Serotonin is also susceptible to regulation *via* inflammatory response[110]. Finally, serotonin is involved in learning and memory, which have been documented to be disrupted following Pb^{2+} exposure[25, 96]. The behavioral disruptions observed with Pb^{2+} exposure during development have given rise to the theory that Pb^{2+} may be a risk factor for autism spectrum disorder[12, 111]. Research so far has focused on Pb^{2+} exposure concentrations much higher than we explore in this paper[98, 99, 112]. While the underlying pathophysiology of ASD is not fully understood, research strongly implicates alterations in brain serotonin, therefore we are interested in assessing the effects of Pb^{2+} on the serotonin system.

In this paper, we determine the effects of acute and chronic Pb^{2+} exposure, at the EPA (Environmental Protection Agency) drinking water limit, on *in vivo* serotonin transmission. Specifically, we ask whether low level Pb^{2+} exposure during pregnancy and lactation can contribute to an increased risk of ASD in mouse models.

5.2 MATERIALS AND METHODS

5.2.1 STUDY DESIGN

The Guide for the Care and Use of Laboratory Animals, as accepted by the Institutional Animal Care and Use Committees of the University of South Carolina (Institution Approval # A3049-01), was followed in all animal care and procedures. C57BL/6J (RRID: IMSR_JAX:000664) mice, 6 weeks old were procured from Jackson Laboratories (Bar Harbor, ME). Mice were offered food and water ad libitum and housed in 12 hours light/dark cycles. Three separate paradigms were followed for acute, chronic, and perinatal exposures, the methods of which are as follows. For the acute exposure, mice between the ages of 7-9 weeks old underwent stereotaxic surgery and FSCV was used to evaluate their serotonin neurochemistry, control files were collected, and they were administered a bolus dose of 15 ppb lead acetate solution in saline (5 ml/kg). For the chronic exposure, 6-8 week old mice were exposed to either drinking water from animal facilities, which goes through a reverse osmosis filter, or the same water with 15 ppb lead acetate added to it, for one week. When the mice reached 7-9 weeks old, they then underwent stereotaxic surgery and FSCV was used to evaluate their serotonin neurochemistry. For the perinatal exposure, male and female mice were paired for breeding at 8 weeks old and upon being paired, mice were exposed to either drinking water from animal facilities, which goes through a reverse osmosis filter, or the same water with 15 ppb lead acetate added to it. The male breeder was removed once the pups were born. The female breeder and pups were exposed to their respective drinking waters up until weening at which point the pups were all offered animal facility drinking water, without any lead added, ad libitum. When the perinatally exposed mice reached 8 weeks old, they underwent

a battery of behavior tests (described below). Following these tests, a short period was allowed for any stress the behavior tests may have caused to abate. Mice then underwent stereotaxic surgery and FSCV was used to evaluate their serotonin neurochemistry.

5.2.2 BEHAVIORAL ANALYSIS

When the mice were 8 weeks old, they underwent a series of behavior tests to assess autism-like behaviors. The tests were administered in the order they are described below with one day between the olfactory test and three-chamber test to reduce any effects of stress on test outcome. As the test order was selected to minimize stress, likewise the order in which animals were underwent each test was also determined in a manner to minimize stress effects on test outcome. For example, a mouse which was used as a "familiar mouse" in the three-chamber social approach would not subsequently be used as the test mouse on the same day. Prior to each test, mice were habituated to the behavior suite for at least one hour. Noldus Ethovision was employed for the recording and scoring of behavior tests when applicable.

5.2.2.1 REPETITIVE BEHAVIOR

Mice were singly housed for the duration of the behavior test and allowed a fifteen-minute habituation period in the clean cage prior to the start of the test. Mice did not have access to food or water throughout the habituation and test periods. The duration of the test was fifteen minutes. The following behaviors were observed and scored: grooming, digging, rearing, and climbing. The test was hand scored by two researchers who were blinded to the identity of the mice. The number of times each behavior was observed was averaged for all mice in a cohort and the two cohorts (exposed vs control) were compared for each behavior. A t-test was used to test for any statistical differences.

5.2.2.2 MARBLE BURYING

For the purpose of this test biofresh comfort bedding was used, as the natural cellulose fibers promote burrowing. Mice were habituated in singly housed cages with the biofresh comfort bedding for a period of ten minutes. Following habituation, mice were temporarily removed from the cage to place 12 marbles in a grid pattern on the bedding. Mice were returned to the cages and allowed a ten-minute test period, after which the marbles were scored as either buried, unburied, or partially buried. A partial burial constituted a marble which was still easily visible but also had some bedding on top of it. Again, two research blindly hand scored the outcome of the test. The results were compared as buried and unburied (assuming partial burial constituted buried) for exposed mice to control mice and a t-test was used to evaluate statistical significance.

5.2.2.3 OLFACTORY HABITUATION/ DISHABITUATION

In the olfactory habituation/dishabituation test, mice were singly house without access to food or water for the test and habituation period, with each period lasting 45 minutes. A series of scents were introduced to the mice *via* a q-tip and the amount of time the mice spent sniffing each scent was recorded. Each scent was presented to the mice three times, each on a new q-tip, for a period of two minutes, with one minute between each presentation. The following scents were introduced in the order listed: water, orange extract, vanilla extract, social scent 1, social scent 2. Each social scent was taken as a swab from the bottom of a cage of unfamiliar mice containing 4-5 mice of the same sex as the test subject. The cage had not been changed for at least two days. The non-social smells were prepared as previously described [113]. The two scoring researchers were again blind to the animal identity and the two tabulated scores averaged. The results were evaluated with

a multi-way analysis of variance (ANOVA), to test for habituation as well as difference in time spent sniffing social vs non-social smells in Pb^{2+} exposed vs control mice.

5.2.2.4 THREE-CHAMBER SOCIAL APPROACH

A custom built three chamber apparatus was utilized with dimensions according to commercially available equivalents from Ugo Basile. The cage cups used were purchased from Ugo Basile. Mice were allowed a 5-minute habituation period in the center chamber without access to the other chambers, followed by a five-minute exploration period with access to all chambers and no other mice present in the apparatus. Following these periods, when the mouse returned to the center chamber, the doors were again closed and a familiar mouse (cage mate) was placed in one of the cups in one of the side chambers. The other side chamber contained an empty cup and the side used was chosen at random, though kept consistent for each test. For a ten-minute test period, the mouse was allowed access to all three chambers. Once the test period was complete and the mouse returned to the center chamber, the familiar mouse was removed, the cage cleaned, and a novel mouse of the same sex placed in that cup. The ten-minute test period was repeated. Noldus ethovision was used to score this test, scoring the time spent in each chamber by the mouse. Multi-way ANOVAs were used to compare time spent in each chamber.

5.2.2.5 ELEVATED ZERO MAZE

The elevated zero maze was used to test for anxiety in the mice, and account for any effects this could be have on other behavioral test outcome. An elevated zero apparatus was used from Maze Engineers (Boston, MA). Mice were placed on the maze at one of the four points, chosen randomly, where the open and closed arm meet. The test period began as soon as the mouse was set down and lasted five minutes. Noldus ethovision was used to

record and score the test. The time spent in open vs closed arms was scored and compared using a t-test.

5.2.3 CARBON-FIBER MICROELECTRODES

CFM's were constructed through the aspiration of a single T-650 carbon fiber (7 μm, Goodfellow, Coraopolis, PA) through a cylindrical glass capillary (internal diameter: 0.4 mm, external diameter: 0.6 mm, Product # 624500, A-M Systems, Carlsborg, WA). This capillary was then placed in a vertical pipette puller (Narishige Group, Setagaya-Ku, Tokyo, Japan) to make a carbon – glass seal by gravity. The protruding carbon fiber was then cut to 150 μm in length. Subsequently, a solution of Nafion (LQ-1105-US-25, 5% by weight Nafion, Ion Power, DE) was electrodeposited, as previously described, onto the exposed carbon fiber [23]. The CFM was then dried for 10 minutes at 70°C.

5.2.4 ANIMAL SURGERY

A urethane solution was produced (25% (w/v)) by dissolving urethane (Sigma Aldrich Co., St. Louis, MO, USA) in sterile saline (0.9% NaCl solution, Hospira, Lake Forest, IL). When the mice were 7 to 10 weeks old the urethane was administered *intraperitoneally* (*i.p.*) at a volume of 7 μL per 1 g mouse weight, followed by stereotaxic surgeries (Model 962, David Kopf Instruments, Tujunga, CA) during the light cycle. To maintain the ideal mouse body temperature of 37° C, a heating pad from Braintree Scientific was utilized. For stereotaxic coordinates of MFB [AP: -1.58, ML: +1.0, DV: -4.8 to -5.0] and mPFC [AP: +1.7, ML: +0.2, DV: -2.0 to -3.0], bregma was used as a reference from Franklin and Paxinos (2008). In order to access the MFB and mPFC, holes were drilled in line with the above stereotaxic coordinates. For stimulation, a stainless-steel electrode (diameter 0.2 mm, MS303/2-A/SPC; Plastics One, Roanoke, VA) was inserted

into the MFB. For measurements, the Nafion-coated CFM was inserted into the mPFC. The reference electrode is made of a silver wire (diameter: 0.010 in, 787000; A-M Systems, Sequim, WA), which was electroplated with chloride through immersion of in hydrochloric acid for 30 seconds (0.1 M, 4 V vs. tungsten). This is then placed into the contralateral hemisphere of the CFM placement.

5.2.5 DATA COLLECTION AND ANALYSIS

FSCV was performed through instrumentation and software (WCCV 3.05) developed by Knowmad Technologies LLC (Tucson, AZ); the "Jackson" waveform [20] was applied for the measurement of serotonin. Measurements were collected every 10 minutes with a 30 second file. Five seconds into the file, a stimulation was applied (60 Hz biphasic 360 μA, 120 pulse stimulation, 2 ms per phase) using a linear constant current stimulus isolator (NL800A Neurolog; Digitimer Ltd.) to elicit the serotonin response. Signals were processed using custom software (*vide supra*) using LabVIEW 2009. The processing used includes signal deconvolution, filtering, and smoothing.

Signals were analyzed to compare the maximum amplitude and $t_{1/2}$. The maximum amplitude was taken as the highest concentration of serotonin elicited following the stimulation. The $t_{1/2}$ was calculated using the curve fitting tool with a custom equation for plotting exponential decay in MatLab R2018B, the natural log of 2 was divided by the mean lifetime yielded to calculate $t_{1/2}$.

5.2.6 EXCLUSION CRITERIA

For all FSCV experiments, the CV of the evoked signal was compared to well-established serotonin cyclic voltammograms (CVs) *in vivo* and *in vitro* and mice in which the CVs did not contain the characteristic serotonin redox peaks were excluded. For

FSCAV experiments, a stimulated serotonin response was collected prior to the start of FSCAV and the same aforementioned test was performed. Data which contained a peak resulting from the stimulation electrode touching the skull that masked, delayed, or minimized the serotonin response (stimulation glitch) were excluded. Electrodes that displayed instability during file collection were excluded.

5.2.9 HISTOLOGY

In order to confirm the spatial placement of the CFM *in vivo*, a small lesion was created at the end of the FSCV experiment, by applying a constant potential at the CFM (~10 V for 1 min). Subsequently, the mice were euthanized *via* cervical dislocation followed by decapitation, and the brain was removed from the skull and stored in 4% paraformaldehyde in PBS solution. At least 2 days prior to sectioning, the brain was transferred into a 30% sucrose solution, until it was saturated with the medium. The brain was then flash-frozen, sectioned into 30 μm slices mounted onto frosted glass slides. The slices were then photographed with an optical microscope.

5.3 RESULTS

5.3.1 ACUTE RESPONSE

The administration of a bolus injection of 15 ppb Pb^{2+} caused a slight reduction in evoked serotonin amplitude 60 minutes following the injection, as seen in Figure 5.1. This reduction was not consistent in every animal and to determine if the reduction was significant the maximum amplitude of the file collected 60 minutes after Pb^{2+} administration was compared to the maximum amplitude of the control files (of which there were four). A q-test was used to determine if the change in amplitude following Pb^{2+} injection was significantly different, and the results are displayed in Table 5.1. The $t_{½}$ was

calculated as the time it takes for the serotonin signal to decay to half of its maximum amplitude. The comparison process using a q-test was repeated for $t_{½}$, shown in Table 5.1, though only one animal displayed significantly slowed reuptake while the other three display non-significant faster or slower reuptakes.

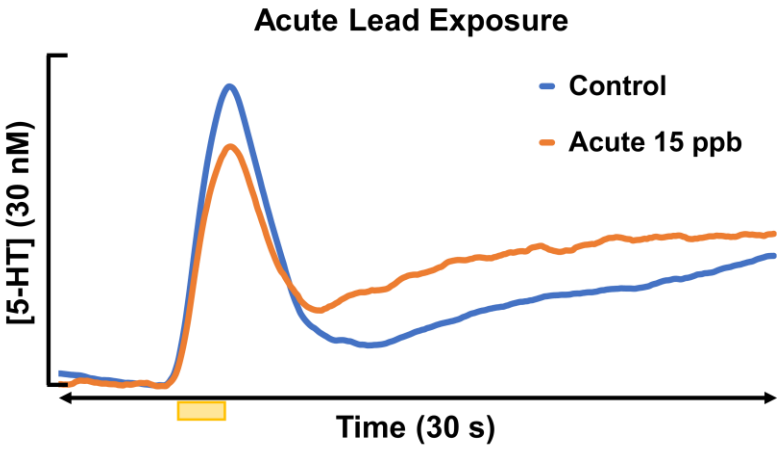

Figure 5.1. Evoked Serotonin Release Pre and Post-Acute Pb^{2+} Administration. The average evoked serotonin release (stimulation is noted by the yellow box) is shown in blue along with the evoked serotonin release 60 minutes following the injection of a bolus dose of 15 ppb Pb^{2+} (n=4).

Table 5.1. Comparison of Max_A and $t_{½}$ Pre and Post-Acute Pb^{2+} Administration.

	Control Max_A Avg ± SEM (nM)	**Post Pb Max_A (nM)**	**Q-Value**	**Control $t_{½}$ Avg ± SEM (s)**	**Post Pb $t_{½}$ (s)**	**Q-Value**
Acute 1	27.71± 1.22	21.72	0.628	2.04±0.113	1.98	0.0848
Acute 2	40.24 ± 1.29	29.95	1.19	2.19±0.227	1.90	0.0126
Acute 3	33.61 ± 0.44	27.92	1.92	1.27±0.0693	1.85	1.25
Acute 4	10.17 ± 0.24	9.32	0.313	0.810±0.0182	0.752	0.0887

5.3.2 CHRONIC ADULT EXPOSURE

Mature mice were exposed to 15 ppb Pb^{2+} in their drinking water for one week, while control mice received filtered water from animal facilities, that is free of Pb^{2+}. The evoked serotonin signals in these animals were compared in Figure 5.2. While the chronic Pb^{2+} exposure mice appeared to have slightly lower amplitude of evoked serotonin, this difference was not significant, as determined with a t-test ($p=0.355$). The reuptake of serotonin was also compared between the two groups by evaluating the $t_{½}$ as the time to reach half of the maximum amplitude. There was no significant difference in the $t_{½}$ between the chronic Pb^{2+} exposure mice and the controls, as determined by a t-test ($p=0.247$). It should be noted that the comparison of the chronic exposure here is complicated by not knowing the starting point of the serotonin signals in the individual animal and at the specific electrode location. The serotonin response varies between each mouse and has a range of evoked concentration of approximately 10-45 nM with the single peak alone. Therefore, it is probable that only drastically different serotonin responses will be discovered without exceedingly large sample size.

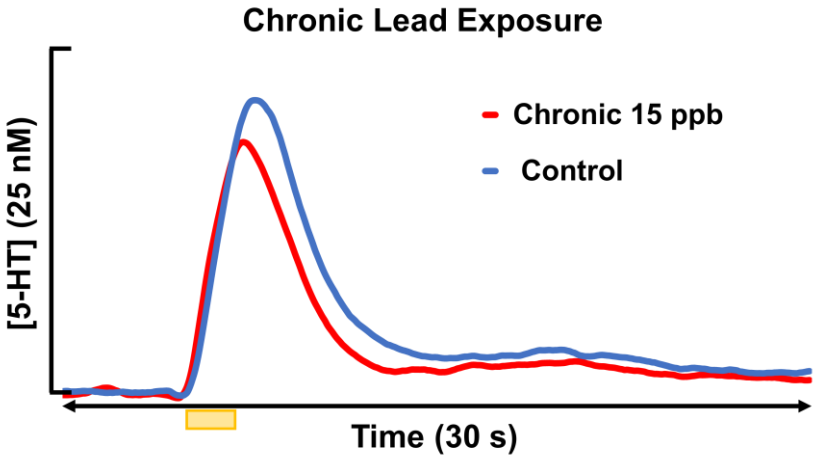

Figure 5.2. Evoked Serotonin Release in Chronic Pb^{2+} Exposed Mice and Controls. The average evoked serotonin release

(stimulation is noted by the yellow box) of control (blue, n=4) and chronic Pb^{2+} exposure (red, n=4) mice are shown here.

5.3.3 PERINATAL EXPOSURE

Breeding pairs were exposed to 15 ppb Pb^{2+} in drinking water until the pups were weaned at 21 days. When the mice reached maturity, they underwent a series of behavior tests to evaluate whether the mice displayed stereotypical ASD behaviors. The results of this tests are seen in Figure 5.3. The mice exposed to Pb^{2+} during development did not display any differences from controls in the three chamber social approach task (Figure 5.3 Panel A), particularly they did not display less preference for the chambers that contained either a familiar (t-test, p=0.362) or novel mouse (t-test, p=0.494) when compared to the control mice. The mice did not display other changes to their social communication on the olfactory habituation/dishabituation test (Panel D), displaying interest for the social scent and the non-social scent equivalent to that of the control mice (ANOVA, p=0.422, p=0.0742, respectively). The exposed mice also demonstrated significantly more interest for the social scents than the non-social scents (ANOVA, p=0.0003), as did the control mice (ANOVA, p=0.000). The exposure mice did not display significantly increased anxiety on the elevated zero test (Panel B), spending only slightly more time on average in the open arms of the apparatus than the control mice (t-test, p=0.0799). Finally, analysis for repetitive behaviors finds that in the marble burying test (Panel C) the Pb^{2+} exposed mice did not bury significantly more marbles compared to controls (t-test, p=0.246). The only behavior found to be statistically different when grooming, digging, rearing, and climbing were scored over a 15-minute period was climbing, with exposed mice climbing significantly less than controls (t-test, p= 0.00238). Exposed mice did appear to rear more

on average than controls, however this was not quite statistically significant (t=test, p= 0.059).

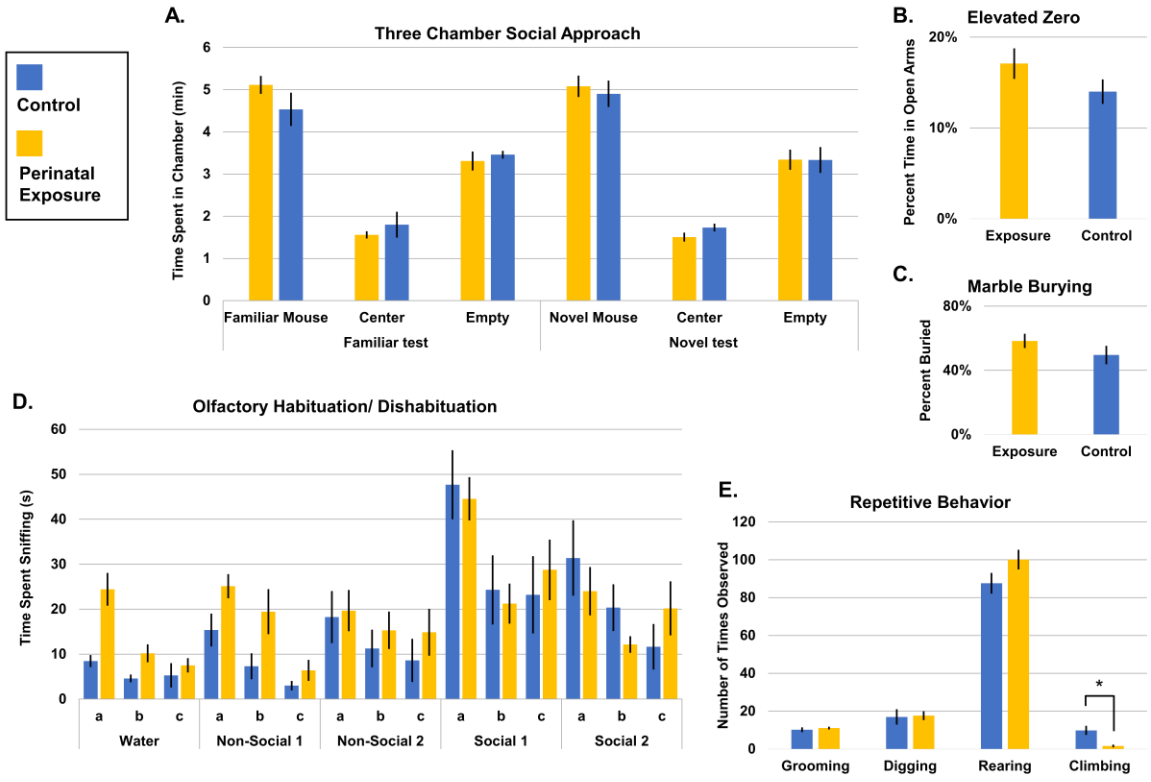

Figure 5.3. Behavioral Outcomes of Perinatal Pb^{2+} Exposed Mice. Perinatal Pb^{2+} exposed mice (yellow) are compared to control mice (blue) across five different behavioral tests. The three chamber social approach (A), elevated zero (B), marble burying (C) and olfactory habituation/dishabituation (D) found no significant differences between exposed and control mice. The repetitive behavior test found that exposed mice displayed less climbing behavior than control mice (t-test, p= 0.00238). (exposure n=22, control n=18)

Several days following the conclusion of the behavior tests, mice underwent stereotaxic surgery and were evaluated for difference in their serotonin neurochemistry. The average evoked serotonin response of the perinatal exposure mice was compared to that of controls, shown in Figure 5.4. The two main features of the curve, maximum amplitude and $t_{½}$, were compared using a t-test and significant differences were not found (p=0.305, p= 0.101, respectively) as shown in Table 5.2.

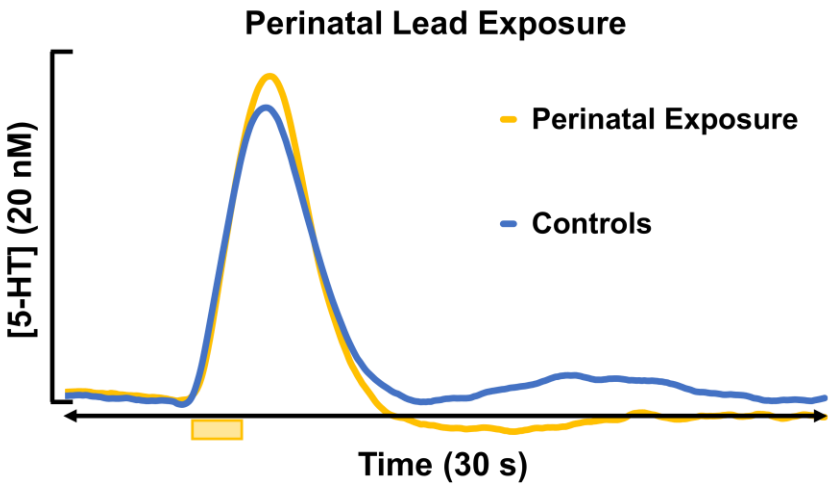

Figure 5.4. Evoked Serotonin Release in Perinatal Pb^{2+} Exposed Mice and Controls. The average evoked serotonin release (stimulation is noted by the yellow box) of control (blue, n=7) and perinatal Pb^{2+} exposure (yellow, n=7) mice are shown here.

Table 5.2. Comparison of Max_A and $t_{½}$ of Perinatal Pb^{2+} Exposure Mice and Control Mice.

Experiment	**Max_A (nM)**	**$T_{1/2}$ (s)**
Exposure 1	20.61	0.879
Exposure 2	9.05	1.04
Exposure 3	11.74	1.31
Exposure 4	9.50	1.88
Exposure 5	35.26	1.17
Exposure 6	29.18	1.21
Exposure 7	22.83	1.61
Control 1	8.85	1.98
Control 2	25.99	2.18
Control 3	8.79	1.12
Control 4	17.49	1.56
Control 5	18.48	0.943
Control 6	17.16	1.85
Control 7	24.48	1.49
p-value	0.305	0.101

5.4 DISCUSSION

5.4.1 AUTORECEPTOR AND TRANSPORTER ALTERATIONS

The evoked serotonin curve obtained with FSCV can inform upon several regulation mechanisms of serotonin transmission. The aspects which we have evaluated in this work *via* analysis of the maximum amplitude and $t_{½}$ are amount released (as a function of serotonin synthesis, vesicular packaging, receptors, and input strength) and rate of reuptake (*via* transporters)[21, 73]. The reduction in amplitude following the acute administration of Pb^{2+} suggests that there may be either direct or indirect effects on the autoreceptors.

There are 7 known serotonin receptor families, most with multiple subtypes, that can act in an excitatory or inhibitory role for serotonin release[4]. We observe their effects on evoked serotonin curves in two areas: the maximum amplitude of serotonin released and a dip in the concentration below baseline following stimulation as a function of prolonged inhibition[21]. As the stimulation occurs, serotonin axons release serotonin into the extracellular space where it binds to receptors and gets taken up by transporters. Once the serotonin binds to the receptor it can inhibit the maximum amplitude observed in two ways, the receptor may inhibit the release of serotonin, as the $5HT_{1A}$ autoreceptor does[114], or it may regulate the serotonin transporter (SERT) and can initiate a faster reuptake of serotonin, as the $5HT_{1B}$ receptor does[94]. The maximum amplitude observed is a summation of released serotonin and the simultaneous reuptake of serotonin by transporters[93]. The transporter function is typically evaluated as the rate of reuptake of serotonin and can be quantified by the time it takes to reach half of the maximum amplitude, $t_{½}$. The receptors in particular can be subject to changes *via* Pb^{2+} since this metal mimics and competes with

Ca^{2+} [100]. When the receptors bind to serotonin, they cause ion channels to open allowing for the influx of specific ions. Any differences in how Pb^{2+} performs once inside the cell could affect serotonin inhibition or excitation and may explain the changes in amplitude observed.

5.4.2 INFLAMMATION RESULTING FROM PB^{2+} EXPOSURE

The effects of Pb^{2+} in the brain are numerous and wide reach, therefore it warrants further consideration of an indirect cause of the alterations observed following Pb^{2+} administration. Pb^{2+} has been observed to cause microgliosis and astrogliosis, indicating a potent neuroinflammatory response[112]. Since immune responses are unique to each individual animal the theories described below may also explain why only some of the animals exhibited statistically lower serotonin signals since each mouse would be subject to a variable inflammatory response.

Inflammation, particularly neuroinflammation, has been found to result in higher histamine levels[115]. We have shown in previous work that histamine acts to modulate serotonin *via* the H_3 receptor, resulting in an inhibition of serotonin when histamine levels are higher[110]. This is one possible theory as to why the serotonin release is lower following Pb^{2+} administration.

Research has shown that the extracellular fluid is reduced during inflammation states which would result in a higher concentration of neurotransmitters, serotonin included, in the extracellular space[116]. This higher concentration may be causing the autoreceptors to activate, thus further inhibiting the release and increasing the uptake. If the extracellular level is already above what it normally would be due to inflammation, the

autoreceptors would activate at a lower stimulated release of serotonin. This provides an addition theory for the decreased summation of serotonin release observed.

5.4.3 CHRONIC AND PERINATAL SEROTONIN EFFECTS

The chronic and perinatal effects observed are more inconsistent than the acute responses to Pb^{2+}, with no statistical difference in variations in uptake or amplitude. This uncertainty is primarily due to a limitation with looking at effects to serotonin following long-term exposures using FSCV. It is more difficult to view changes to serotonin with this technique following long-term exposures because we do not know the starting point of the individual animal and electrode location. Bearing this in mind and as no dramatic differences have been observed, we will assume that the alterations are negligible since the signals observed still fall within the range of controls.

Acute effects indicate that after a single dose, alterations to serotonin are possible. Based upon this, we assumed that longer-term exposures would elicit more dramatic changes. However, as that does not appear to be the case for either chronic or perinatal exposure, we must assume that the serotonin system has compensated for these changes to maintain equilibrium. It is not surprising that the compensations are made for longer-term exposures since serotonin is very tightly regulated in the brain and falling out of its narrow range of operation can have severe, even deadly consequences[39, 117].

In the case of the perinatal exposure, the low dose utilized was either not enough to result in the altered gene expression observed in other studies at higher exposure doses, or the serotonin system was able to compensate for these changes in inflammatory response. It must also be noted that our technique reveals only evoked serotonin and that changes in basal serotonin could still be present and should be investigated in the future.

The general lack of behavioral changes following perinatal exposure are unsurprising as the dose utilized was much lower than any previously reported to have behavioral changes. There are some trends, such as more rearing observed and less anxiety displayed, that may prove to be significant with a slightly larger cohort. Nonetheless, at this time we must assume that perinatal exposure to 15 ppb Pb^{2+} is not substantial enough to induce any stereotypical ASD behaviors.

5.4 CONCLUSION

We observed variable but significant effects of 15 ppb Pb^{2+} exposure on serotonin transmission during an acute administration. This effect was not preserved or exacerbated during chronic or perinatal exposures. We also found no significant behavioral changes to suggest that Pb^{2+} perinatal exposure at only 15 ppb induces stereotypical ASD behaviors.

To better understand the acute effects of Pb^{2+} a higher concentration of Pb^{2+} must be utilized, potentially revealing a more consistent and severe reduction in amplitude. Additionally, expanding the sample size may result in statistical significance across the average of the animals. Discerning which of the proposed theories holds the most weight would best be accomplished by evaluating the basal serotonin concentrations and also assessing markers of inflammation in each of the mice. This data combined with the FSCV signals would present a more complete picture of what is happening to alter serotonin neurotransmission. It would also indicate if the chronic and perinatal exposures are being affected by inflammation at this low dose and what regulatory mechanisms have been employed to reinstate equilibrium in the serotonin system.

The serotonin system is perhaps more robust and adaptive to outside influence than we initially assumed. The main concern raised by this study is that if there are effects on

serotonin transmission following one dose of Pb^{2+} at the EPA drinking water standard, albeit variable, what are the consequences for dose much higher than this such as those resulting from cases in Flint, MI and D.C.? The serotonin system proves to be resilient and adaptive following a long-term exposure to Pb^{2+}, but this may reach a breaking point at higher exposure concentrations or for longer periods of time.

REFERENCES

1. Mohammad-Zadeh, L. F.; Moses, L.; Gwaltney-Brant, S. M., Serotonin: a review. *J Vet Pharmacol Ther* **2008,** *31* (3), 187-99.
2. Lucki, I., The spectrum of behaviors influenced by serotonin. *Biol Psychiatry* **1998,** *44* (3), 151-62.
3. Monti, J. M., Serotonin control of sleep-wake behavior. *Sleep Med Rev* **2011,** *15* (4), 269-81.
4. Pytliak, M.; Vargova, V.; Mechirova, V.; Felsoci, M., Serotonin receptors - from molecular biology to clinical applications. *Physiol Res* **2011,** *60* (1), 15-25.
5. Daws, L. C., Unfaithful neurotransmitter transporters: focus on serotonin uptake and implications for antidepressant efficacy. *Pharmacol Ther* **2009,** *121* (1), 89-99.
6. Muller, C. L.; Anacker, A. M.; Veenstra-VanderWeele, J., The serotonin system in autism spectrum disorder: From biomarker to animal models. *Neuroscience* **2016,** *321*, 24-41.
7. Grzadzinski, R.; Huerta, M.; Lord, C., DSM-5 and autism spectrum disorders (ASDs): an opportunity for identifying ASD subtypes. *Mol Autism* **2013,** *4* (1), 12.
8. Jon Baio; Lisa Wiggins; Deborah L. Christensen; Matthew J Maenner, J. D. Z. W. M. K.-S. W. Z. C. R. R. T. W. M. S., Prevalence of Autism Spectrum Disorder Among Children Aged 8 Years — Autism and Developmental Disabilities Monitoring Network, 11 Sites, United States, 2014. *Surveillance Summaries* **2018,** *67* (6), 1-23.
9. Karimi, P.; Kamali, E.; Mousavi, S. M.; Karahmadi, M., Environmental factors influencing the risk of autism. *J Res Med Sci* **2017,** *22*, 27.
10. SFARI Gene. https://sfari.org/resources/sfari-gene (accessed October 13).
11. Lyall, K.; Croen, L.; Daniels, J.; Fallin, M. D.; Ladd-Acosta, C.; Lee, B. K.; Park, B. Y.; Snyder, N. W.; Schendel, D.; Volk, H.; Windham, G. C.; Newschaffer, C., The Changing Epidemiology of Autism Spectrum Disorders. *Annu Rev Public Health* **2017,** *38*, 81-102.
12. Landrigan, P. J.; Lambertini, L.; Birnbaum, L. S., A research strategy to discover the environmental causes of autism and neurodevelopmental disabilities. *Environ Health Perspect* **2012,** *120* (7), a258-60.
13. Modabbernia, A.; Velthorst, E.; Reichenberg, A., Environmental risk factors for autism: an evidence-based review of systematic reviews and meta-analyses. *Mol Autism* **2017,** *8*, 13.
14. Veenstra-Vanderweele, J.; Jessen, T. N.; Thompson, B. J.; Carter, M.; Prasad, H. C.; Steiner, J. A.; Sutcliffe, J. S.; Blakely, R. D., Modeling rare gene variation to gain insight into the oldest biomarker in autism: construction of the serotonin transporter Gly56Ala knock-in mouse. *J Neurodev Disord* **2009,** *1* (2), 158-71.
15. Walsh, J. J.; Christoffel, D. J.; Heifets, B. D.; Ben-Dor, G. A.; Selimbeyoglu, A.; Hung, L. W.; Deisseroth, K.; Malenka, R. C., 5-HT release in nucleus accumbens rescues social deficits in mouse autism model. *Nature* **2018,** *560* (7720), 589-594.

16. Sodhi, M. S.; Sanders-Bush, E., Serotonin and brain development. *Int Rev Neurobiol* **2004,** *59*, 111-74.
17. Farrelly, L. A.; Thompson, R. E.; Zhao, S.; Lepack, A. E.; Lyu, Y.; Bhanu, N. V.; Zhang, B.; Loh, Y. E.; Ramakrishnan, A.; Vadodaria, K. C.; Heard, K. J.; Erikson, G.; Nakadai, T.; Bastle, R. M.; Lukasak, B. J.; Zebroski, H., 3rd; Alenina, N.; Bader, M.; Berton, O.; Roeder, R. G.; Molina, H.; Gage, F. H.; Shen, L.; Garcia, B. A.; Li, H.; Muir, T. W.; Maze, I., Histone serotonylation is a permissive modification that enhances TFIID binding to H3K4me3. *Nature* **2019,** *567* (7749), 535-539.
18. Scahill L, B. S., Psychopharmacology in children with PDD: review of current evidence. In *Evidence-Based Practices and Treatments for Children with Autism*, Reichow B, D. P., Cicchetti DV, Volkmar FR, Ed. Springer: NY, USA, 2011; pp 231-243.
19. Yang, H.; Thompson, A. B.; McIntosh, B. J.; Altieri, S. C.; Andrews, A. M., Physiologically relevant changes in serotonin resolved by fast microdialysis. *ACS Chem Neurosci* **2013,** *4* (5), 790-8.
20. Jackson, B. P.; Dietz, S. M.; Wightman, R. M., Fast-Scan Cyclic Voltammetry of 5-Hydroxytryptamine. *Analytical Chemistry* **1995,** *67* (6), 1115-1120.
21. Wood, K. M.; Zeqja, A.; Nijhout, H. F.; Reed, M. C.; Best, J.; Hashemi, P., Voltammetric and mathematical evidence for dual transport mediation of serotonin clearance in vivo. *J Neurochem* **2014,** *130* (3), 351-9.
22. Abdalla, A.; Atcherley, C. W.; Pathirathna, P.; Samaranayake, S.; Qiang, B.; Pena, E.; Morgan, S. L.; Heien, M. L.; Hashemi, P., In Vivo Ambient Serotonin Measurements at Carbon-Fiber Microelectrodes. *Anal Chem* **2017,** *89* (18), 9703-9711.
23. Hashemi, P.; Dankoski, E. C.; Petrovic, J.; Keithley, R. B.; Wightman, R. M., Voltammetric detection of 5-hydroxytryptamine release in the rat brain. *Anal Chem* **2009,** *81* (22), 9462-71.
24. Azmitia, E. C.; Singh, J. S.; Whitaker-Azmitia, P. M., Increased serotonin axons (immunoreactive to 5-HT transporter) in postmortem brains from young autism donors. *Neuropharmacology* **2011,** *60* (7-8), 1347-54.
25. Kolb, B.; Mychasiuk, R.; Muhammad, A.; Li, Y.; Frost, D. O.; Gibb, R., Experience and the developing prefrontal cortex. *Proc Natl Acad Sci U S A* **2012,** *109 Suppl 2*, 17186-93.
26. Calipari, E. S.; Godino, A.; Peck, E. G.; Salery, M.; Mervosh, N. L.; Landry, J. A.; Russo, S. J.; Hurd, Y. L.; Nestler, E. J.; Kiraly, D. D., Granulocyte-colony stimulating factor controls neural and behavioral plasticity in response to cocaine. *Nat Commun* **2018,** *9* (1), 9.
27. Guise, K. G.; Shapiro, M. L., Medial Prefrontal Cortex Reduces Memory Interference by Modifying Hippocampal Encoding. *Neuron* **2017,** *94* (1), 183-192 e8.
28. Kim, C. K.; Adhikari, A.; Deisseroth, K., Integration of optogenetics with complementary methodologies in systems neuroscience. *Nat Rev Neurosci* **2017,** *18* (4), 222-235.
29. Whitaker-Azmitia, P. M., Serotonin and brain development: Role in human developmental diseases. *Brain Research Bulletin* **2001,** *56* (5), 479-485.
30. Robbins, T. W., Chemistry of the mind: Neurochemical modulation of prefrontal cortical function. *J Comp Neurol* **2005,** *493* (1), 140-146.

31. Hranilovic, D.; Blazevic, S., Hyperserotonemia in Autism: 5HT-Regulating Proteins. *Comprehensive Guide to Autism* **2014**, 717-739.
32. Dufour-Rainfray, D.; Vourc'h, P.; Le Guisquet, A. M.; Garreau, L.; Ternant, D.; Bodard, S.; Jaumain, E.; Gulhan, Z.; Belzung, C.; Andres, C. R.; Chalon, S.; Guilloteau, D., Behavior and serotonergic disorders in rats exposed prenatally to valproate: a model for autism. *Neurosci Lett* **2010,** *470* (1), 55-9.
33. Nakamura, K.; Sekine, Y.; Ouchi, Y.; Tsujii, M.; Yoshikawa, E.; Futatsubashi, M.; Tsuchiya, K. J.; Sugihara, G.; Iwata, Y.; Suzuki, K.; Matsuzaki, H.; Suda, S.; Sugiyama, T.; Takei, N.; Mori, N., Brain serotonin and dopamine transporter bindings in adults with high-functioning autism. *Arch Gen Psychiatry* **2010,** *67* (1), 59-68.
34. Guo, Y. P.; Commons, K. G., Serotonin neuron abnormalities in the BTBR mouse model of autism. *Autism Res* **2017,** *10* (1), 66-77.
35. Gould, G. G.; Hensler, J. G.; Burke, T. F.; Benno, R. H.; Onaivi, E. S.; Daws, L. C., Density and function of central serotonin (5-HT) transporters, 5-HT1A and 5-HT2A receptors, and effects of their targeting on BTBR T+tf/J mouse social behavior. *J Neurochem* **2011,** *116* (2), 291-303.
36. Nakai, R.; Fukuda, S.; Kawase, M.; Yamashita, Y.; Ashida, H., Curcumin and its derivatives inhibit 2,3,7,8,-tetrachloro-dibenzo-p-dioxin-induced expression of drug metabolizing enzymes through aryl hydrocarbon receptor-mediated pathway. *Biosci Biotechnol Biochem* **2017**, 1-13.
37. Shaskan, E. G.; Snyder, S. H., Kinetics of serotonin accumulation into slices from rat brain: relationship to catecholamine uptake. *J Pharmacol Exp Ther* **1970,** *175* (2), 404-18.
38. Paxinos, G. W., C., *The Mouse Brain in Stereotaxic Coordinates*. 4th ed.; Academic Press: 2012.
39. Hashemi, P.; Dankoski, E. C.; Lama, R.; Wood, K. M.; Takmakov, P.; Wightman, R. M., Brain dopamine and serotonin differ in regulation and its consequences. *Proc Natl Acad Sci U S A* **2012,** *109* (29), 11510-5.
40. Sombers, L. A.; Beyene, M.; Carelli, R. M.; Wightman, R. M., Synaptic Overflow of Dopamine in the Nucleus Accumbens Arises from Neuronal Activity in the Ventral Tegmental Area. *Journal of Neuroscience* **2009,** *29* (6), 1735-1742.
41. Samaranayake, S.; Abdalla, A.; Robke, R.; Wood, K. M.; Zeqja, A.; Hashemi, P., In vivo histamine voltammetry in the mouse premammillary nucleus. *Analyst* **2015,** *140* (11), 3759-3765.
42. Walters, S. H.; Robbins, E. M.; Michael, A. C., Modeling the Kinetic Diversity of Dopamine in the Dorsal Striatum. *Acs Chemical Neuroscience* **2015,** *6* (8), 1468-1475.
43. Ikemoto, S., Dopamine reward circuitry: two projection systems from the ventral midbrain to the nucleus accumbens-olfactory tubercle complex. *Brain Res Rev* **2007,** *56* (1), 27-78.
44. Vertes, R. P., A Pha-L Analysis of Ascending Projections of the Dorsal Raphe Nucleus in the Rat. *J Comp Neurol* **1991,** *313* (4), 643-668.
45. Vertes, R. P.; Fortin, W. J.; Crane, A. M., Projections of the median raphe nucleus in the rat. *J Comp Neurol* **1999,** *407* (4), 555-582.
46. Gerfen, C. R.; Herkenham, M.; Thibault, J., The neostriatal mosaic: II. Patch- and matrix-directed mesostriatal dopaminergic and non-dopaminergic systems. *J Neurosci* **1987,** *7* (12), 3915-34.

47. Graybiel, A. M.; Ragsdale, C. W., Jr.; Yoneoka, E. S.; Elde, R. P., An immunohistochemical study of enkephalins and other neuropeptides in the striatum of the cat with evidence that the opiate peptides are arranged to form mosaic patterns in register with the striosomal compartments visible by acetylcholinesterase staining. *Neuroscience* **1981,** *6* (3), 377-97.
48. Brimblecombe, K. R.; Cragg, S. J., Substance P Weights Striatal Dopamine Transmission Differently within the Striosome-Matrix Axis. *J Neurosci* **2015,** *35* (24), 9017-23.
49. Tellez, R.; Gomez-Viquez, L.; Meneses, A., GABA, glutamate, dopamine and serotonin transporters expression on memory formation and amnesia. *Neurobiol Learn Mem* **2012,** *97* (2), 189-201.
50. Gasser, P. J.; Orchinik, M.; Raju, I.; Lowry, C. A., Distribution of Organic Cation Transporter 3, a Corticosterone-Sensitive Monoamine Transporter, in the Rat Brain. *J Comp Neurol* **2009,** *512* (4), 529-555.
51. Brennum, L.; Larsen, A.; Andersen, P.; Halldin, C., Escitalopram - the most selective SSRI; in vitro data and in vivo binding studies using the new selective SERT ligand 3H-MADAM. *Eur Neuropsychopharm* **2002,** *12*, S209-S209.
52. Andrade, R., Serotonergic regulation of neuronal excitability in the prefrontal cortex. *Neuropharmacology* **2011,** *61* (3), 382-386.
53. Kosofsky, B. E.; Molliver, M. E., The Serotoninergic Innervation of Cerebral-Cortex - Different Classes of Axon Terminals Arise from Dorsal and Median Raphe Nuclei. *Synapse* **1987,** *1* (2), 153-168.
54. Kiyasova, V.; Fernandez, S. P.; Laine, J.; Stankovski, L.; Muzerelle, A.; Doly, S.; Gaspar, P., A Genetically Defined Morphologically and Functionally Unique Subset of 5-HT Neurons in the Mouse Raphe Nuclei. *Journal of Neuroscience* **2011,** *31* (8), 2756-2768.
55. Hajos, M.; Richards, C. D.; Szekely, A. D.; Sharp, T., An electrophysiological and neuroanatomical study of the medial prefrontal cortical projection to the midbrain raphe nuclei in the rat. *Neuroscience* **1998,** *87* (1), 95-108.
56. Owens, M. J.; Nemeroff, C. B., Role of serotonin in the pathophysiology of depression: focus on the serotonin transporter. *Clin Chem* **1994,** *40* (2), 288-95.
57. Abi-Dargham, A.; Laruelle, M.; Aghajanian, G. K.; Charney, D.; Krystal, J., The role of serotonin in the pathophysiology and treatment of schizophrenia. *J Neuropsychiatry Clin Neurosci* **1997,** *9* (1), 1-17.
58. Oades, R. D., Dopamine-serotonin interactions in attention-deficit hyperactivity disorder (ADHD). *Prog Brain Res* **2008,** *172*, 543-65.
59. Volkow, N. D.; Fowler, J. S., Addiction, a disease of compulsion and drive: involvement of the orbitofrontal cortex. *Cereb Cortex* **2000,** *10* (3), 318-25.
60. Johnson, J. A.; Rodeberg, N. T.; Wightman, R. M., Measurement of Basal Neurotransmitter Levels Using Convolution-Based Nonfaradaic Current Removal. *Anal Chem* **2018,** *90* (12), 7181-7189.
61. Shen, M.; Qu, Z.; DesLaurier, J.; Welle, T. M.; Sweedler, J. V.; Chen, R., Single Synaptic Observation of Cholinergic Neurotransmission on Living Neurons: Concentration and Dynamics. *J Am Chem Soc* **2018,** *140* (25), 7764-7768.

62. Meunier, C. J.; Roberts, J. G.; McCarty, G. S.; Sombers, L. A., Background Signal as an in Situ Predictor of Dopamine Oxidation Potential: Improving Interpretation of Fast-Scan Cyclic Voltammetry Data. *ACS Chem Neurosci* **2017,** *8* (2), 411-419.
63. Parsons, L. H.; Justice, J. B., Jr., Serotonin and dopamine sensitization in the nucleus accumbens, ventral tegmental area, and dorsal raphe nucleus following repeated cocaine administration. *J Neurochem* **1993,** *61* (5), 1611-9.
64. Palkovits, M.; Brownstein, M.; Saavedra, J. M., Serotonin content of the brain stem nuclei in the rat. *Brain Res* **1974,** *80* (2), 237-49.
65. Gyorfi, O.; Nagy, H.; Bokor, M.; Moustafa, A. A.; Rosenzweig, I.; Kelemen, O.; Keri, S., Reduced CA2-CA3 Hippocampal Subfield Volume Is Related to Depression and Normalized by l-DOPA in Newly Diagnosed Parkinson's Disease. *Front Neurol* **2017,** *8*, 84.
66. Schumann, C. M.; Bauman, M. D.; Amaral, D. G., Abnormal structure or function of the amygdala is a common component of neurodevelopmental disorders. *Neuropsychologia* **2011,** *49* (4), 745-59.
67. Nestler, E. J.; Barrot, M.; DiLeone, R. J.; Eisch, A. J.; Gold, S. J.; Monteggia, L. M., Neurobiology of depression. *Neuron* **2002,** *34* (1), 13-25.
68. Jin, Y.; Dougherty, S. E.; Wood, K.; Sun, L.; Cudmore, R. H.; Abdalla, A.; Kannan, G.; Pletnikov, M.; Hashemi, P.; Linden, D. J., Regrowth of Serotonin Axons in the Adult Mouse Brain Following Injury. *Neuron* **2016,** *91* (4), 748-62.
69. Frodl, T.; Schaub, A.; Banac, S.; Charypar, M.; Jager, M.; Kummler, P.; Bottlender, R.; Zetzsche, T.; Born, C.; Leinsinger, G.; Reiser, M.; Moller, H. J.; Meisenzahl, E. M., Reduced hippocampal volume correlates with executive dysfunctioning in major depression. *J Psychiatry Neurosci* **2006,** *31* (5), 316-23.
70. Bremner, J. D.; Narayan, M.; Anderson, E. R.; Staib, L. H.; Miller, H. L.; Charney, D. S., Hippocampal volume reduction in major depression. *Am J Psychiatry* **2000,** *157* (1), 115-8.
71. Bremner, J. D.; Vythilingam, M.; Vermetten, E.; Nazeer, A.; Adil, J.; Khan, S.; Staib, L. H.; Charney, D. S., Reduced volume of orbitofrontal cortex in major depression. *Biol Psychiatry* **2002,** *51* (4), 273-9.
72. Rigucci, S.; Serafini, G.; Pompili, M.; Kotzalidis, G. D.; Tatarelli, R., Anatomical and functional correlates in major depressive disorder: the contribution of neuroimaging studies. *World J Biol Psychiatry* **2010,** *11* (2 Pt 2), 165-80.
73. West, A.; Best, J.; Abdalla, A.; Nijhout, F.; Reed, M.; Hashemi, P., Voltammetric evidence for discrete serotonin circuits, linked to specific reuptake domains, in the mouse medial prefrontal cortex. *Neurochem Int* **2018**.
74. Srejic, L. R.; Wood, K. M.; Zeqja, A.; Hashemi, P.; Hutchison, W. D., Modulation of serotonin dynamics in the dorsal raphe nucleus via high frequency medial prefrontal cortex stimulation. *Neurobiol Dis* **2016,** *94*, 129-38.
75. Charan, J.; Kantharia, N. D., How to calculate sample size in animal studies? *J Pharmacol Pharmacother* **2013,** *4* (4), 303-6.
76. Cohen, J., *Statistical Power Analysis for the Behavioral Sciences*. 2nd edition ed.; Lawrence Erlbaum Associates: 1988.
77. Uhlig, C.; Krause, H.; Koch, T.; de Abreu, M. G.; Spieth, P. M., Anesthesia and Monitoring in Small Laboratory Mammals Used in Anesthesiology, Respiratory and

Critical Care Research: A Systematic Review on the Current Reporting in Top-10 Impact Factor Ranked Journals. *Plos One* **2015,** *10* (8).
78. Michael, D. J.; Joseph, J. D.; Kilpatrick, M. R.; Travis, E. R.; Wightman, R. M., Improving data acquisition for fast-scan cyclic voltammetry. *Anal Chem* **1999,** *71* (18), 3941-7.
79. Gong, S.; Zheng, C.; Doughty, M. L.; Losos, K.; Didkovsky, N.; Schambra, U. B.; Nowak, N. J.; Joyner, A.; Leblanc, G.; Hatten, M. E.; Heintz, N., A gene expression atlas of the central nervous system based on bacterial artificial chromosomes. *Nature* **2003,** *425* (6961), 917-25.
80. Lane, R.; Baldwin, D., Selective serotonin reuptake inhibitor-induced serotonin syndrome: review. *J Clin Psychopharmacol* **1997,** *17* (3), 208-21.
81. Gina L. Forster, A. M. N., Jamie L. Scholl, Michael J. Watt, The Role of the Amygdala in Anxiety Disorders. In *The Amygdala*, Ferry, B., Ed. IntechOpen: 2012.
82. Muhammad, A.; Carroll, C.; Kolb, B., Stress during development alters dendritic morphology in the nucleus accumbens and prefrontal cortex. *Neuroscience* **2012,** *216*, 103-9.
83. Zhou, F. C.; Tao-Cheng, J. H.; Segu, L.; Patel, T.; Wang, Y., Serotonin transporters are located on the axons beyond the synaptic junctions: anatomical and functional evidence. *Brain Res* **1998,** *805* (1-2), 241-54.
84. Kim, T. H.; Choi, J.; Kim, H. G.; Kim, H. R., Quantification of neurotransmitters in mouse brain tissue by using liquid chromatography coupled electrospray tandem mass spectrometry. *J Anal Methods Chem* **2014,** *2014*, 506870.
85. Horlin, C.; Falkmer, M.; Parsons, R.; Albrecht, M. A.; Falkmer, T., The Cost of Autism Spectrum Disorders. *Plos One* **2014,** *9* (9).
86. Devlin, B.; Scherer, S. W., Genetic architecture in autism spectrum disorder. *Curr Opin Genet Dev* **2012,** *22* (3), 229-37.
87. Hallmayer, J.; Cleveland, S.; Torres, A.; Phillips, J.; Cohen, B.; Torigoe, T.; Miller, J.; Fedele, A.; Collins, J.; Smith, K.; Lotspeich, L.; Croen, L. A.; Ozonoff, S.; Lajonchere, C.; Grether, J. K.; Risch, N., Genetic Heritability and Shared Environmental Factors Among Twin Pairs With Autism. *Archives of General Psychiatry* **2011,** *68* (11), 1095-1102.
88. Tordjman, S.; Gutknecht, L.; Carlier, M.; Spitz, E.; Antoine, C.; Slama, F.; Carsalade, V.; Cohen, D. J.; Ferrari, P.; Roubertoux, P. L.; Anderson, G. M., Role of the serotonin transporter gene in the behavioral expression of autism. *Mol Psychiatr* **2001,** *6* (4), 434-439.
89. Veenstra-VanderWeele, J.; Muller, C. L.; Iwamoto, H.; Sauer, J. E.; Owens, W. A.; Shah, C. R.; Cohen, J.; Mannangatti, P.; Jessen, T.; Thompson, B. J.; Ye, R.; Kerr, T. M.; Carneiro, A. M.; Crawley, J. N.; Sanders-Bush, E.; McMahon, D. G.; Ramamoorthy, S.; Daws, L. C.; Sutcliffe, J. S.; Blakely, R. D., Autism gene variant causes hyperserotonemia, serotonin receptor hypersensitivity, social impairment and repetitive behavior. *Proc Natl Acad Sci U S A* **2012,** *109* (14), 5469-74.
90. Bozdagi, O.; Sakurai, T.; Papapetrou, D.; Wang, X. B.; Dickstein, D. L.; Takahashi, N.; Kajiwara, Y.; Yang, M.; Katz, A. M.; Scattoni, M. L.; Harris, M. J.; Saxena, R.; Silverman, J. L.; Crawley, J. N.; Zhou, Q.; Hof, P. R.; Buxbaum, J. D., Haploinsufficiency of the autism-associated Shank3 gene leads to deficits in synaptic function, social interaction, and social communication. *Molecular Autism* **2010,** *1*.

91. Grabrucker, A. M.; Schmeisser, M. J.; Schoen, M.; Boeckers, T. M., Postsynaptic ProSAP/Shank scaffolds in the cross-hair of synaptopathies. *Trends Cell Biol* **2011,** *21* (10), 594-603.
92. Jiang, Y. H.; Ehlers, M. D., Modeling Autism by SHANK Gene Mutations in Mice. *Neuron* **2013,** *78* (1), 8-27.
93. Wightman, R. M.; Amatore, C.; Engstrom, R. C.; Hale, P. D.; Kristensen, E. W.; Kuhr, W. G.; May, L. J., Real-Time Characterization of Dopamine Overflow and Uptake in the Rat Striatum. *Neuroscience* **1988,** *25* (2), 513-523.
94. Montanez, S.; Munn, J. L.; Owens, W. A.; Horton, R. E.; Daws, L. C., 5-HT1B receptor modulation of the serotonin transporter in vivo: Studies using KO mice. *Neurochemistry International* **2014,** *73*, 127-131.
95. Nadeau, J.; Sulkowski, M. L.; Ung, D.; Wood, J. J.; Lewin, A. B.; Murphy, T. K.; May, J. E.; Storch, E. A., Treatment of comorbid anxiety and autism spectrum disorders. *Neuropsychiatry-Lond* **2011,** *1* (6), 567-578.
96. Needleman, H., Lead poisoning. *Annu Rev Med* **2004,** *55*, 209-22.
97. Bressler, J. P.; Goldstein, G. W., Mechanisms of lead neurotoxicity. *Biochem Pharmacol* **1991,** *41* (4), 479-84.
98. Dou, J. F.; Farooqui, Z.; Faulk, C. D.; Barks, A. K.; Jones, T.; Dolinoy, D. C.; Bakulski, K. M., Perinatal Lead (Pb) Exposure and Cortical Neuron-Specific DNA Methylation in Male Mice. *Genes-Basel* **2019,** *10* (4).
99. Kasten-Jolly, J.; Pabello, N.; Bolivar, V. J.; Lawrence, D. A., Developmental lead effects on behavior and brain gene expression in male and female BALB/cAnNTac mice. *Neurotoxicology* **2012,** *33* (5), 1005-1020.
100. Simons, T. J. B., Lead-Calcium Interactions in Cellular Lead Toxicity. *Neurotoxicology* **1993,** *14* (2-3), 77-86.
101. Neal, A. P.; Guilarte, T. R., Molecular Neurobiology of Lead (Pb2+): Effects on Synaptic Function. *Mol Neurobiol* **2010,** *42* (3), 151-160.
102. Ziegler, E. E.; Edwards, B. B.; Jensen, R. L.; Mahaffey, K. R.; Fomon, S. J., Absorption and Retention of Lead by Infants. *Pediatr Res* **1978,** *12* (1), 29-34.
103. Carpenter, S. J., Placental permeability of lead. *Environ Health Perspect* **1974,** *7*, 129-31.
104. Ettinger, A. S.; Tellez-Rojo, M. M.; Amarasiriwardena, C.; Bellinger, D.; Peterson, K.; Schwartz, J.; Hu, H.; Hernandez-Avila, M., Effect of breast milk lead on infant blood lead levels at 1 month of age. *Environ Health Persp* **2004,** *112* (14), 1381-1385.
105. Bornschein, R.; Pearson, D.; Reiter, L., Behavioral effects of moderate lead exposure in children and animal models: part 1, clinical studies. *Crit Rev Toxicol* **1980,** *8* (1), 43-99.
106. Bornschein, R.; Pearson, D.; Reiter, L., Behavioral effects of moderate lead exposure in children and animal models: part 2, animal studies. *Crit Rev Toxicol* **1980,** *8* (2), 101-52.
107. Renner, R., Plumbing the depths of the DC Crisis. *Environmental Science and Technology* **2004**, 224-227.
108. Pieper, K. J.; Tang, M.; Edwards, M. A., Flint Water Crisis Caused By Interrupted Corrosion Control: Investigating "Ground Zero" Home. *Environ Sci Technol* **2017,** *51* (4), 2007-2014.

109. National Primary Drinking Water Regulations. https://www.epa.gov/ground-water-and-drinking-water/national-primary-drinking-water-regulations.
110. Samaranayake, S.; Abdalla, A.; Robke, R.; Nijhout, H. F.; Reed, M. C.; Best, J.; Hashemi, P., A voltammetric and mathematical analysis of histaminergic modulation of serotonin in the mouse hypothalamus. *J Neurochem* **2016,** *138* (3), 374-83.
111. Yassa, H. A., Autism: a form of lead and mercury toxicity. *Environ Toxicol Pharmacol* **2014,** *38* (3), 1016-24.
112. Peng, J.; Zhou, F.; Wang, Y.; Xu, Y.; Zhang, H.; Zou, F.; Meng, X., Differential response to lead toxicity in rat primary microglia and astrocytes. *Toxicol Appl Pharmacol* **2019,** *363*, 64-71.
113. Yang, M.; Crawley, J. N., Simple behavioral assessment of mouse olfaction. *Curr Protoc Neurosci* **2009,** *Chapter 8*, Unit 8 24.
114. Richardson-Jones, J. W.; Craige, C. P.; Nguyen, T. H.; Kung, H. F.; Gardier, A. M.; Dranovsky, A.; David, D. J.; Guiard, B. P.; Beck, S. G.; Hen, R.; Leonardo, E. D., Serotonin-1A autoreceptors are necessary and sufficient for the normal formation of circuits underlying innate anxiety. *J Neurosci* **2011,** *31* (16), 6008-18.
115. Saraiva, C.; Barata-Antunes, S.; Santos, T.; Ferreiro, E.; Cristovao, A. C.; Serra-Almeida, C.; Ferreira, R.; Bernardino, L., Histamine modulates hippocampal inflammation and neurogenesis in adult mice. *Sci Rep* **2019,** *9* (1), 8384.
116. Sykova, E., Extrasynaptic volume transmission and diffusion parameters of the extracellular space. *Neuroscience* **2004,** *129* (4), 861-876.
117. Lane, R.; Baldwin, D., Selective serotonin reuptake inhibitor-induced serotonin syndrome: Review. *J Clin Psychopharm* **1997,** *17* (3), 208-221.

APPENDIX A
CHAPTER 1 SUPPLEMENTARY MATERIAL

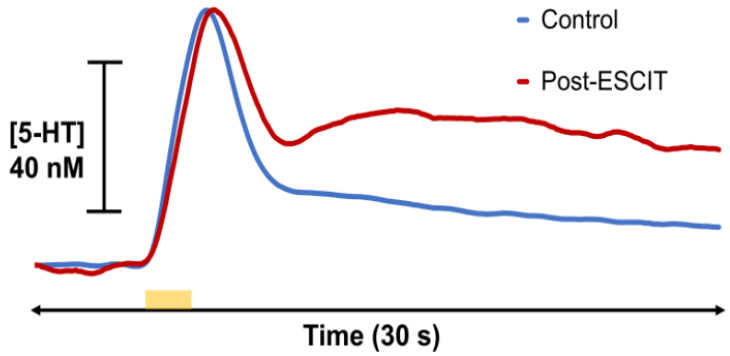

Figure A.1 mPFC Double Peak Response to Escitalopram. An additional representative plot of a serotonin double peak control (blue) signal and ESCIT (red) response in layers 5-6 of the mPFC.

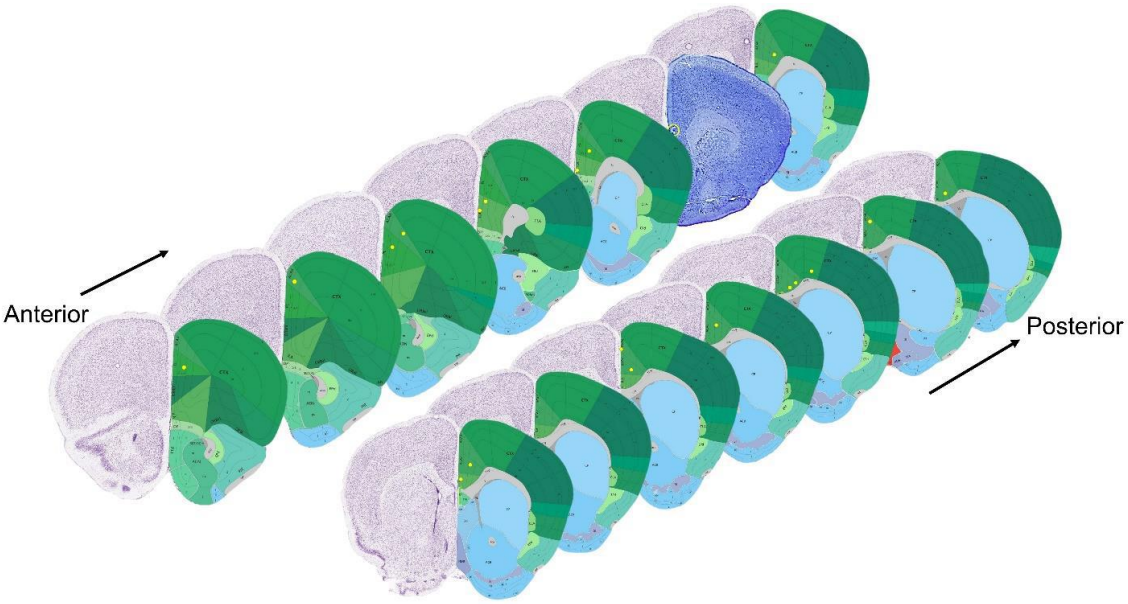

Figure A.2 Histology of Experiments. A physical representation of the histology for each data point, corresponding to the data in Table 1. The location of the lesion can be identified

by the yellow dot. A representative stained slice is shown with the lesion appearing in the infralimbic sub-region, layer 1.

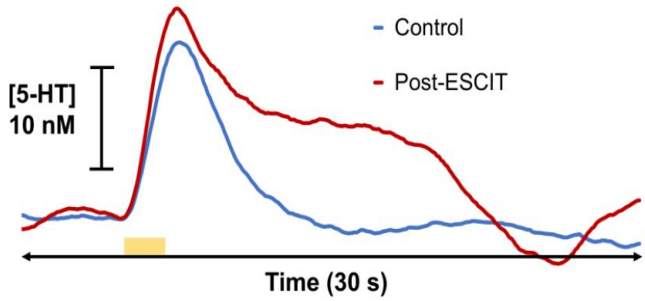

Figure A.3 mPFC Single Peak Response to Escitalopram. An additional representative plot of a serotonin single peak control (blue) signal and ESCIT (red) response in layers 1-3 of the mPFC. A second peak is induced following the administration of ESCIT.

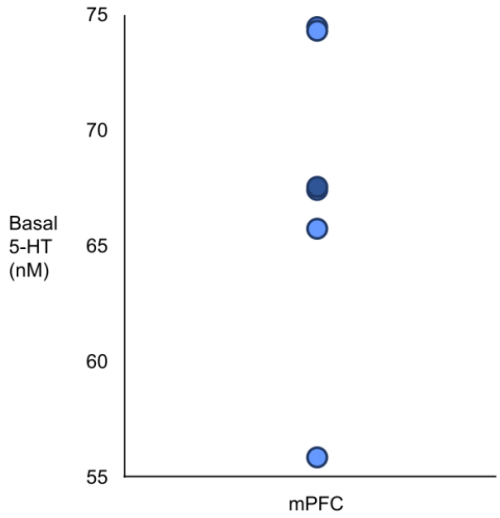

Figure A.4 The basal concentration of serotonin in the mPFC (n=5) as determined by fast-scan controlled adsorption voltammetry (FSCAV). The region has a range from 55-75 nM with an average (dark blue) of 67.56 nM.

APPENDIX B
CHAPTER 2 SUPPLEMENTARY MATERIAL

Table B.1 Preliminary Study Data Used for the Power Analysis

	Max Amplitude
Animal 1	
Control	0.645
Drug Effect	2.01
Animal 2	
Control	1.39
Drug Effect	2.54
Animal 3	
Control	1.36
Drug Effect	2.86
Animal 4	
Control	1.03
Drug Effect	2.60
Animal 5	
Control	1.47
Drug Effect	5.72
	Average± Std Dev
Control	1.18±0.34
Drug Effect	3.15±1.47

APPENDIX C
COPYRIGHT RELEASE

Chapter 2 Release. Screenshots obtained at:

https://www.elsevier.com/about/policies/copyright

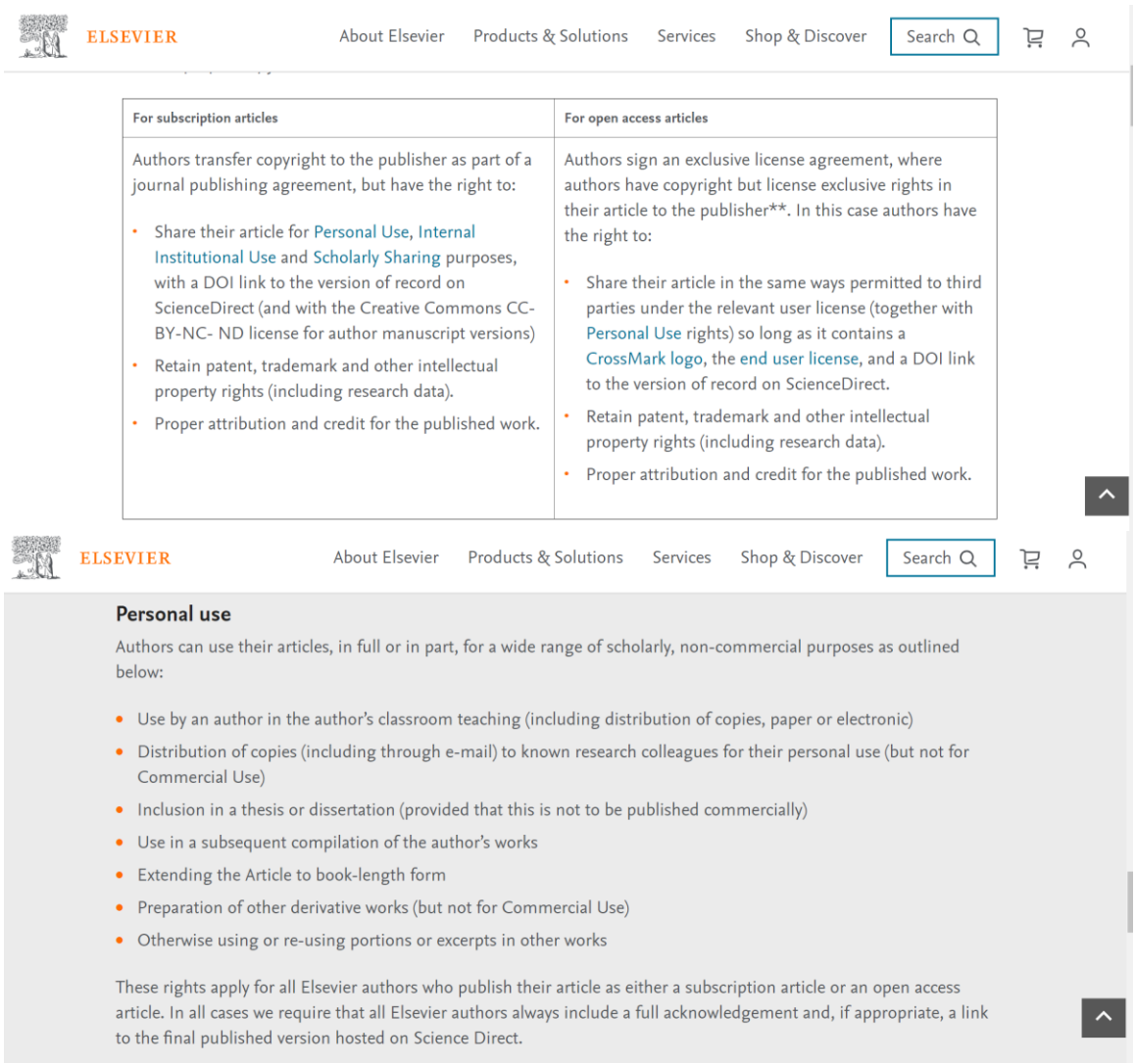

ELSEVIER About Elsevier Products & Solutions Services Shop & Discover Search

For subscription articles	For open access articles
Authors transfer copyright to the publisher as part of a journal publishing agreement, but have the right to: • Share their article for Personal Use, Internal Institutional Use and Scholarly Sharing purposes, with a DOI link to the version of record on ScienceDirect (and with the Creative Commons CC-BY-NC- ND license for author manuscript versions) • Retain patent, trademark and other intellectual property rights (including research data). • Proper attribution and credit for the published work.	Authors sign an exclusive license agreement, where authors have copyright but license exclusive rights in their article to the publisher**. In this case authors have the right to: • Share their article in the same ways permitted to third parties under the relevant user license (together with Personal Use rights) so long as it contains a CrossMark logo, the end user license, and a DOI link to the version of record on ScienceDirect. • Retain patent, trademark and other intellectual property rights (including research data). • Proper attribution and credit for the published work.

ELSEVIER About Elsevier Products & Solutions Services Shop & Discover Search

Personal use

Authors can use their articles, in full or in part, for a wide range of scholarly, non-commercial purposes as outlined below:

- Use by an author in the author's classroom teaching (including distribution of copies, paper or electronic)
- Distribution of copies (including through e-mail) to known research colleagues for their personal use (but not for Commercial Use)
- Inclusion in a thesis or dissertation (provided that this is not to be published commercially)
- Use in a subsequent compilation of the author's works
- Extending the Article to book-length form
- Preparation of other derivative works (but not for Commercial Use)
- Otherwise using or re-using portions or excerpts in other works

These rights apply for all Elsevier authors who publish their article as either a subscription article or an open access article. In all cases we require that all Elsevier authors always include a full acknowledgement and, if appropriate, a link to the final published version hosted on Science Direct.

Chapter 3 Release. Screenshots obtained at:

https://onlinelibrary.wiley.com/page/journal/14714159/homepage/permissions.html